



HAL
open science

Impact of climate changes on vegetation and human societies during the Holocene in the South Caucasus (Vanevan, Armenia): A multiproxy approach including pollen, NPPs and brGDGTs

Mary Robles, Odile Peyron, Elisabetta Brugiapaglia, Guillemette Ménot, Lucas Dugerdil, Vincent Ollivier, Salomé Ansanay-Alex, Anne-Lise Develle, Petros Tozalakyan, Khachatur Meliksetian, et al.

► To cite this version:

Mary Robles, Odile Peyron, Elisabetta Brugiapaglia, Guillemette Ménot, Lucas Dugerdil, et al.. Impact of climate changes on vegetation and human societies during the Holocene in the South Caucasus (Vanevan, Armenia): A multiproxy approach including pollen, NPPs and brGDGTs. *Quaternary Science Reviews*, 2022, 277, pp.107297. 10.1016/j.quascirev.2021.107297 . insu-03710173

HAL Id: insu-03710173

<https://insu.hal.science/insu-03710173v1>

Submitted on 18 Nov 2022

HAL is a multi-disciplinary open access archive for the deposit and dissemination of scientific research documents, whether they are published or not. The documents may come from teaching and research institutions in France or abroad, or from public or private research centers.

L'archive ouverte pluridisciplinaire **HAL**, est destinée au dépôt et à la diffusion de documents scientifiques de niveau recherche, publiés ou non, émanant des établissements d'enseignement et de recherche français ou étrangers, des laboratoires publics ou privés.

1 **Impact of climate changes on vegetation and human societies during the**
2 **Holocene in the South Caucasus (Vanevan, Armenia): a multiproxy**
3 **approach including pollen, NPPs and brGDGTs**

4 Mary Robles^{1,2}, Odile Peyron², Elisabetta Brugiapaglia¹, Guillemette Ménot³, Lucas Dugerdil^{2,3}, Vincent
5 Ollivier^{4,5}, Salomé Ansanay-Alex³, Anne-Lise Develle⁶, Petros Tozalakyan⁷, Khachatur Meliksetian⁷, Kristina
6 Sahakyan⁷, Lilit Sahakyan⁷, Bérengère Perello⁸, Ruben Badalyan⁹, Claude Colombié¹⁰, Sébastien Joannin²

7
8 1 - Univ. Molise, Department Agriculture, Environment and Alimentation, Italy
9 2 - Univ. Montpellier, CNRS, IRD, EPHE, UMR 5554 ISEM, Montpellier, France
10 3 - Univ. Lyon, ENSL, UCBL, UJM, CNRS, LGL-TPE, F-69007 Lyon, France
11 4 - Aix-Marseille Univ., CNRS, MCC, UMR 7269 LAMPEA, Aix-en-Provence, France
12 5 - Aix-Marseille Univ., CNRS, FR ECCOREV, Aix-en-Provence, France
13 6 - Univ. Savoie Mont Blanc, CNRS, UMR 5204 EDYTEM, Le Bourget-du-Lac, France
14 7 - National Academy of Sciences of Armenia, Institute of Geological Sciences, Yerevan, Armenia
15 8 - Univ. Lyon, CNRS, UMR 5133 'Archéorient', Maison de l'Orient et de la Méditerranée, Lyon, France
16 9 - National Academy of Sciences of Armenia, Institute of Archaeology and Ethnography, Yerevan, Armenia
17 10 - Univ. Lyon, UCBL, ENSL, UJM, CNRS, LGL-TPE, F-69622, Villeurbanne, France

18
19 E-mail: mary.robles@umontpellier.fr
20

21 **Abstract**

22 Relationships between steppe vegetation, human practices and climate changes in the past are
23 crucial to disentangle human development in Eurasia. In this frame, our study investigates (1) modern
24 pollen-vegetation relationships and (2) changes in vegetation, human activity and climate in the
25 Holocene record of Vanevan peat (south-eastern shore of Lake Sevan, Armenia), using a multiproxy
26 approach including sediment geochemistry (XRF), pollen, Non-Pollen Palynomorphs (NPPs), and
27 branched Glycerol Dialkyl Glycerol Tetraethers (brGDGTs). Climate reconstructions are provided by
28 (1) water-level changes, (2) brGDGTs, and (3) pollen transfer functions (multi-method approach:
29 Modern Analogue Technique, Weighted Averaging Partial Least Squares regression, Random Forest,
30 and Boosted Regression Trees). Modern pollen assemblages are selected along an altitudinal transect in
31 Armenia. They show a dominance of Chenopodiaceae in semi-desert/steppe regions while meadows
32 steppes, subalpine, and alpine meadows are dominated by Poaceae. Past vegetation is characterized by
33 steppes dominated by Poaceae surrounded during the Mid-Holocene (8200-4200 a cal BP) by scarce
34 open woodlands. Humans have influenced the local vegetation, mainly through their agricultural
35 practices present since 5200 a cal BP with several intensification steps. Our reconstruction indicates a
36 climate shift from a cold and arid Early Holocene toward a warmer and more humid Mid-Late Holocene.
37 An aridification trend marks the last 5000 years causing a drop in water level, which allowed humans
38 to live and cultivate on Lake Sevan shores. Arid events are recorded at 6.2 ka, 5.2 ka, 4.2 ka and 2.8 ka
39 a cal BP, which are commonly related to multi-centennial-scale variations of Westerlies activity (North
40 Atlantic Oscillation). Through our temperature reconstruction, we can assign (1) the 5.2 and 2.8 ka
41 events as being cold and probably related to a strong Siberian High, and (2) the 4.2 ka event as being
42 warm associated with high Arabian subtropical pressures in the South Caucasus and the Near East. Our
43 study suggests a significant impact of these arid events on the Lake Sevan shore populations and they
44 are consistent with cultural phases in the South Caucasus, thus showing the impact of climatic variations
45 on cultural, land use and occupation mode development in this crossroad region between Europe, Africa
46 and Asia.

47

48 **Keywords: Vegetation dynamics; Human impact; Agriculture; Water level changes;**
49 **Paleoclimate; Arid climate events; Transfer functions; XRF**

50

51 **1. Introduction**

52

53 Understanding relationships between vegetation, climate, and anthropogenic impact over long
54 time periods is a major goal to stress out human development in arid and steppe environments of Eurasia.
55 Paleoecology is therefore a mandatory approach for the regions characterized by a strong human impact
56 such as the Mediterranean basin or the Near East. The Caucasus is among the areas that have been
57 influenced by humans the longest, since the Neolithic, which witness the rise of agriculture and animal
58 husbandry (ca. around 6000 BC) (Badalyan et al., 2004; Chataigner et al., 2014). The variety of
59 landscapes of the region also resulted from its complex orography, geology, and climate (Volodicheva,
60 2002). The Caucasus is recognized as a “hotspot” of biodiversity (Connor and Kvavadze, 2008; Solomon
61 et al., 2014) and was an important tree refugium during glacial periods (Connor and Kvavadze, 2008).
62 The current vegetation of the South Caucasus is mainly dominated by steppe or desert (Bohn et al.,
63 2000) and only 8% of Armenia’s area is covered by exploited or deteriorated forests (Sayadyan, 2011).
64 In contrast, in the 18th century, the forest covered 18% (Sayadyan, 2011), thus questioning the
65 afforestation rate during the Holocene, either before or after the increasing impact of human societies
66 on the environment and the respective impact of climate and humans on ecosystems.

67 Paleoecological studies of the South Caucasus have recorded forested phases during the
68 Holocene (e.g. Connor et al., 2018; Messager et al., 2013; 2017). In Armenia however, the vegetation
69 dynamic is more complex and suggests steppes dominance throughout the Holocene (Joannin et al.,
70 2014; Leroyer et al., 2016; Cromartie et al., 2020). At Vanevan, on Lake Sevan’s shores, Leroyer et al.
71 (2016) also revealed steppes expansion but, as their core only covers the Mid-Holocene (from 7800 to
72 5100 a cal BP), this vegetation dynamic cannot be extrapolated for the whole Holocene. Old studies
73 based on palynological records with low temporal resolution have suggested that broadleaf deciduous
74 forests existed around 6000 uncalibrated years on the slopes of Lake Sevan (Takhtajyan, 1941;
75 Tumanyan, 1971; Tumajanov and Tumanyan, 1973; Sayadyan et al., 1977; Sayadyan, 1978, 1983;
76 Moreno-Sanchez and Sayadyan, 2005); archaeological sites have revealed animal remains and statues
77 of animals (deer, bears, wolf and foxes) associated with deciduous forests (Lalayan, 1931;
78 Mnatsakanyan, 1952; Mezhlumyan, 1972) but their chronological frame is not precise enough. Further
79 investigations are required to better understand the history of forest and steppes in the South Caucasus
80 over the Holocene and to connect to nowadays issues with aridification and land use impact on soil
81 erosion.

82 Several studies suggest that humans have an impact on their environment since the Early
83 Holocene in the Near East, by fostering the maintenance of steppic vegetation with fires (Roberts et al.,
84 2002; Turner et al., 2008, 2010). However, in the South Caucasus the regional fire activities do not

85 increase at this period (Messager et al., 2017; Joannin et al., 2014) and climate seems to play an
86 important role in the delayed regional postglacial reforestation in the Near East and the South Caucasus
87 (Wright et al., 2003; Stevens et al., 2001; Djamali et al., 2010; Leroy et al., 2013; Joannin et al., 2014;
88 Messager et al., 2013, 2017; Leroyer et al., 2016). On the shores of Lake Sevan, humans have a long
89 history and agriculture is attested since 5500 a cal BP (Biscione et al., 2002; Parmegiani and Poscolieri,
90 2003; Hovsepyan, 2013, 2017). As human activities (e.g. agriculture and deforestation) modify the
91 vegetation structure, composition and diversity, a major challenge is to identify and to distinguish the
92 relationships between climate, human, and vegetation. This issue is particularly difficult to address in
93 places (1) where human neolithization already took place during the Early to Mid-Holocene, (2) where
94 the openness of the landscape is not primarily determined by human pressure, and (3) when the
95 technological advancement (e.g. water management systems, winery and fishery) preserves societies
96 from climate and environmental sudden changes (Lawrence et al., 2016; McGovern et al., 2017; Ollivier
97 et al., 2018; Roberts et al., 2019; Ritchie et al., 2021). Human influence is generally detected in
98 paleoecological records during the Early Bronze Age and becomes obvious during the last 3000 years
99 (e.g. Wick et al., 2003; Cromartie et al., 2020). Moreover, wild cereals and other Poaceae produce pollen
100 grains of *Cerealia*-type pollen, which may have biased the interpretation of anthropogenic pollen
101 occurrence (Van Zeist et al., 1975).

102 Climate role on vegetation during the Holocene is not very well understood in the Caucasus
103 region because of its complexity, mainly due to seasonality influence and climate mechanisms. Few
104 climate reconstructions based on pollen data are available (Connor and Kvavadze, 2008; Joannin et al.,
105 2014; Leroyer et al., 2016; Cromartie et al., 2020) and the climate of Armenia during the Holocene is
106 poorly documented (Joannin et al., 2014; Cromartie et al., 2020). The abrupt climate changes are
107 difficult to detect and until now the 4.2 ka event, a major climate event around the Mediterranean basin
108 (e.g. Bini et al., 2019), has not yet been detected in the South Caucasus. The climate mechanisms are
109 not totally understood although the role of the North Atlantic Oscillation and the Siberian High is
110 undeniable in this region (e.g. Joannin et al., 2014; Bini et al., 2019). Moreover, human impact can
111 substantially influence pollen-climate relationships even if the impact of this influence on climate
112 reconstructions is often difficult to quantify (Chevalier et al., 2020). Accordingly, pollen-based climate
113 reconstructions from records characterized by a strong human influence need to be evaluated carefully,
114 by comparison with independent climate reconstructions based on other proxies. Molecular biomarkers
115 are an emerging proxy that allow quantitative reconstruction of paleotemperature changes from lake or
116 peat sediments. Specifically, brGDGTs (branched Glycerol Dialkyl Glycerol Tetraethers) or glycerol
117 tetraethers are ubiquitous organic compounds synthesized by bacteria (Weijers et al., 2006; Dearing
118 Crampton-Flood et al., 2020). Although bacteria that produce brGDGTs are still unknown (Sinninghe
119 Damsté et al., 2018), the relationship between brGDGTs assemblages and temperature is well
120 established (Weijers et al., 2004; Schouten et al., 2007) and this new proxy allows annual
121 paleotemperature reconstructions (e.g. Dearing Crampton-Flood et al., 2020; Dugerdil et al., 2021;

122 [Stockhecke et al., 2021](#)). To date, there are very few studies based on comparative approaches including
123 pollen and molecular biomarkers to quantify climate variability over time and more particularly abrupt
124 climate events ([Watson et al., 2018](#); [Martin et al., 2020](#); [Dugerdil et al., 2021](#)).

125 This study aims to document vegetation and climate changes around Lake Sevan in Armenia for
126 the Holocene period. Based on a multi-proxy approach, we provide Holocene high-resolution sediment
127 geochemistry, pollen, Non-Pollen Palynomorphs (NPPs), and molecular biomarkers records from a
128 newly retrieved core in the Vanevan peat, located on the south-eastern shore of Lake Sevan. Our study
129 goals are to:

- 130 1) based on a collection of new modern samples from Armenia, understand the modern
131 relationships between pollen and vegetation and reinforce the reliability of pollen-based climate
132 reconstructions by the addition of new samples.
- 133 2) reconstruct the Holocene wetland dynamics and water level changes based on XRF data, aquatic
134 pollen taxa and NPPs.
- 135 3) reconstruct the Holocene vegetation dynamics and identify the existence of deciduous forests
136 or the persistence of steppes on the slopes of Lake Sevan.
- 137 4) identify human activity traces on vegetation records by distinguishing the “agricultural”
138 practices present on the south-eastern shore of Lake Sevan.
- 139 5) provide a reliable climate reconstruction for the South Caucasus based on a multi-proxy
140 approach including both brGDGTs and pollen (multi-method approach: MAT (Modern
141 Analogue Technique), WAPLS (Weighted Averaging Partial Least Squares regression), RF
142 (Random Forest) and BRT (Boosted Regression Forest)).
- 143 6) finally infer relationships between vegetation dynamics, climate changes, and human practices
144 at a local scale and discuss these results at a regional scale (South Caucasus and Near East).

145

146 2. Study site

147

148 2.1 Geological and geographical setting

149 The Caucasus Mountains are situated at the eastern edge of the Near East, between the Black
150 Sea and the Caspian Sea ([Fig. 1A](#)). They were formed by the Alpine and Himalayan orogeny with the
151 collision between the Arabian and Eurasian plates ([Volodicheva, 2002](#)). Located in the Lesser Caucasus
152 (i.e. a geological structure of the South Caucasus), Lake Sevan has a volcano-tectonic origin. Its
153 northeastern shore is characterized by an ophiolitic structure dating from the Middle Jurassic to Early
154 Cretaceous while the western and southern shores are defined by volcanic ridges dating from the
155 Quaternary ([Karakhanian et al., 2000](#); [Sosson, et al., 2010](#)). The lava flows from Porak volcano, located
156 in the southeast, spread towards Lake Sevan and Vanevan peat (40°12'8.83"N, 45°40'24.03"E, [Fig.](#)
157 [1AB](#)). Several lava flows may date from the Holocene ([Karakhanian et al., 2002](#)). The most important
158 fault system in Armenia, the Pambak-Sevan-Syunik fault system extends through the Porak volcano and

159 Lake Sevan. Seven strong earthquakes on this fault are attested during the Holocene (Karakhanian et
160 al., 2017).

161 The hydrological system of Lake Sevan has a negative water balance and a slow turnover (50
162 years) due to higher evaporation (800 mm/year) than precipitation (360 mm/year) (Leroyer et al., 2016).
163 During the Soviet period, its water was intensively used for irrigation and electricity (Jenderedjian,
164 2005). Consequently, its level dropped approximately 20 m and its volume decreased by more than 40%.
165 The lake passed from oligotrophic to eutrophic conditions, accompanied by changes in the flora and
166 fauna (Lind and Taslakyian, 2005). Among the 28 rivers draining the lake catchment (3650 km²), the
167 Masrik River is located in the South-East. Prior to the lake lowering and field management during the
168 Soviet time, it crossed a wetland area named Gilli (Jenderedjian, 2005). After the drying of the wetland,
169 the area was used for agricultural (mainly wheat and barley), pastoralism (sheep and cattle), and peat
170 exploitation for fuel.

171

172 2.2 Modern climate and vegetation

173 The climate of Armenia is dominated in winter by dry and cold air masses from Siberian High.
174 However, when these masses are weak, they are replaced by the Westerlies (associated with North
175 Atlantic Oscillation, NAO) with snowfall in winter and rainfall in spring. In summer, the climate is
176 warm and dry, and it is linked to Arabian subtropical high pressure in the west and Asian depression in
177 the east (Volodicheva, 2002; Joannin et al., 2014). In the north of Lake Sevan, the annual precipitation
178 is about 500 mm and the annual temperature is 3°C, with a minimum in January of -8°C and a maximum
179 in August of 15°C (Sevan City meteorological station). The coastal belt of the lake receives between
180 350 and 450 mm of annual precipitation while the mountain zones receive around 800 mm
181 (Baghdasaryan, 1958). Thunderstorms are common around the lake in late spring, particularly in May-
182 June.

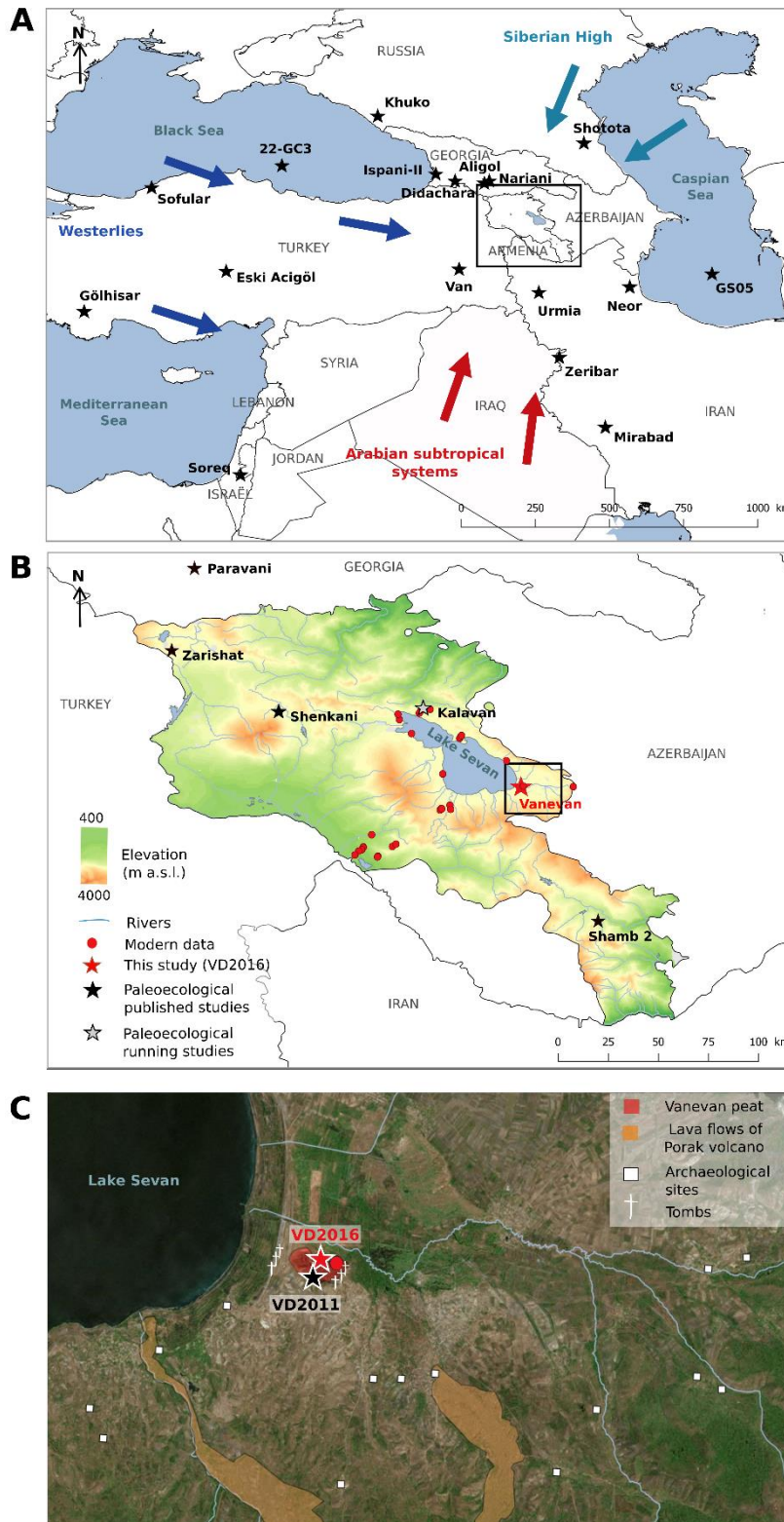
183 The Armenian vegetation is dominated by steppes and only 8% are represented by forests
184 (Sayadyan, 2011). Armenia has a rich biodiversity and a high level of endemism (Fayvush et al., 2013).
185 The mountainous relief favors very different ecological environments (Stanyukovich, 1973;
186 Volodicheva, 2002; Fayvush et al., 2017). The lower landscapes (480–1200 m a.s.l.) are covered by
187 semi-desert vegetation, dominated by *Artemisia fragrans*. The middle mountains (1200-1800 m a.s.l.)
188 are covered by steppes, mainly dominated by *Stipa* spp., or sparse arid woodland composed by *Pistacia*
189 *atlantica* subsp. *mutica*, *Amygdalus fenzliana* and *Rhamnus pallasii*. On the slopes (1700-2300 m a.s.l.)
190 arid woodland may develop with *Juniperus* spp. The upper mountains (1900-2300 m a.s.l.) are
191 characterized by meadow steppe, rich in Poaceae. The subalpine mountains (2300-2900 m a.s.l.) are
192 covered by subalpine meadows, generally dominated by *Festuca varia*, and some *Quercus macranthera*
193 woodlands. The alpine mountains (2700-3700 m a.s.l.) are covered by alpine meadows rich in Poaceae
194 (such as *Poa alpina*) and including *Taraxacum stevenii*, *Alchemilla* spp., *Potentilla* spp., *Primula* spp.,
195 *Geranium* spp., *Campanula* spp. and *Pedicularis* spp. The vegetation around Lake Sevan is mostly

196 composed of meadow steppes dominated by Poaceae. Only the borders of the lake have trees, principally
197 pines planted during the 1980s and some arid woodland on north-facing slopes. In the southeast slopes
198 of Lake Sevan, some *Juniperus* spp. are also present. The detailed description of potential vegetation of
199 [Bohn et al. \(2000\)](#) around Lake Sevan is presented in [Leroyer et al. \(2016\)](#). At a local scale, the
200 vegetation of Vanevan peat is dominated by Poaceae, Cyperaceae and Juncaceae.

201

202 2.3 Archeology and modern human activities

203 During the Holocene, the first signs of human occupation (hunter-gatherers) in Armenia have
204 been recorded during the Mesolithic in the lower Kasakh valley ([Arimura et al., 2012](#)). Agriculture is
205 established during the Late Neolithic (8000-7500 a cal BP) on the Ararat plain ([Badalyan et al., 2004](#);
206 [Hovsepian and Willcox, 2008](#); [Badalyan and Harutyunyan, 2014](#)) where cereals, vetch and lentil have
207 all been recorded along with the presence of sheep (*Ovis aries*), goat (*Capra hircus*), cattle (*Bos taurus*)
208 and scant evidence of pigs (*Sus domesticus*) ([Hovsepian and Willcox, 2008](#)). On the shore of Lake
209 Sevan, the first traces of agriculture date around 5500 a cal BP during the Early Bronze Age ([Hovsepian,](#)
210 [2013, 2017](#)). During the Early, Mid-, and Late Bronze Ages, Early Iron Age, and medieval period,
211 cereals are the primary subsistence crop in the southeast of Lake Sevan around Gilli wetland ([Biscione](#)
212 [et al., 2002](#); [Parmegiani and Poscolieri, 2003](#); [Hovsepian, 2013, 2017](#)). The long-term occupation of
213 this area is also attested by the presence of many tombs in Gilli wetland ([Fig. 1C](#)). Several empires
214 including the Persians (Achaemenids and Sassanids), Arabs, and Mongols and states including Urartu,
215 Ottoman Turkey, Imperial Russia, and the USSR have succeeded in Armenia ([Lindsay and Smith, 2006](#)).
216 The Urartian Empire was present during the Iron Age and centered around Lake Sevan ([Biscione et al.,](#)
217 [2002](#); [Parmegiani and Poscolieri, 2003](#)). During this period subsistence focused on the cultivation of
218 cereals, vines, fruit trees, and pastoralism. Today, the activities are centered around agriculture and
219 extensive pastoralism. To date, no pollen study has been able to compare pollen indicators of human
220 activities with archeological findings in the Sevan area. In the work done by [Leroyer et al. \(2016\)](#) at
221 Vanevan, the pollen sequence does not cover the last 5700 years BP.



222

223 Figure 1. A) East Mediterranean region with selected paleoenvironmental studies: Lake Khuko (Grachev et al.,
 224 2020), Shotota swamp (Ryabogina et al., 2018), 22-GC3 (Shumilovskikh et al., 2012), Ispani-II mire (Connor and
 225 Kvavadze, 2008), Lake Aligol (Connor and Kvavadze, 2008), Didachara Mire (Connor et al., 2018), Nariani
 226 wetland (Messenger et al., 2017), Sofular cave (Göktürk et al., 2011), Lake Van (Wick et al., 2003), Eski Acigöl
 227 (Roberts et al., 2001), Lake Neor (Sharifi et al., 2015), Lake Urmia (Djamali et al., 2008), Lake Gölhisar (Eastwood
 228 et al., 2007), GS05 (Leroy et al., 2013), Lake Zeribar (Stevens et al., 2001), Lake Mirabad (Stevens et al., 2006),
 229 Soreq cave (Bar-Matthews et al., 1997). B) Topography of Armenia with the location of Vanevan peat and modern
 230 samples (mosses, soils and botanical records). Black and gray stars represent published and ongoing

231 paleoecological studies, respectively: Lake Paravani (Messager et al., 2013; 2073 m), Zarishat fen (Joannin et al.,
232 2014; 2116 m), Lake Shenkani (Cromartie et al., 2020; 2193 m), Lake Kalavan (Joannin et al., in prep; 1603 m),
233 Shamb 2 (Ollivier et al., 2011). C) Southeastern shore of Lake Sevan with the location of Vanevan peat (VD2016
234 core, this study; VD2011 core, Leroyer et al., 2016) and archeological sites (Biscione et al., 2002; Parmegiani and
235 Poscolieri, 2003; Hovsepyan, 2013, 2017). Image modified from Google Earth (Image © 2020 CNES/Airbus, ©
236 2019 Google, © 2019 Basarsoft).

237

238 3. Material and methods

239

240 3.1 Field campaign

241 3.1.1 Core retrieval

242 The present study focuses on a new core VD2016 (40°12'8.83"N, 45°40'24.03"E, 1916 m a.s.l.)
243 retrieved from approximately 850 meters north of the previous Vanevan study (Fig. 1C). Two parallel
244 cores (cores A and B) were taken with a 1 m Russian corer with a 6.3 cm diameter chamber. The
245 mastercore (MC), was built from sections of both cores using the lithology and XRF data for correlation.
246 The complete continuous sequence measures 601 cm in total.

247

248 3.1.2 Modern samples

249 A total of 28 modern pollen samples along an altitudinal transect from the Ararat plain (808 m
250 a.s.l.) to the mountains of Lake Sevan (2699 m a.s.l.) were collected in May 2016, 2017, and 2019 (Fig.
251 1B and Supplementary Table S1). This transect records the vegetation in semi-desert steppes, meadow
252 steppes, subalpine, and alpine meadows in Armenia (Stanyukovitch, 1973; Volodicheva, 2002). Several
253 sampling sites are located around Lake Sevan and three altitudinal transects were performed in the
254 mountains around it (Mount Artanish, Mount Armaghan, and Mount Katarajayr). In each sampling site,
255 2-5 moss polsters or soil were collected within a radius of 5 m and then combined into one sample. The
256 vegetation within a radius of 10 m, representing the local vegetation, was recorded by visual estimation
257 of percentage cover for 19 sites (adaptation of the Braun-Blanquet method; Braun-Blanquet and
258 Schoenichen, 1964). For the other sites, the local vegetation was not quantitatively identified but
259 qualitatively estimated. The vegetation within a radius of 100 m is considered as the extra-local
260 vegetation and beyond this distance as the regional vegetation. The modern climate data were calculated
261 with the *New_LocClim 1.10* software (Grieser et al., 2006) and then corrected according to the site
262 elevation.

263

264 3.2 Age model, lithology, and geochemistry

265 3.2.1 Age model and lithology

266 The core chronology is based on 12 accelerator mass spectrometry (AMS) ¹⁴C dates (Table 1).
267 For seven samples, plant macrofossils (plant fibers, seeds) and charcoal were selected for dating. In
268 addition, bulk sediment was used for another set of 5 samples in which the quantity of macrofossils was
269 insufficient. Radiocarbon ages were calibrated in years cal BP using *Calib 8.2* software with the

270 IntCal20 calibration curve (Reimer et al., 2020) and the median calibrated ages with the 2 σ confidence
 271 intervals (95%) are reported in Table 1. The age-depth model was constructed using an interpolated
 272 linear curve with the R ‘Clam’ program with 95% confidence intervals (Blaauw, 2010). Three zones
 273 were defined upon visual differences in lithology.

274

275 Table 1. AMS-radiocarbon dates (Radiocarbon Laboratory, Poznań), calibrated median ages, with 2 σ range of
 276 calibration from Vanevan peat A and B cores. *: Age rejected

Sample ID	Depth MC (cm)	Lab code	Material	AMS 14C age (a BP)	Age (a cal BP) (2 σ)	Median age (a cal BP)
A0 15-17	15	Poz-111218	Plant fibers	875 \pm 30	692-903	768
A0 42-43	42	Poz-88797	Plant fibers	1860 \pm 50	1623-1916	1773
A1 16-17	59	Poz-110035	Plant fibers, seeds	2355 \pm 35	2326-2665	2377
A1 55-57	98	Poz-89222	Plant fibers	4380 \pm 40	4848-5255	4943
A2 16-17	126	Poz-110036	Plant fibers, seeds	4400 \pm 35	4859-5263	4966
A2 56-57	165	Poz-119280	Plant fibers, charcoals, seeds	4450 \pm 30	4885-5284	5112
A2 86-87*	195	Poz-122005	Bulk	6605 \pm 35	7429-7568	7495
A3 39-40	247	Poz-122006	Bulk	6690 \pm 35	7479-7651	7554
A3 81-82	289	Poz-119285	Bulk	6920 \pm 40	7670-7842	7746
A5 80-81	486	Poz-119281	Bulk	7980 \pm 50	8646-8998	8844
B5 29-31	534	Poz-89221	Plant fibers	8230 \pm 40	9026-9401	9197
A6 91-92*	597	Poz-121074	Bulk	6980 \pm 50	7690-7931	7810

277

278 3.2.2 Geochemistry

279 The running chemical composition of the sediment cores was performed using an Avaatech
 280 XRF (EDYTEM Laboratory) core scanner at a 0.5 cm interval (elements presented here: Si, K, Ti, Al,
 281 S, Fe, Ca, Mg, P). XRF measurements were carried out on split cores with a duration step of 10 s. A 10
 282 kV voltage and a 1000 μ A current was applied to detect elements. Because of the influences of variable
 283 water content and grain size on the sediment matrix, the XRF scanner provides an estimate of the
 284 geochemical composition, and the acquired counts are semi-quantitative. The selected elements are
 285 indicative of the sediment geochemistry itself depending on erosive and deposit conditions, and of
 286 sources in the catchment (Croudace and Rothwell, 2015). Principal component analysis (PCA) was
 287 performed on XRF data with *FactoMineR 2.4* package (Lê et al., 2008). Titanium (Ti) content is
 288 considered as a terrigenous indicator because it is weakly affected by weathering and redox conditions
 289 (Arnaud et al., 2012). Silicon (Si) content may be derived from diatoms, radiolaria, siliceous sponges,
 290 or from phytoliths contained in aquatic and terrestrial plants. The ratio Si/Ti allows to understand the
 291 respective role of organic production or terrigenous inputs (Brown et al., 2007).

292

293 3.3 Pollen, NPP analysis, and pollen-inferred climate reconstruction

294

295 3.3.1 Pollen, NPP extraction, and counting

296 A total of 28 modern and 94 fossil pollen samples from the Vanevan core (2 cm resolution
297 between 43-99 cm, 4 cm resolution between 99-170 cm, 10 cm resolution between 170-600 cm) were
298 extracted for analysis. For each sample, 1 cm³ of sediment was processed and 3 *Lycopodium* tablets
299 were added to calculate the absolute abundance of pollen grains. The core samples were treated with the
300 standard procedure (Fægri et al., 1989; Moore et al., 1991) including HCl, KOH, acetolysis and HF. The
301 pollen and NPP counts were carried out with a Leica DM1000 LED microscope at a standard
302 magnification of 400x. Pollen and NPP taxa were identified using photo atlases (Reille, 1992–1998;
303 Komárek and Jankovská, 2001; Van Geel, 2002; Beug, 2004) and a modern reference collection (ISEM,
304 University of Montpellier). A minimum of 300 or 200 pollen grains of terrestrial taxa (excluding aquatic
305 plants, mainly Cyperaceae) was counted by slide for the richest and the poorest samples, respectively,
306 to obtain a representative assessment of pollen types (Lytle and Wahl, 2005; Djamali and Cilleros,
307 2020). Grass pollen grains greater than 40 µm were classified as *Cerealia*-type (Beug, 2004). Aquatic
308 taxa, fern spores, and NPPs (algae and fungal spores) were counted alongside pollen. The pollen
309 diagrams were constructed with the R package *Rioja* (Juggins, 2020).

310

311 3.3.2 Pollen-inferred climate reconstruction

312 To reconstruct climate parameters from pollen data, currently available methods have their own
313 set of advantages and limitations and the selection of the most appropriate technique to be used on the
314 fossil pollen record can be complex. A multi-method approach is the best choice to increase the
315 reliability of the climate reconstruction (e.g. Brewer et al., 2008; Peyron et al., 2013; Salonen et al.,
316 2019). Four methods have been selected here among the most accurate (Chevalier et al., 2020): the
317 Modern Analog Technique (MAT; Guiot, 1990), Weighted Averaging Partial Least Squares regression
318 (WAPLS; Ter Braak and Van Dam, 1989; Ter Braak et al., 1993), and regression Trees: Random Forest
319 (RF; Breiman, 2001; Prasad et al., 2006) and Boosted Regression Trees (BRT; De'ath, 2007; Elith et al.,
320 2008). The MAT and the WAPLS are often selected to reconstruct past climate changes while RF and
321 BRT have been developed recently to reconstruct palaeoclimate changes (Salonen et al., 2016, 2019)
322 and have never been tested on Caucasus pollen records. Based on machine learning, these classification
323 trees are used to partition the data by separating the pollen assemblages based on the relative pollen
324 percentages. RF is based on a large number of regression trees, each tree being estimated from a
325 randomized ensemble of different subsets of the modern pollen dataset by bootstrapping. BRT is also
326 based on regression trees and differs from RF in the definition of the random modern datasets. In RF,
327 each sample gets the same probability of being selected, while in BRT the samples that were
328 insufficiently described in the previous tree get a higher probability of being selected. This approach is
329 called ‘boosting’ and increases the performance of the model over the elements that are least well
330 predicted.

331 The modern pollen dataset used here (382 samples) is part of the large Eurasian/Mediterranean
332 dataset compiled by [Peyron et al., \(2013, 2017\)](#) which include more than 3200 modern pollen samples
333 (moss polster, soils and top-cores). A recent study showed that (1) large databases are not reliable for
334 the reconstruction of steppic environment/climate and (2) local calibrations including data from steppe
335 and desert–steppe sites are necessary to better calibrate arid environments ([Dugerdil et al., 2021](#)).
336 Therefore, the large database has been cropped to optimize the selection of surface samples consistent
337 with our paleosequence environment: we used here a reduced dataset of 382 “cold steppe” samples,
338 including new samples from Mongolia ([Peyron et al., 2013, 2017; Dugerdil et al., 2021](#)), Georgia
339 ([Connor et al., 2004](#)) and Armenia (seventy-five new modern samples, [this study](#)). We applied here a
340 biome constraint ([Guiot et al., 1993](#)), which is essential to define steppe environments and to distinguish
341 between cold and warm steppes. Therefore, we have finally used for the calibration of each method the
342 samples attributed to the biomes “cold steppes” following the biomization procedure ([Prentice et al.,](#)
343 [1996; Peyron et al., 1998](#)). The location of these 382 cold steppe samples is given in the [Supplementary](#)
344 [Fig. S2](#). The surface calibration methods and datasets to reconstruct paleoclimate in arid environments
345 are discussed in [Dugerdil et al., \(2021\)](#). In order to estimate the performance of each method, the transfer
346 functions have been tested on the modern “cold steppe” dataset, 60% of the dataset has been used to
347 calibrate and 40% to test the transfer functions, thereby preventing a circular reasoning. Correlations
348 have been realized between the current climate parameters extracted from WorldClim 2 ([Fick and](#)
349 [Hijmans, 2017](#)) and the estimated climate parameters reconstructed by each method ([Supplementary](#)
350 [Fig. S3](#)). Then, the performance of each method and each calibration training was statistically tested
351 with a bootstrap technique (for more details, see [Dugerdil et al., 2021](#)). The transfer functions have been
352 applied 500 times on the modern “cold steppe” dataset, thereby obtaining the Root Mean Square Error
353 (RMSE) and the R^2 and determining if modern samples are suitable for quantitative climate
354 reconstructions ([Supplementary Table S4](#)). Thereafter, the function transfers have been applied on the
355 Vanevan core samples with the modern “cold steppe” dataset. Four climate parameters were
356 reconstructed, mean annual air temperature (MAAT), mean annual precipitation (MAP), mean
357 temperature of the warmest month (MTWA), and summer precipitation (Psummer) including July,
358 August, and September. For each climate parameter, the methods fitting with the higher R^2 and the lower
359 RMSE were selected. The WAPLS and the MAT methods were applied with the R package Rioja
360 ([Juggins, 2020](#)), the RF with the R package randomForest ([Liaw and Wiener, 2002](#)) and the BRT with
361 the R package dismo ([Hijmans et al., 2020](#)). Cyperaceae and ferns of Vanevan record have been
362 excluded because they indicate local dynamics in Armenia ([Joannin et al., 2014; Cromartie et al., 2020](#)).
363
364 3.4 GDGT analysis and annual temperature reconstruction
365

366 3.4.1 BrGDGT analyses

367 A total of 46 core samples (4-20 cm resolution) were used for GDGT analysis. After freeze-
 368 drying and grinding, a subsample (0.8 g for soil, 1 g for clay and 0.6 g for peat sediments) was extracted
 369 using a Microwave oven (MARS 6; CEM) with a mix of dichloromethane and methanol (3:1). The total
 370 lipid extract was split on a silica SPE cartridge, using hexane: DCM (1:1) and DCM:MeOH (1:1).
 371 GDGTs were analyzed using a High-Performance Liquid Chromatography Mass Spectrometry (HPLC-
 372 APCI-MS, Agilent 1200) with detection via selective ion monitoring (SIM) of m/z 1050, 1048, 1046,
 373 1036, 1034, 1032, 1022, 1020, and 1018 for brGDGTs (Hopmans et al., 2016; Davtian et al., 2018).
 374 GDGT concentrations were calculated based on the internal standard (C₄₆ GDGT, Huguet et al., 2006).
 375 The linearity and analytic reproducibility were assessed based on an internal standard sediment.

376

377 3.4.2 brGDGT-based proxy calculation and global calibration datasets

378 The formulae for the brGDGT indexes are presented in Table 2. The proportions of tetra- (I),
 379 penta- (II) and hexa- (III) methylated brGDGTs were calculated with the fractional abundances of
 380 brGDGTs including the 5-methyl (X), the 6-methyl (X') and the 7-methyl brGDGT (X₇) (Ding et al.,
 381 2016). The ΣIIIa/ΣIIa ratio proposed by Xiao et al. (2016) was calculated according to the equation
 382 modified by Martin et al. (2019) including the 5-, 6- and 7-methyl brGDGTs. The CBT and MBT
 383 indexes were developed by Weijers et al. (2007) and the MBT'_{5me}, only based on the 5-methyl brGDGTs,
 384 by De Jonge et al. (2014). The mean annual temperature was calculated with the global soil calibration
 385 developed by Naafs et al. (2017a) and the global lacustrine calibration developed by Sun et al. (2011).
 386 The calibrations are applied according to the sediment types in paleorecords (e.g. Martin et al., 2019)
 387 and can be homogenized using a ΔMAAT based on the mean value of each sediment type. The analytic
 388 reproducibility corresponds to 0.005 for CBT, 0.006 for MBT, 0.008 for MBT'_{5me}, 0.3 for MAAT_{soil5me}
 389 and 0.2 for MAAT_{lake}.

390

391 Table 2. Synthesis of the formulae for the main brGDGT indices

Indice	Formula	Reference
%tetra	$\frac{Ia + Ib + Ic}{\Sigma brGDGTs}$	Ding et al., 2016
%penta	$\frac{IIa + IIa' + IIa_7 + IIb + IIb' + IIb_7 + IIc + IIc' + IIc_7}{\Sigma brGDGTs}$	Ding et al., 2016
%hexa	$\frac{IIIa + IIIa' + IIIa_7 + IIIb + IIIb' + IIIb_7 + IIIc + IIIc' + IIIc_7}{\Sigma brGDGTs}$	Ding et al., 2016
Σ IIIa/Σ IIa	$\frac{IIIa + IIIa' + IIIa_7}{IIa + IIa' + IIa_7}$	Martin et al., 2019
CBT	$-\log \frac{Ib + IIb}{Ia + IIa}$	Weijers et al., 2007

<i>MBT</i>	$\frac{Ia + Ib + Ic}{\Sigma brGDGTs}$	Weijers et al., 2007
MBT'_{5me}	$\frac{Ia + Ib + Ic}{Ia + Ib + Ic + IIa + IIb + IIc + IIIa}$	De Jonge et al., 2014
$MAAT_{soil5me} (^{\circ}C)$	$39.09 \times MBT'_{5me} - 14.50$	Naafs et al., 2017a
	$(n = 177, R^2 = 0.76, RMSE = 4.1^{\circ}C)$	
$MAAT_{lake} (^{\circ}C)$	$3.949 - 5.593 \times CBT + 38.213$	Sun et al., 2011
	$\times MBT (n = 100, R^2 = 0.73, RMSE = 4.27^{\circ}C)$	

392

393 4. Results

394

395 4.1 Sediment analysis

396 4.1.1 Age-depth model

397 The Clam age-depth model (Fig. 2B) is based on ten calibrated ¹⁴C dates (Table 1). Two ¹⁴C
398 dates (A2 86-87 at depth 195 cm and A6 91-92 at depth 597) were excluded from the age-depth model.
399 The age-depth model constructed with the R ‘Bacon’ program (Blaauw and Christen, 2011; not shown)
400 has rejected the two dates and the same information was used with the ‘Clam’ program. The VC2016
401 record extends from 9700 a cal BP to 800 a cal BP. The age-depth model has an error of ~50–260 years
402 between 15-550 cm and ~210–470 years for the base of the core (550-600 cm) (Fig. 2B and
403 Supplementary Table S5). The age–depth curve shows a sedimentation rate (16.7 cm.100 yr⁻¹) that
404 decreases at 7560 a cal BP (3.3 cm.100 yr⁻¹) except between 5100 and 4950 a cal BP (43.5 cm.100 yr⁻¹).
405 From the base of the core to 43 cm depth, an average temporal resolution of 77 years was achieved for
406 pollen records and 202 years for brGDGTs.

407

408 4.1.2 Lithology changes

409 The core lithology is divided into 3 units (Fig. 2B). Unit 1 (600-558 cm) is characterized by a
410 light gray clay and sand sediment. Unit 2 (558-170 cm) is composed of a gray clay sediment. Unit 3
411 (170-15 cm) is divided into 4 subzones. Unit 3a (170-144 cm) is composed of a brown peat silt sediment.
412 Unit 3b (144-125 cm) is characterized by alternating yellow and dark peat silt sediments. Unit 3c (125-
413 113 cm) is marked by a gray clay sediment. Unit 3d (113-15 cm) is composed of a peat silt sediment
414 with brown, dark and orange colors. The clay sediments are interpreted as open underwater
415 environments while the peat sediments indicate the accumulation of plant remains growing in place in
416 restricted underwater or near-surface environments.

417

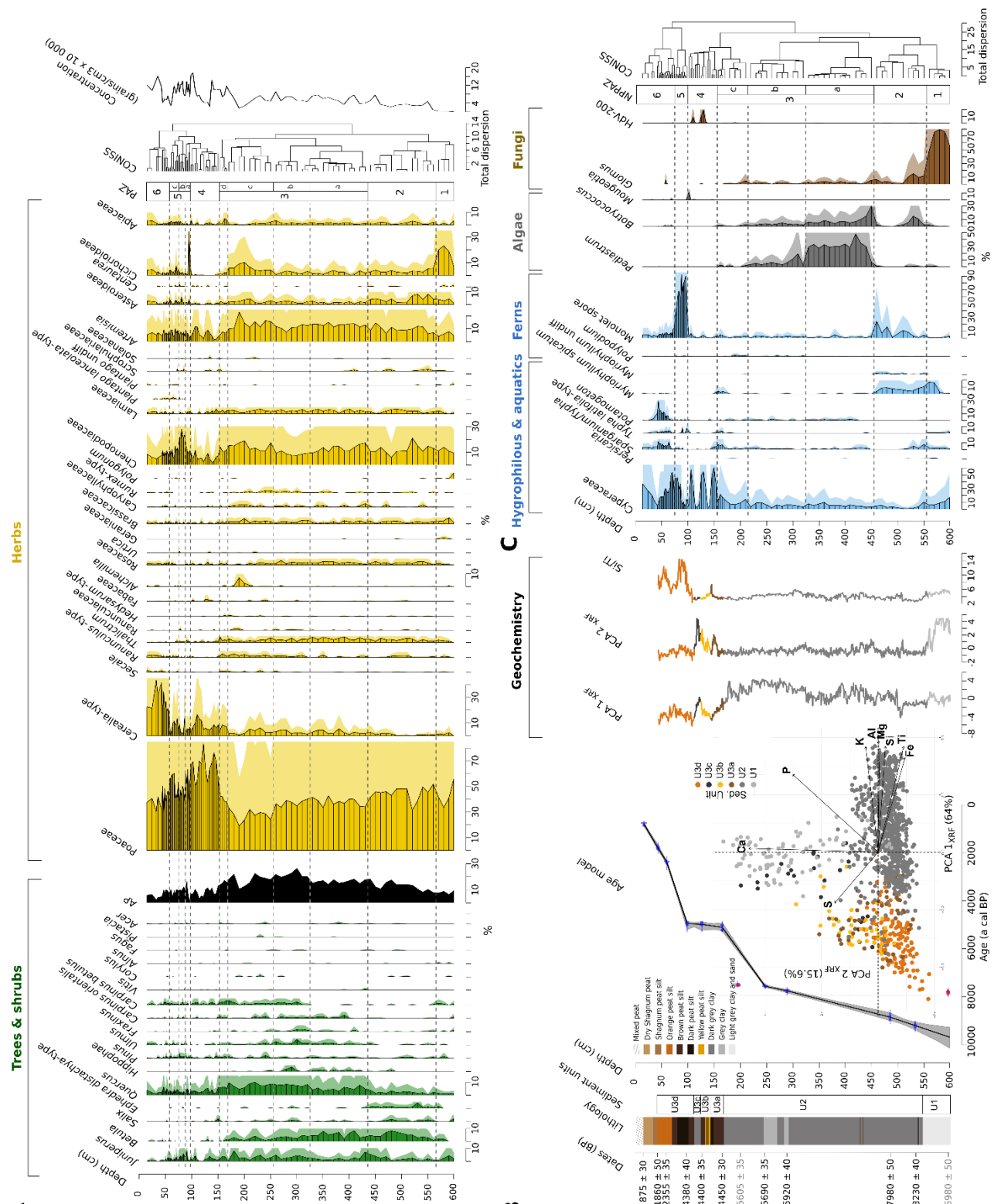
418 4.1.3 Geochemical composition

419 A principal component analysis (PCA) was conducted on XRF elements (Fig. 2B) and the
420 sample map was colored according to the lithology units. The first two dimensions (PCA 1_{XRF} and PCA

421 2_{XRF}) explain 80% of the variability (64% and 16% respectively). Two major geochemical end-members
422 are identified: the first one represents terrigenous inputs (K, Al, Mg, Si, Ti, Fe) and are positively
423 correlated with PCA 1_{XRF} . Terrigenous elements are associated with clay sediments (Units 1 and 2)
424 deposited in open underwater environments, and are opposed to organic sediments (Unit 3) mainly
425 composed of peat sediments formed in restricted underwater or near-surface environments.

426 The second end-member represents carbonate components (Ca), sulfur (S) and phosphorus (P)
427 and are positively correlated with PCA 2_{XRF} . Calcium is abundant at the base of the core (Unit 1) and in
428 the first organic levels (Units 3a, 3b, 3c). Sulfur and phosphorus are only abundant in the first organic
429 levels (Units 3a, 3b, 3c). The upper part of the core (Unit 3d) is distinguished by a biogenic silica
430 production, visible in the ratio Si/Ti ([Brown et al., 2007](#)).

431
432



433
434
435
436
437
438
439
440
441
442

A Figure 2. Pollen and sedimentology of Vanevan peat against core depth. A) Selected terrestrial pollen taxa. Tree, shrub, and herb pollen taxa are expressed in percentages of total terrestrial pollen. AP: Arboreal Pollen. PAZ: Pollen Assemblage Zones. B) Sediment lithology, age-depth model and geochemical data. The age–depth model is based on calibrated radiocarbon ages (with 2 σ errors) (AMS, see Table 1). Principal component analysis (PCA) was done on XRF data according to the lithological units. The first two dimensions (PCA 1_{XRF} and PCA 2_{XRF}) of PCA are arranged by depth. C) Selected hygrophilous and aquatic pollen taxa and NPPs. Hygrophilous and aquatic pollen taxa are expressed in percentages of total pollen. Fern spores, algae and fungi are expressed in percentages of total terrestrial pollen and NPPs. NPPAZ: Non-Pollen Palynomorph Assemblage Zones.

443 4.2 Pollen analysis and pollen-based climate reconstruction

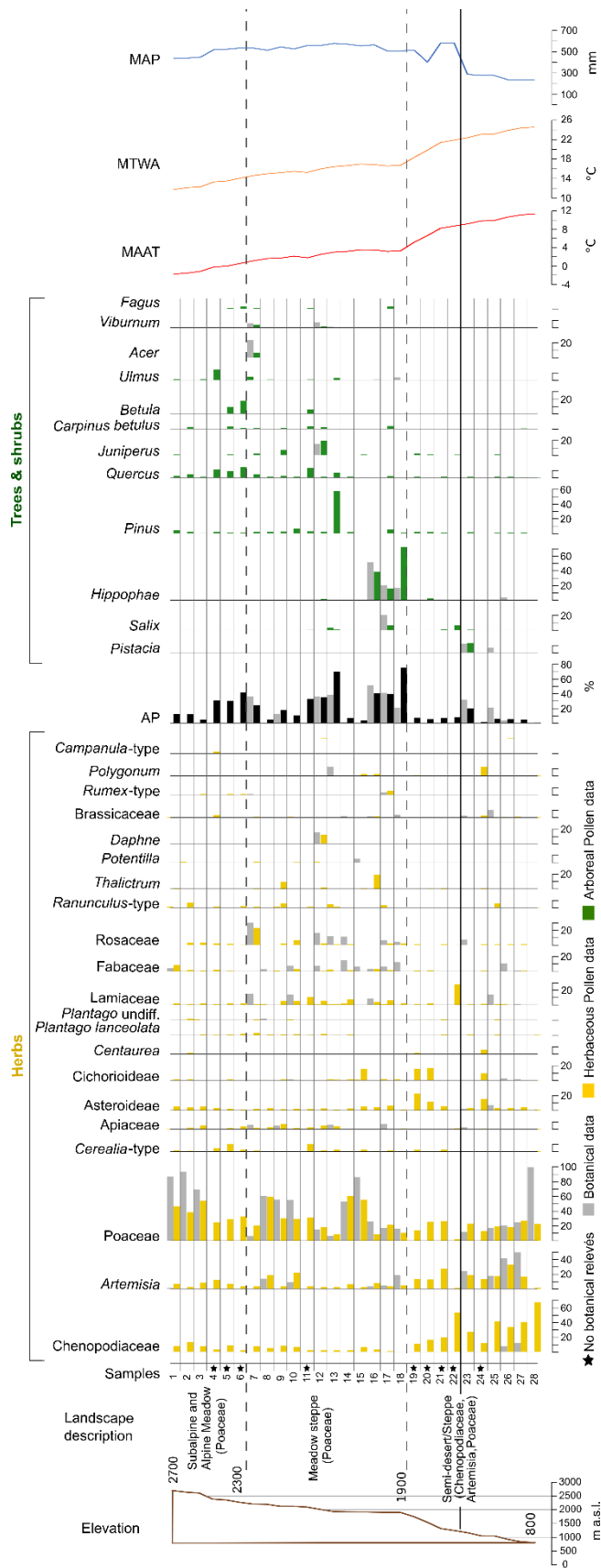
444 4.2.1 Surface samples, vegetation, and climate

445 The modern pollen assemblages (Fig. 3) are dominated by herbaceous pollen taxa, including
446 Poaceae, Chenopodiaceae and *Artemisia*. By comparing the pollen data with the vegetation, it appears
447 that Poaceae is well associated with the local vegetation, while Chenopodiaceae, *Artemisia*, Asteroideae
448 and Cichorioideae are over-represented. Arboreal taxa such as *Hippophae* is well associated with the
449 local vegetation while *Quercus* and *Pinus* are over-represented.

450 The altitudinal vegetation gradient is well recorded in the modern pollen rain. The lower and
451 middle elevations (800-1900 m) are dominated by pollen of Chenopodiaceae (33%), Poaceae (19%),
452 *Artemisia* (16%), and indicate a semi-desert or steppe vegetation. A few pollen grains of *Pistacia* and
453 *Salix* are also recorded. These levels are distinguished by high percentages of Chenopodiaceae and
454 *Artemisia* and by low percentages of arboreal pollen taxa (7%). The upper elevations (1900-2300 m)
455 record high percentages of Poaceae (30%), characteristic of meadow steppes, except when trees or
456 shrubs are present in the local (*Hippophae*, *Salix*, *Juniperus*, *Acer*, *Viburnum*) or extra-local vegetation
457 (*Pinus*). *Pinus* was present in the extralocal vegetation of sites number 13 and 18. However, only site
458 number 13 records *Pinus* pollen. *Quercus*, *Carpinus betulus* and *Fagus* are recorded with low
459 percentages (<4%). *Artemisia* and Chenopodiaceae represent only 7% and 4%, respectively. The
460 subalpine and alpine environments are dominated by Poaceae pollen (38%) and few arboreal pollen
461 taxa, such as *Quercus* (7%), *Betula* (6%), *Ulmus* (3%), are recorded. At these elevations, *Artemisia* and
462 Chenopodiaceae represent 7% each.

463 Although the modern sites are distant from agricultural areas, pollen of *Cerealia*-type are
464 recorded, reaching up to 11%. Pollen indicator of pastoralism activities, such as *Plantago lanceolata*-
465 type or *Rumex*-type, represent less than 1% on average and a maximum of 6%. Otherwise, the pollen
466 rain shows correspondence to climatic gradients (Fig. 3). The highest percentages of Chenopodiaceae
467 and *Artemisia* pollen correspond to high temperature (>5°C) and low precipitation (MAP<500 mm).
468 The limit between cool and warm steppe biomes correspond to a change in Chenopodiaceae percentages
469 and in MAP. In contrast, percentages of Poaceae pollen increase when MAAT decreases.

470



471

472 Figure 3. Selected modern pollen assemblages, botanical relevés and climate values along an altitudinal transect
 473 in Armenia. MAAT=mean annual air temperature, MTWA= mean temperature of the warmest month, MAP=
 474 mean annual precipitation.

475

476 4.2.2 Pollen sequence: terrestrial, hygrophilous vegetation, and Non-Pollen Palynomorphs

477 A total of 76 terrestrial pollen taxa were identified in the Vanevan core VC2016. Herbaceous
 478 pollen taxa dominate the pollen assemblages along the sequence ranging from 73 to 99%. The pollen
 479 diagram is divided into 6 pollen assemblage zones (PAZ) according to the CONISS method (Grimm,
 480 1987) and visual differences for subzones transitions (PAZ 3a/3b) (Fig. 2A, Table 3). The diagram of
 481 NPPs and hygrophilous vegetation is divided into 6 Non-Pollen Palynomorph assemblage zones
 482 (NPPAZ) according to the CONISS method (Grimm, 1987) (Fig. 2C, Table 3). The limits of NPPAZ
 483 generally follow changes in lithology.

484

485 Table 3. Inventory of pollen assemblage zones (PAZ), depth, estimated ages, total of arboreal pollen (AP_t),
 486 common and rare pollen types (CPT, RPT) for arboreal and herbaceous taxa, Non-Pollen Palynomorph assemblage
 487 zones (NPPAZ) and main hygrophilous pollen taxa and Non-Pollen Palynomorphs (NPPs). Common pollen types
 488 (CPT) include pollen taxa with percentages > 5% and rare pollen taxa (RPT) percentages < 5%

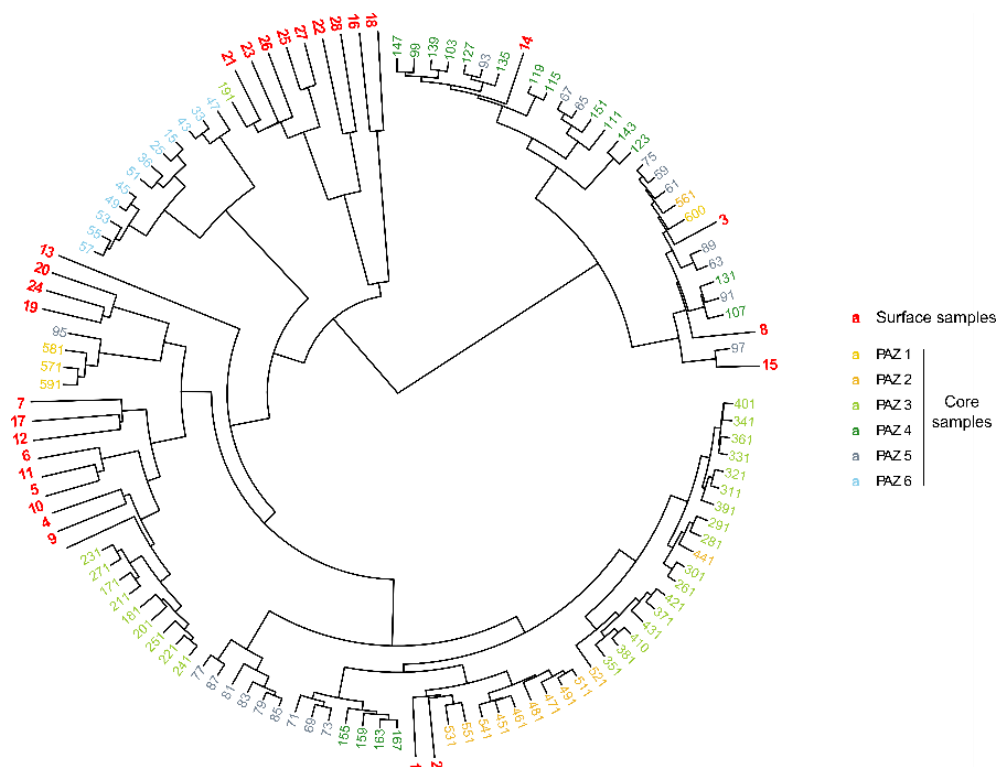
PAZ	Depth (cm)	Total of Age (a cal BP)	Arboreal Pollen %	AP _t	Arboreal and herbaceous pollen Common pollen types (CPT) Rare pollen types (RPT)	NPPAZ	Hygrophilous pollen NPPs
6	58-15 2350-790			AP _t 7	CPT: Poaceae, <i>Cerealia</i> -type, Chenopodiaceae, <i>Artemisia</i> RPT: Cichorioideae, Asteroideae, Apiaceae Rosaceae, <i>Ranunculus</i> -type, <i>Quercus</i> , <i>Carpinus betulus</i> , <i>Juniperus</i>	6	Cyperaceae, <i>Potamogeton</i> , <i>Sparganium/Typha</i> , Cyperaceae
5c	76-58 3500-2350				CPT: Poaceae, Chenopodiaceae, <i>Cerealia</i> -type, <i>Artemisia</i> RPT: Cichorioideae, Asteroideae, Apiaceae; <i>Quercus</i> , <i>Juniperus</i> , <i>Carpinus betulus</i> , <i>Pinus</i>		
5b	88-76 4300-3500				CPT: Poaceae, Chenopodiaceae, <i>Artemisia</i> , <i>Cerealia</i> - type RPT: Asteroideae, Cichorioideae, Apiaceae, <i>Juniperus</i> , <i>Quercus</i> , <i>Pinus</i> , <i>Carpinus betulus</i>		
5a	98-88 4950-4300				CPT: Poaceae, Cichorioideae, Chenopodiaceae, <i>Artemisia</i> RPT: <i>Cerealia</i> -type, Asteroideae, Lamiaceae, <i>Thalictrum</i> ; <i>Quercus</i> , <i>Juniperus</i> , <i>Pinus</i> , <i>Carpinus</i> <i>betulus</i>		
5	98-58 4950-2350			AP _t 9		5	Monolete spores, <i>Typha</i> <i>latifolia</i> -type, Cyperaceae
4	153-98 5100-4950			AP _t 8	CPT: Poaceae, <i>Cerealia</i> -type, Chenopodiaceae, <i>Artemisia</i> RPT: Lamiaceae; <i>Quercus</i> , <i>Juniperus</i> , <i>Carpinus betulus</i>	4	Alternating episodes with or without Cyperaceae accompanied by <i>Sparganium/Typha</i> , <i>Myriophyllum spicatum</i> , fungi HdV-200, <i>Mougeotia</i>
3d	256-153 5200-5100				CPT: Poaceae, Chenopodiaceae, <i>Cerealia</i> -type, <i>Artemisia</i> RPT: Cichorioideae, Asteroideae, <i>Quercus</i> , <i>Carpinus</i> <i>betulus</i> , <i>Juniperus</i> , <i>Carpinus orientalis</i>		
3c	256-169 7600-5200				CPT: Poaceae Chenopodiaceae, <i>Artemisia</i> , <i>Cichorioideae</i> , <i>Quercus</i> , <i>Alchemilla</i> RPT: <i>Cerealia</i> -type, Asteroideae, <i>Thalictrum</i> , Brassicaceae, Lamiaceae, Rosaceae, <i>Ranunculus</i> -type, <i>Caryophyllaceae</i> , <i>Rumex</i> -type; <i>Betula</i> , <i>Juniperus</i> , <i>Carpinus betulus</i>		
3b	326-256 8000-7600				CPT: Poaceae, <i>Artemisia</i> , Chenopodiaceae, <i>Quercus</i> RPT: <i>Cerealia</i> -type, <i>Thalictrum</i> , Cichorioideae, Brassicaceae, Apiaceae, Lamiaceae, Rosaceae, Asteroideae, <i>Caryophyllaceae</i> , <i>Ranunculus</i> -type,		

3a	436-326 8600-8000		<i>Rumex</i> -type; <i>Betula</i> , <i>Juniperus</i> , <i>Ulmus</i> , <i>Fraxinus</i> , <i>Hippophae</i> , <i>Carpinus betulus</i> , <i>Carpinus orientalis</i> CPT: Poaceae, <i>Artemisia</i> , Chenopodiaceae RPT: <i>Cerealia</i> -type, <i>Thalictrum</i> , Cichorioideae, Brassicaceae, Apiaceae, Lamiaceae, Rosaceae, Asteroideae, <i>Caryophyllaceae</i> ; <i>Betula</i> , <i>Quercus</i> , <i>Ulmus</i> , <i>Fraxinus</i> , <i>Carpinus orientalis</i> , <i>Hippophae</i> , <i>Pinus</i>		
3	436-153 8600-5100	AP ₁ 17	Maximum of arboreal pollen percentages and diversity. Progressive decrease in Poaceae and trees until 5900 a cal BP.	3	Planktonic algae (<i>Pediastrum</i> , <i>Botryococcus</i>), Cyperaceae
2	566-436 9400-8600	AP ₁ 13	CPT: Poaceae Chenopodiaceae, <i>Artemisia</i> RPT: <i>Cichorioideae</i> , Asteroideae, <i>Thalictrum</i> , Brassicaceae, Apiaceae, Lamiaceae, Rosaceae; <i>Betula</i> , <i>Quercus</i> , <i>Juniperus</i> , <i>Ephedra distachya</i> -type, <i>Salix</i> , <i>Hippophae</i>	2	<i>Myriophyllum spicatum</i> , Monolete spores. At 9200 a cal BP, peak of <i>Botryococcus Glomus</i> , <i>Sparganium/Typha</i>
1	600-566 9700-9400	AP ₁ 8	CPT: Poaceae, Cichorioideae, Chenopodiaceae <i>Artemisia</i> RPT: Asteroideae, <i>Polygonum</i> , <i>Thalictrum</i> , Brassicaceae, Apiaceae; <i>Juniperus</i> , <i>Quercus</i> , <i>Betula</i> , <i>Carpinus betulus</i>	1	<i>Glomus</i> , Cyperaceae, <i>Myriophyllum spicatum</i>

489

490 4.2.3 Comparison between surface and core samples

491 A classification by hierarchical cluster analysis was conducted on Armenian surface samples
492 and core VD2016 samples (Fig. 4). The surface samples are well distributed within the core samples:
493 the surface samples dominated by Poaceae (n. 1-3, 8, 14, 15), are close to core samples which record a
494 large percentage of Poaceae (PAZ 1, 2, 4, 5) whereas those recording regional arboreal taxa (n. 4-7, 9-
495 12, 17) approach the core samples of PAZ 3 representing the most forested phase. At lower and middle
496 elevations, the surface samples with a large percentage of Cichorioideae (19, 20, 24) are close to the
497 PAZ 1 core samples recording a large proportion of this taxon whereas those dominated by
498 Chenopodiaceae, *Artemisia* and Poaceae (n. 13, 16, 18, 21-23, 25-28; i.e. mainly lowland samples) seem
499 more different of the core samples.



500

501 Figure 4. Classification by hierarchical cluster analysis on surface samples of Armenia (presented in Fig. 3) and
 502 core samples of VD2016 expressed in depth (presented in Fig. 2). The color of core samples corresponds to the
 503 six pollen assemblage zones (PAZ) defined with the CONISS method. The distance matrix was calculated using
 504 Euclidean distance and Ward's algorithm was applied for clustering.

505

506 4.2.4 Pollen-inferred climate reconstruction

507 Climate changes at Vanevan are estimated using four methods: MAT, WAPLS, RF, and BRT
 508 (Fig. 5). The climate patterns reconstructed are consistent and do not seem method-dependent. The MAT
 509 and the BRT appear as the most sensitive methods and the results show important sample-to-sample
 510 variability; the WAPLS method shows large variations along the Holocene and the inferred values are
 511 significantly higher than the modern values; the RF is the less sensitive method (Fig. 5). Correlations
 512 between current and estimated climate parameters show the maximum R^2 for the RF and BRT methods
 513 (Supplementary Fig. S3). However, the RF method does not reconstruct correctly the high or the low
 514 current climate values. Statistical results of the model performances are presented in Supplementary
 515 Table S4; the BRT method presents the maximum R^2 and the minimum RMSE for all climatic
 516 parameters.

517 Based on the multi-method approach, the Vanevan climate reconstruction (Fig. 5) shows
 518 remarkably consistent trends during the Holocene, except for the most recent periods. Five climatic
 519 phases have been defined and are described below.

520 **Phase 1 (9700 – 8200 a cal BP)** is first characterized by warm and wet conditions. For temperature and
 521 annual precipitation, all methods show the same trend although the reconstructed values can be different.
 522 Then, the reconstructions show a drop in temperature and precipitation with a minimum between 8600
 523 and 8200 a cal BP.

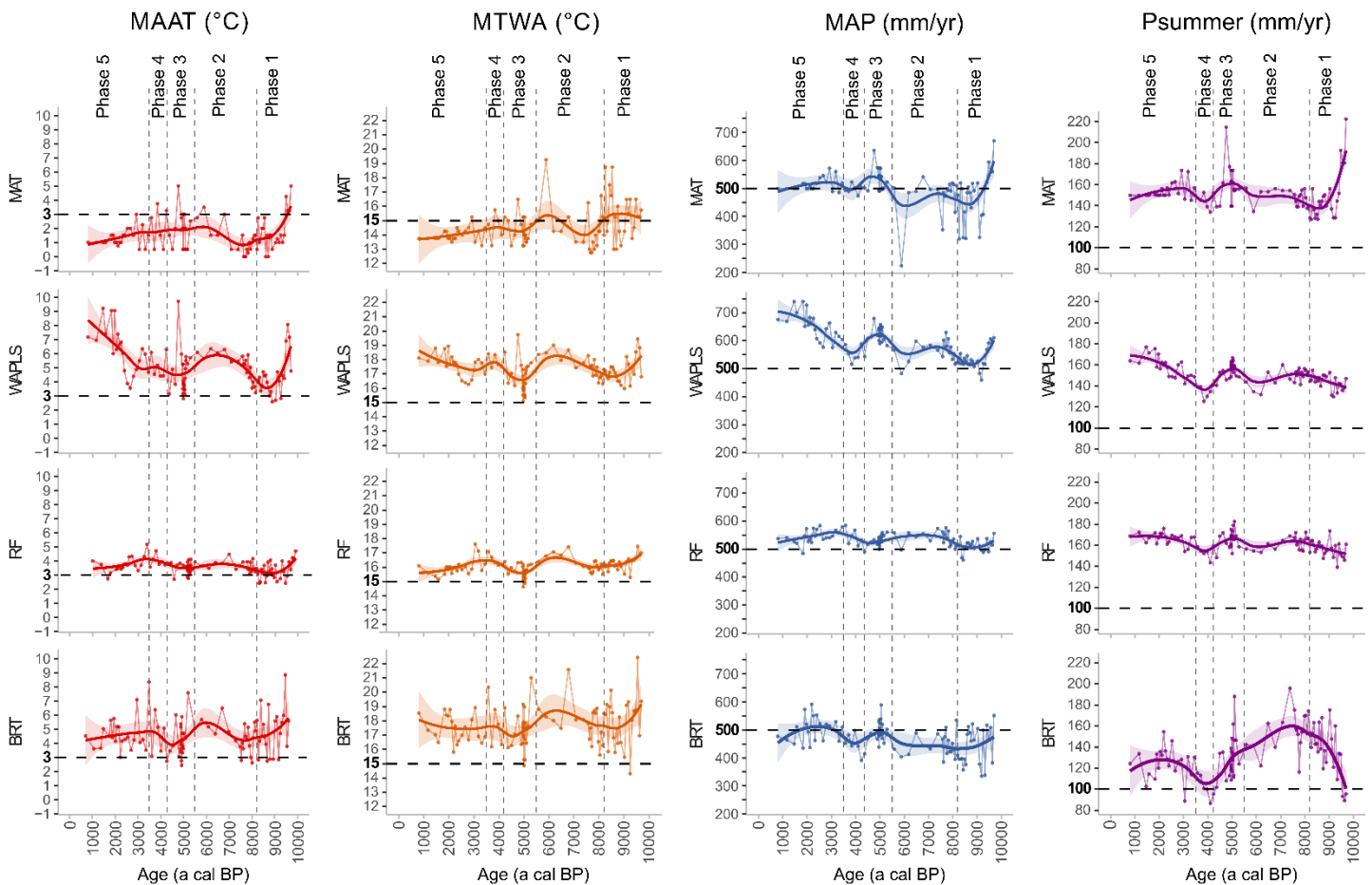
524 **Phase 2 (8200 – 5500 a cal BP)** is marked by warmer conditions than previously. Temperatures increase
 525 and reach an optimum around 6000 a cal BP (2.5-6°C for MAAT and 17-19°C for MTWA). Considering
 526 precipitation, it first increases and then declines around 6000 a cal BP (350-530 mm/year for MAP and
 527 130-150 mm/year for Psummer).

528 **Phase 3 (5500 – 4300 a cal BP)** shows cooler and wetter conditions than previously. Precipitation
 529 increases for all methods reaching 460-550 mm/year for MAP and 130-170 mm/year for Psummer.

530 **Phase 4 (4300 - 3500 a cal BP)** is mainly characterized by a drop in annual precipitation and particularly
 531 in Psummer with a minimum at 4100 a cal BP (90-150 mm/year).

532 **Phase 5 (3500 - 800 a cal BP)** is marked by divergent trends according to the methods. The MAT, RF,
 533 and BRT methods record a decrease of temperature and precipitation. In contrast, the WAPLS method
 534 shows the warmest and the wettest conditions of the Holocene. At 2800 a cal BP, a decrease in
 535 temperature and precipitation are recorded by WAPLS and RF methods.

536



557
 558 Figure 5. Pollen-inferred climate changes estimated using four methods: MAT (Modern Analogue Technique),
 559 WAPLS (Weighted Averaging Partial Least Squares regression), RF (Random Forest) and BRT (Boosted
 560 Regression Trees). Dotted lines correspond to modern values (Sevan city meteorological station). MAAT: mean
 561 annual air temperature. MTWA: mean temperature of the warmest month. MAP: mean annual precipitation.
 562 Psummer: summer precipitation.

563

564

565 4.3 GDGT analysis

566

567 *4.3.1 Distribution of brGDGTs*

568 The concentration of brGDGTs (Fig. 6D) ranges from 0.04 to 11.6 µg/g dry sediment. The
569 fractional abundances of brGDGTs (Fig. 6A) show a dominance of pentamethylated brGDGTs (II, 49%)
570 in particular brGDGT IIa (20%), brGDGT IIa' (11%), and brGDGT IIb (9%). The relative abundance
571 of tetramethylated brGDGTs (III, 26%) is explained by the abundance of brGDGT Ia (14%) and
572 brGDGT Ib (10%). Finally, the relative abundance of hexamethylated brGDGTs (III, 25%) can be
573 explained by the presence of brGDGT IIIa (11%) and brGDGT IIIa' (9%). The relative abundances of
574 tetra, penta- and hexamethylated brGDGTs (Fig. 6B) differ according to the type of sediment in the
575 core. The peat sediment samples are close to global soils and peats, whereas the clay sediment samples
576 are closer to global lakes.

577 A principal component analysis (PCA) and a hierarchical clustering on principal components
578 (HCPC) were conducted on the fractional abundances of brGDGTs with *FactoMineR 2.4* package (Lê
579 et al., 2008) (Fig. 6C). The first two dimensions (PCA 1 and PCA 2) explain 86% of the variability (54%
580 and 32% respectively). Three groups are identified by HCPC: the first one is associated with
581 tetramethylated brGDGTs and the samples are negatively correlated with PCA 1. This group is
582 composed of peat sediment samples. The second one is associated with brGDGTs ΣIIa and the samples
583 are negatively correlated with PCA 1 and PCA 2. The group is composed of samples mainly located in
584 the lithological transition zone of the core between peat and clay sediments. The third one is associated
585 with hexamethylated brGDGTs, brGDGTs ΣIIb and brGDGTs ΣIIc and the samples are positively
586 correlated with PCA 1. The group is mainly composed of lake-type sediment samples.

587

588 *4.3.2 Ratio and indices*

589 The ΣIIIa/ΣIIa ratio shows a general decreasing trend from the beginning to the end of the core
590 (Fig. 6D). From 9700 to 5100 a cal BP (lake sediment), the average ΣIIIa/ΣIIa ratio is equal to 0.83 and
591 then from 5100 a cal BP to today (peat sediment), the average ratio is equal to 0.52. The MBT and the
592 MBT'5Me show similar variations but different absolute values (Fig. 6D). The MBT varies between
593 0.15 and 0.40 and the MBT'5Me between 0.30 and 0.51. From 9700 to 7300 a cal BP, the index values
594 increase and then remain relatively stable. From 7300 a cal BP, they decline and from 5000 a cal BP
595 they largely increase. From 4200 to 3000 a cal BP, the index values progressively decrease and then
596 remain stable except at 1800 a cal BP. The CBT index shows variation between 0.17 and 0.42 except at
597 9200, 8900 and 5000 a cal BP where the values vary from 0.5 to 0.71 (Fig. 6D).

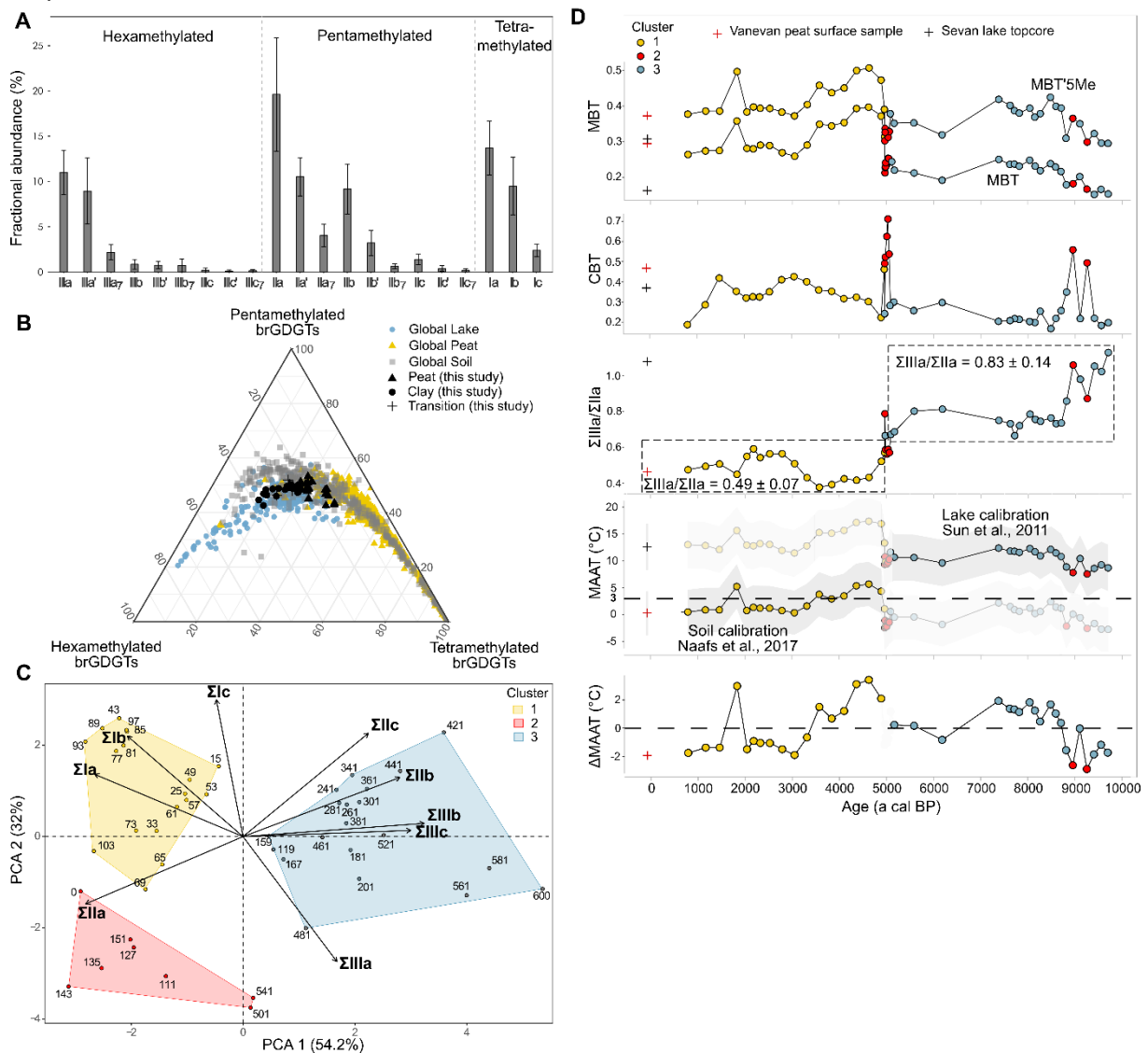
598

599 *4.3.3 Temperature reconstructions*

600 The reconstructed mean annual air temperature (MAAT) using soil (Naafs et al., 2017a) and
601 lake calibrations (Sun et al., 2011) show similar trends but different absolute values (Fig. 6D). For soil,

602 the average MAAT is equal to 0.66 °C during the Holocene and for lake the average MAAT is equal to
 603 11.9 °C. Between 9700 to 7300 a cal BP, MAAT reconstructed values increase and then remain
 604 relatively stable. For this period, the average MAAT is equal to 10.4 °C for lake calibration. From 7300
 605 a cal BP, the MAAT reconstructed values decline, reaching 9.6°C for lake calibration at 6200 a cal BP.
 606 Then shifting to soil calibration, a large increase is recorded from 5000 a cal BP and the MAAT reaches
 607 5.7°C. From 4200 to 3000 a cal BP, the MAAT progressively decrease and then remains stable until the
 608 present at around 0.86°C for soil calibration except at 1800 a cal BP when a peak is recorded. The
 609 Δ MAAT records low temperatures between 9700 and 8700 a cal BP and a plateau until 7400 a cal BP
 610 followed by a continuous decrease onward. Inner variability in this last trend occurs at 4900-3600 a cal
 611 BP and a single peak at 1800 a cal BP.

612
 613



614
 615 Figure 6. A) Average fractional abundance of individual brGDGT, B) Ternary diagram showing the fractional
 616 abundances of tetra-, penta-, and hexamethylated brGDGTs. The dataset of Vanevan core are plotted against that
 617 of lakes (Wang et al., 2012; Günther et al., 2014; Li et al., 2016; Zink et al., 2016; Dang et al., 2018; Weber et al.,
 618 2018; Martin et al., 2019; Ning et al., 2019), of global peat (Naafs et al., 2017b), and of soils (Yang et al., 2014;

619 Naafs et al., 2017a). C) Principal component analysis (PCA) and hierarchical clustering on principal components
620 (HCPC) with fractional abundances of brGDGTs. Labels correspond to sample depth. D) Degree of methylation
621 (MBT, MBT*5Me), Cyclisation ratio (CBT), $\Sigma\text{IIIa}/\Sigma\text{IIa}$ ratio, Mean annual air temperature values (MAAT) based
622 on Naafs et al., 2017a and Sun et al., 2011, Difference of temperature (ΔMAAT) against age. ΔMAAT corresponds
623 to the centered values based on the mean value of the two sediment types (peat and lake).
624
625

626 5. Discussion

627

628 5.1 Pollen representation in modern vegetation and relationship with climate variables

629 The relationship between pollen assemblages and modern vegetation depends on various
630 factors, including pollen production, type of pollination, dispersion mechanisms, surrounding
631 vegetation, topography and microclimatic parameters (Jacobson and Bradshaw, 1981). Pollen rain
632 integrates local to regional vegetation (Jacobson and Bradshaw, 1981; Prentice, 1985). In Armenia, the
633 vegetation is largely open which contributes to a greater pollen dispersion, but topography and
634 microclimatic parameters may also play significant roles. Understanding the representation of pollen
635 and their origins are important for the reliability of the fossil record in vegetation and climate
636 reconstructions.

637 In our study (Fig. 3), the modern vegetation shows the dominance of herbaceous taxa whose
638 pollen representation largely depends on the type of pollination. The insect-pollinated nature of
639 Fabaceae and Rosaceae explain their under-representation whereas the wind-pollinated nature of
640 Asteraceae (*Artemisia*, Asteroideae and Cichorioideae) and Chenopodiaceae explain their over-
641 representation (Fig. 3). These results are consistent with previous studies in semi-arid regions of the
642 Caucasus where Chenopodiaceae represent 30% to 80 % of the pollen signal (Connor et al., 2004). In
643 the desert regions of East Asia, Chenopodiaceae is the most abundant taxa and represents more than
644 60% of the pollen signal in China (e.g. Zhao and Herzschuh, 2009; Wei and Zhao, 2015; Zhang et al.,
645 2018) and Mongolia (Ma et al., 2008). *Artemisia*, another taxa characterizing the semi desert-steppe
646 environments of Armenia, is associated with the local vegetation along our sample gradient but is also
647 present without local presence (Fig. 3), indicating over-representation. This is consistent with
648 observations from the arid and semi-arid areas of Iran (up to 80% of the pollen signal in Djamali et al.,
649 2009), China (e.g. Li et al., 2005; Xu et al., 2007, 2009; Zhang et al., 2018), and Mongolia (Ma et al.,
650 2008) where *Artemisia* is the dominant taxa in steppe regions. In contrast, in Georgia (Connor et al.,
651 2004) and Armenia, *Artemisia* is never the dominant taxa in modern pollen assemblages, although it is
652 well recorded in semi desert-steppe environments of Armenia. According to previous studies in East
653 Asia (e.g. Li et al., 2008; Zheng et al., 2008), the over-representation of Chenopodiaceae and *Artemisia*
654 could be explained by wind transport dispersal, their long-distance transport capacity and a high pollen
655 production. In our study, Chenopodiaceae and *Artemisia* are registered in all modern samples although
656 they are not necessarily present in the local vegetation. Chenopodiaceae is even well registered in

657 subalpine and alpine meadows whereas they do not appear in the vegetation, confirming the previous
658 assumptions.

659 In steppes, subalpine and alpine meadows of Armenia, Poaceae is the dominant taxa and it is
660 reliably associated with the local vegetation (Fig. 3). In East Asia, Poaceae is very common in the semi-
661 desert and steppe vegetation, even though it is generally not the dominant taxa in pollen assemblages
662 due to under-representation (e.g. Ma et al., 2008; Xu et al., 2014). However, in protected areas of
663 Mongolia, Poaceae is better recorded in pollen assemblages (Ma et al., 2008). Anthropogenic activities,
664 such as overcultivation and overgrazing, may prevent the flowering of Poaceae plants (Ma et al., 2008;
665 Wei and Zhao, 2015). The rapid deterioration of Poaceae pollen after their deposition may also
666 contribute to the low representation of Poaceae in pollen assemblages of soils and mosses (Cao et al.,
667 2007). In general, Poaceae is under-represented in pollen assemblages and often represents a quarter of
668 vegetation (Ge et al., 2017). However, our study and Connor et al. (2004) show that in Georgia and
669 Armenia, Poaceae is well associated with the vegetation. In our case, the p/v ratio (average pollen
670 percentages/average vegetation cover percentages) is equal to 0.99, indicating a good correspondence
671 between pollen and local vegetation. The reliable representation of Poaceae could be explained by the
672 abundance of Poaceae in Armenia and a limited anthropogenic pressure with extensive pastoralism.

673 Anthropogenic indicators, such as *Plantago lanceolata* and *Rumex*-type are present in very low
674 proportion even with extensive pastoralism which is not easily detectable in the modern pollen
675 assemblages. Considering *Cerealia*-type, the pollen percentages are low and no relationship was found
676 between pollen and vegetation. These results are consistent since the selection of modern sites was done
677 in areas remote from agricultural zones.

678 Arboreal pollen taxa are registered in all modern samples, but they are mainly present at mid-
679 and high elevations (Fig. 3). In meadow steppes, trees and shrubs come primarily from local or extra-
680 local vegetation whereas in subalpine and alpine meadows, trees come from regional vegetation. The
681 long-distance component varies depending on the location and the elevation of modern sites and it also
682 favored by the vegetation openness in Armenia. Arboreal pollen taxa representative of the local
683 vegetation are *Hippophae*, *Pistacia*, *Salix*, *Juniperus*, *Acer* and *Viburnum*. In semi desert-steppe
684 environments, *Pistacia* can be present in areas close to sparse arid woodlands. In meadow steppes,
685 *Hippophae* is present in areas close to humid zones (Lake Sevan, rivers), *Salix* in riparian areas and
686 *Juniperus* on south-facing slopes. In the sample from the Lake Sevan surrounding, *Hippophae* is well
687 associated with the local vegetation even if it is a wind-pollinated tree (Li et al., 2005).

688 Other trees (*Pinus*, *Quercus*, *Carpinus betulus*, *Betula*, *Ulmus* and *Fagus*) recorded in our
689 samples come from regional vegetation. Their over-representation may be partly explained by a wind
690 pollination. *Pinus* pollen is registered at all elevations even if it is not present in the vegetation, except
691 around Lake Sevan. There, *Pinus* was planted during afforestation program of USSR in the eighties.
692 However, these pine plantations do not seem to produce pollen, as indicated by the low percentages of
693 *Pinus* for the sample 18. A similar result occurs around the Mount Aragats in Armenia where *Pinus* is

694 poorly registered despite the presence of planted pine trees for approximately 40 years (Cromartie et al.,
695 2020). *Pinus* is considered as a high pollen producer and it has a good pollen dispersion by wind (Connor
696 et al., 2004). In subalpine and alpine meadows, *Quercus* pollen averages 7% when oak forests are not
697 present. Interestingly, oak pollen is recorded at the same elevations inhabited by oaks on the reverse
698 slopes of the northeast mountains of Armenia and Azerbaijan. The over-representation of *Quercus* is
699 also reported from Georgia (Connor et al., 2004) and Iran (Ramezani et al., 2013) although *Quercus* has
700 a good pollen representation in the eastern part of Iran (Djamali et al., 2009). *Quercus* is a high pollen
701 producer and it is often well represented in the modern pollen assemblages of the Near East (Connor et
702 al., 2004). Our study confirms that *Quercus* pollen can be transported over long distance, even where
703 topographic barriers are high.

704 The relationship between modern pollen assemblages and climate variables is marked across
705 the altitudinal transect. Chenopodiaceae and *Artemisia* pollen dominate in semi desert-steppe vegetation
706 of Armenia when MAAT is high and MAP is low whereas Poaceae are dominant in meadow steppes,
707 subalpine and alpine meadows when MAAT decreases. Chenopodiaceae and *Artemisia* are indicators
708 of continental climate characterized by cold winters and dry summers (El-Moslimany, 1990). In the
709 Near East and Asia, the *Artemisia*/Chenopodiaceae (A/C) ratio is used as an aridity index for desert and
710 steppe environments (e.g. Herzschuh, 2007; Zhao and Herzschuh, 2009). However, in Georgia a low
711 relationship between A/C ratio and precipitation is observed compared to Chenopodiaceae percentages
712 alone (Connor et al., 2004). In our study, Chenopodiaceae dominance also has higher relationship to
713 MAP ($R^2=0.40$) and MAAT ($R^2=0.58$) than A/C ratio to MAP ($R^2=0.02$) and MAAT ($R^2=0.16$). In the
714 South Caucasus, Chenopodiaceae changes seem to be a better aridity index than the A/C ratio.

715

716 5.2 Holocene reconstruction at a local scale: wetland dynamics and human activities at Vanevan

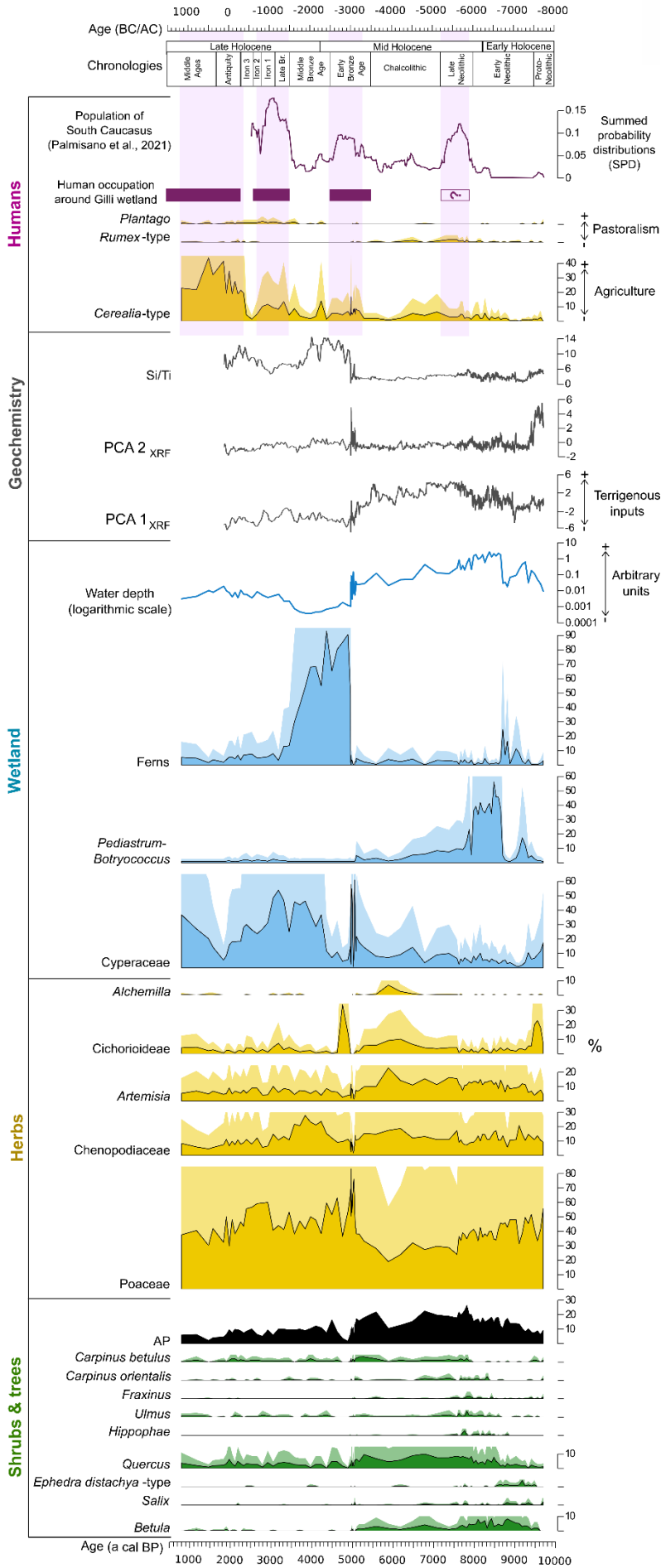
717

718 *5.2.1 Validation of age-depth model*

719 The comparison of the vegetation dynamics with that of the closest site (Shenkani, Cromartie et
720 al., 2020) validates the age model. Similar trends are observed in both sites: occurrence of *Carpinus*
721 *betulus* from 9700 to 9300 a cal BP, *Betula* beginning at 9600 a cal BP (Fig. 7), an arboreal taxa
722 maximum at 7800 a cal BP, and a drop of *Betula* at 5000-4700 a cal BP.

723 At Vanevan, however, the trends evidenced in cores VD2016 (this study) and VD2011 (Leroyer
724 et al., 2016) are closely related but changes are not simultaneously (Supplementary Fig. S6). For
725 example, the maximum of arboreal pollen dates to 7800 and 6800 a cal BP for VD2016 and VD2011,
726 respectively. Similarly, both sequences end with a peak of arboreal pollen at 5900 and 5600 a cal BP for
727 VD2011 and VD2016 followed by an increase of Poaceae, Cyperaceae, and then ferns at 5100 and 4900
728 a cal BP for VD2011 and VD2016. This comparison therefore reveals a temporal gap between the two
729 cores ranging from 2200 years at the base to 300 years at the top of the VD2011 sequence.
730 Underestimation of the ages in the VD2011 sequence could be explained by an age model based on plant

731 macrofossils imbedded in clay sediments. It should, moreover, be noted that the most basal date of
732 VD2011 core, rejected by the authors, is consistent with the older ages of the VD2016 core.
733



735 Figure 7. Selected Pollen taxa, NPPs, XRF, and archeological data of Vanevan peat against age. Water depth =
736 $(\text{Algae}+1)/(\text{semi-aquatic plants}+1)/(\text{ferns} +1)$ plotted on a logarithmic scale. Algae: *Pediastrum*, *Botryococcus*.
737 Semi-aquatic plants: Cyperaceae, *Sparganium*, *Typha*. Ferns: Monolote spore, *Botrychium*, *Polypodium*,
738 *Selaginella*, *Asplenium*.
739

740 5.2.2 Wetland dynamics and water-level changes

741 Aquatic taxa, fern spores, and NPP variations are environmental indicators of the type of
742 wetland, the openness of the waterbody, and its water depth. Following Joannin et al. (2012), a ratio
743 between such environmental indicators is used to estimate changes in water-level (Fig. 7), and for
744 comparison with the conditions indicated by the lithology and XRF data. The ratio increases from 9700
745 to 8600 a cal BP, progressively decreases until 5100 a cal BP and remains low afterwards.

746 From 9700 to 5100 a cal BP, the Vanevan sequence is characterized by clay sediments formed
747 by inputs of detrital elements (PCA 1_{XRF}, Fig. 7). The poorly developed semi-aquatic vegetation and the
748 presence of freshwater algae suggest a lake system seen in the water-depth reconstruction. This is
749 consistent with a transgression of Lake Sevan reported in Sayadyan's works (1977-1983). Within this
750 period, however, we can distinguish a low water-level phase from 9700 to 9400 a cal BP consistent with
751 the regressive phase reported by Sayadyan (1977-1983) at the same period. Such conditions would
752 create an erosional context and may explain both the dominance of the mycorrhizal root-fungi *Glomus*
753 (Fig. 2C) and high calcium concentrations (PCA 2_{XRF}, Fig. 7). *Glomus* is often interpreted as an indicator
754 of close distance soil-related input (Wünnemann et al., 2010; Mudie et al., 2011) and the proportion of
755 calcium may be derived from evaporative concentration, biogenic production (Cohen, 2003) or
756 dissolution of the basaltic outcrops around or in the lake (detrital or in situ; Gudbrandsson et al., 2011).
757 This raises the question of whether the calcium recorded in Vanevan was produced during the regression
758 phase or produced before and washed down during this phase. According to Sayadyan (2009), Lake
759 Sevan was high at the onset of the Holocene and it could have been connected with the Gilli wetland.
760 As calcium concentrations were high in Lake Sevan before the Soviet lowering (Alekin and Ulyanova,
761 1986), it could be due to the remobilization of previous carbonates formed during a high stand of the
762 paleoSevan. The high percentages of Cichorioideae also fit in a regression scenario as it is not connected
763 to known regional vegetation development and therefore suggest local development or taphonomic
764 processes in erosive conditions leading to an over-representation of this resistant pollen taxa (Lebreton
765 et al., 2010).

766 A transitional phase is recorded between 5100 and 4950 a cal BP and shows large variations in
767 Cyperaceae percentages. Successive peaks of the saprophyte fungi HdV-200 may indicate alternating
768 drying conditions followed by aquatic phases (Kuhry, 1985; van Geel et al., 1989). A peak of the green
769 algae *Mougeotia* (Zygnemataceae) is recorded and may indicate changes in the trophic conditions and
770 could play a role in the water-plant succession (Van Geel and van der Hammen, 1978; Van Geel and
771 Grenfell, 1996). This phase is also characterized by high proportions of calcium, sulfur and phosphorus
772 (PCA 2, Fig. 7) and corresponds to high fire activity (core VD2011, Leroyer et al., 2016; Supplementary

773 **Fig. S6**). The macrocharcoals reported in [Leroyer et al. \(2016\)](#) are assumed to reconstruct local scale
774 fires and the chemistry of the fire byproducts is likely recorded through the XRF data ([Smith, 1969](#)).
775 The fire activity seems to have burned Cyperaceae sedges or grassland and favored developments of
776 ferns and Poaceae. The same vegetation dynamic after fire events are recorded at Shenkani ([Cromartie
777 et al., 2020](#)). In the Vanevan wetland, the ecological perturbation of fire also results in a brief but massive
778 peak of Cichorioideae recorded at 4800 a cal BP. Again, the presence of this taxa suggests a local
779 development on perturbed soil or a drying phase leading to an over-representation of the resistant pollen
780 taxa ([Lebreton et al., 2010](#)). The relative impact of human activities and climate changes on the rapid
781 water-level fluctuations between 5100 and 4800 a cal BP remains to be determined because agricultural
782 activities are present around Gilli wetland and climate changes are recorded at this period in the region.

783 After 4800 a cal BP, the Vanevan wetland then evolves towards a peatland characterized by peat
784 deposits produced by a semi-aquatic vegetation, primarily Cyperaceae. The water level is low until 4500
785 a cal BP before the development of semi-aquatic vegetation. Abundant ferns are associated with the
786 increase of the ratio Si/Ti. The biogenic silica production is likely due to phytoliths associated with the
787 ferns ([Brown et al., 2007](#)). The water-level remains low and the wetland is dominated by Cyperaceae,
788 except from 2300 to 1800 a cal BP when *Potamogeton*, *Sparganium* and *Typha* dominated the signal
789 (**Fig. 2C**). This corroborates the Lake Sevan transgression (through underground influence) dating from
790 2350 to 1700 a cal BP ([Sayadyan et al., 1977](#); [Sayadyan, 1978, 1983](#)). In Armenia, a water-level rise is
791 also registered at Shenkani between 2200 and 1500 a cal BP ([Cromartie et al., 2020](#)).

792

793 5.2.3 Human impact

794

795 **Agriculture**

796 In our record, human activities are principally expressed through agricultural practices identified
797 by *Cerealia*-type pollen. Although, *Cerealia*-type pollen may come from Poaceae species or wild cereals
798 commonly present in the Near East ([Van Zeist et al., 1975](#)), our record matches the estimates of the
799 population in the South Caucasus (**Fig. 7**) ([Palmisano et al., 2021](#)).

800 Low percentages of *Cerealia*-type pollen are recorded between 8300 and 6300 a cal BP (Late
801 Neolithic-Chalcolithic). However, there is limited evidence of a Neolithic presence around Vanevan
802 during this period evidenced only by an obsidian source, (Khorapor) located ~20 km away from the
803 Vanevan peatland, which may have been used by Neolithic populations ([Chataigner and Gratuze, 2014](#)).
804 Some evidence of Neolithic occupations is also recorded in the Kasakh valley, ~50 km from Lake Sevan
805 ([Colonge et al., 2013](#)) and agriculture during this period is primarily recorded on the Ararat plain at an
806 elevation of 850 m a.s.l. ([Badalyan et al., 2004](#); [Hovsepyan and Willcox, 2008](#); [Badalyan and
807 Harutyunyan, 2014](#)). During the Early and Middle Chalcolithic, the archeological site of Getahovit-2 in
808 north-eastern Armenia shows the presence of cereals. According to [Chataignier et al., 2020](#), cereals were
809 not locally cultivated ([Chataignier et al., 2020](#)), however, such a transport of cereals at this period is not

810 evidenced around the Lake Sevan. The presence of *Cerealia*-type pollen in our record questions the
811 conservation of archeological remains on the shores of Lake Sevan. The high degree of mobility of
812 Neolithic population (Ricci et al., 2018) has certainly not helped to the conservation of archeological
813 material.

814 Since 5200 a cal BP, archeological remains and *Cerealia*-type pollen occur simultaneously
815 when the environmental conditions shift from a lake to a peatland due to an abrupt drop of water level.

816 Percentages of *Cerealia*-type pollen are more important from 5200 to 4500 a cal BP during the
817 Early Bronze Age, a period marked by an increase of the population in the South Caucasus (Fig. 7) and
818 the first archeological evidence of agriculture around Gilli wetland (Hovsepyan, 2013, 2017). During
819 this period, the Kura-Araxes culture is present in the South Caucasus and archeological data show the
820 development of permanent village communities and agro-pastoral systems at any elevation in Armenia
821 (Badalyan, 2014).

822 Then, a maximum of *Cerealia*-type pollen is recorded at 4300 a cal BP followed by a strong
823 decrease from 4100 to 3700 a cal BP. The decline of agricultural practices at Vanevan is consistent with
824 few archeological remains around Gilli wetland and with a decline of the population in the South
825 Caucasus (Hovsepyan, 2013, 2017; Palmisano et al., 2021). However, very little is known about the
826 Middle Bronze Age and archeological sites for this period are scarce. According to Smith (2015), this
827 period is characterized by a shift to more mobile lifeways and not necessarily accompanied by a decline
828 of the population. Our record indicates that agriculture, which was present at the beginning of the Middle
829 Bronze Age on the Sevan shores, became less important around the 4.2 ka climate event, which is
830 characterized by arid conditions around the Mediterranean basin (e.g. Kaniewski et al., 2018; Bini et al.,
831 2019).

832 From 3600 to 2600 a cal BP (Late Bronze Age, Iron Age I and II), an increase of *Cerealia*-type
833 pollen is recorded and is consistent with the large quantity of archeological sites located on the shores
834 of Lake Sevan and an increase of the population in the South Caucasus (Biscione et al., 2002; Parmegiani
835 and Poscolieri, 2003; Hovsepyan, 2013, 2017; Palmisano et al., 2021). At this period, the Lchashen-
836 Metsamor culture is present around the Lake Sevan and the Urartu empire appears during the Iron Age
837 II. The conception of forts, territory, politics and the development of agriculture, irrigation systems and
838 pastoralism characterized this period (Badalyan et al., 2003).

839 From 2700 to 2400 a cal BP (Iron Age II and III), a strong decline of *Cerealia*-type pollen is
840 recorded (Fig. 7) probably connected to the end of the Urartu empire and Lchashen-Metsamor culture
841 centered on the north-west of Lake Sevan at 2600 a cal BP (Smith, 2015). At the scale of the Lesser
842 Caucasus, a decline of population seems to occur at around 2700 a cal BP although the data from
843 Palmisano et al. (2021) are rather incomplete for this period. This period is also marked by the arrival
844 of domination of the Persian Achaemenid Empire in Armenia between 2540 and 2281 a cal BP (Briant,
845 1996).

846 From 2300 to 800 a cal BP, *Cerealia*-type pollen strongly increase during the Antiquity and
847 Medieval Period and are consistent with the presence of archeological sites located on the shores of Gilli
848 wetland and Lake Sevan (Parmegiani and Poscolieri, 2003; Hovsepian, 2013, 2017). *Cerealia*
849 percentages up to 40% suggest crops close or within the wetland. If located in the wetland, a drainage
850 system would have been required in conjunction with fire utilization to suppress semi-aquatic
851 vegetation. At this period, increase of fire activity is recorded in Armenia (Joannin et al., 2014;
852 Cromartie et al., 2020) and Georgia (Connor, 2011). This period is also consistent with the conquest of
853 Alexander the Great in 2281 a cal BP (Briant, 1996) and the foundation of the Kingdom of Armenia,
854 which contributed to a change of human practices.

855

856 **Pastoralism**

857 Pastoral activities are complex to detect in pollen records (Fig. 7). Similarly to the modern pollen
858 samples, anthropogenic indicators such as *Plantago lanceolata* and *Rumex*-type (Behre, 1981) are
859 present in very low proportion whereas extensive pastoralism existed since the Neolithic in Armenia
860 (Badalyan et al., 2004; Hovsepian and Willcox, 2008; Badalyan and Harutyunyan, 2014). During the
861 Late Neolithic and the Chalcolithic (7900-6000 a cal BP), the occurrence of *Rumex*-type suggests two
862 phases of grazing (Behre, 1981), corresponding to increases in cereal cultivation and population in the
863 South Caucasus (Fig. 7) and was already observed by Leroyer et al. (2016).

864 From 4100 to 3700 a cal BP (Middle Bronze Age), no pollen indicators of pastoralism are
865 recorded. At Vanevan, the decline of agriculture is not accompanied by a shift to more mobile lifeways
866 centered on pastoralism as mentioned by Smith (2015). Several studies show a significant impact of the
867 4.2 ka climate event on Near East societies, hypothesize population decline or migration (Kaniewski et
868 al., 2018; Palmisano et al., 2021). Our data seem to agree for a decline of local population around Lake
869 Sevan.

870 During the last 3700 a cal BP, pollen of *Plantago lanceolata*, are continuously recorded at
871 Vanevan, although in low percentages. This pollen may be an indicator of pastoralism activities (Behre,
872 1981). Since the Early Bronze Age (5500 a cal BP), bones of domestic animals are recorded in
873 archaeological materials and confirm the presence of herds of cattle around Gilli wetland (Hovsepian,
874 2017). At Zarishat, the last 3000 a cal BP are also marked by a continuous record for *Plantago* and
875 *Rumex*-type (Joannin et al., 2014).

876 The succession of *Rumex*-type then *Plantago* along the Holocene raises questions about pastoral
877 practices and particularly livestock types for each period (cow, sheep, goat, horse). However, these
878 anthropogenic taxa are also common in mountain steppe environment and it is difficult to unequivocally
879 associate them with specific practices.

880

881 5.3 Holocene vegetation dynamics for the Lesser Caucasus

882

883 **Steppe grassland vegetation with pioneer trees during the Early Holocene (9700-8000 a cal BP)**

884 The Vanevan sequence covers most of the Holocene but does not document the Chenopodiaceae
885 steppe recorded before 10,000 a cal BP when it got replaced by grassland steppes (Wick et al., 2003;
886 Messenger et al., 2013; Joannin et al., 2014; Cromartie et al., 2020). From 9700 to 8000 a cal BP, the
887 steppe vegetation is primarily dominated by Poaceae and secondarily by Chenopodiaceae and *Artemisia*
888 (Fig. 7). During this period, open vegetation is also recorded in the Southern Caucasus and the Near
889 East mainly, although the dominant steppic taxa varies from (1) Poaceae (this study; Roberts et al., 2001;
890 Stevens et al., 2001; Wick et al., 2003; Stevens et al., 2006; Ryabogina et al., 2018; Cromartie et al.,
891 2020), to (2) *Artemisia*, (Djamali et al., 2008; Joannin et al., 2014; also in Central Asia: Chen et al.,
892 2008; Zhao et al., 2009, 2020) or (3) Chenopodiaceae (Leroy et al., 2013; Messenger et al., 2013). In
893 contrast, the sites north-west of Armenia document forested phases during the same part of the Early
894 Holocene (Connor, 2011; Shumilovskikh et al., 2012; Messenger et al., 2017; Connor et al., 2018;
895 Grachev et al., 2020). At Vanevan, a low proportion of arboreal pollen taxa is recorded (Fig. 7). There,
896 the occurrence of *Carpinus betulus*, *Betula* and *Quercus* observed is also recorded at Shenkani
897 (Cromartie et al., 2020), suggesting that these taxa mostly represent regional vegetation. From 9500 to
898 8500 a cal BP, *Ephedra distachya*-type, *Hippophae*, and *Betula* expand. *Ephedra*, which has a long-
899 distance dispersal by wind (Herzschuh, 2007; Djamali et al., 2009), is indicative of dry climate
900 conditions and is also observed at Lake Van during the Early Holocene (Wick et al., 2003). *Hippophae*,
901 according to the modern relationship between pollen and vegetation, represents the local vegetation
902 bordering Gilli wetland (Fig. 3). *Betula*, which is simultaneously recorded at Shenkani (Cromartie et al.,
903 2020) and Lake Van (Wick et al., 2003), is a pioneer taxon. After this pioneer phase, the arboreal taxon
904 richness increases from 8500 a cal BP with the appearance of several deciduous trees that represent the
905 regional vegetation such as *Carpinus orientalis* and *Carpinus betulus*.

906

907 **Mixed steppe and open woodlands during a truncated Mid Holocene (8000-5100 a cal BP)**

908 During the Mid Holocene, the vegetation remains steppic but becomes more mixed with
909 Poaceae, *Artemisia*, Chenopodiaceae and Cichorioideae (Fig. 7). From 5900 a cal BP, Poaceae decrease
910 progressively with the same dynamic recorded at Shenkani (Cromartie et al., 2020). The arboreal pollen
911 are dominated by *Quercus* (<10%) and the percentages remain low with a maximum recorded at 7800 a
912 cal BP. Older palynological studies have suggested the presence of deciduous forests on the slopes of
913 Lake Sevan during the Middle Holocene in particular around 6000 years (e.g. Sayadyan et al., 1977;
914 Sayadyan, 1978, 1983; Moreno-Sanchez and Sayadyan, 2005). However, modern pollen-vegetation
915 relationships demonstrated that *Quercus* pollen could represent up to 15% even if no trees were present
916 in the catchment (Fig. 3). More likely, a *Quercus* forest was not present on the slopes of Lake Sevan
917 during the Mid-Holocene. In contrast, *Juniperus* is also well recorded at this period. According to Figure
918 3, *Juniperus* is mainly an indicator of the local vegetation and could have lived on the slopes such as
919 today where it grows as open woodland. Therefore, the Vanevan's landscape, with nearby grasslands

920 and scarce open woodlands, resembles similar pollen assemblages from Armenia (Joannin et al., 2014;
921 Cromartie et al., 2020) and Iran (Djamali et al., 2008) during the Mid-Holocene. However, Vanevan's
922 pollen record differs by an abrupt drop of arboreal taxa between 6300-5700 a cal BP. The increase of
923 *Artemisia*, Chenopodiaceae, Cichorioideae and *Alchemilla* can be an indicator of both dry climate and
924 pastoralism activities.

925

926 **Steppe grassland and limited tree diversity (5100-700 a cal BP)**

927 The major vegetation change, initiated at 5400 and which fully settled after 5100 a cal BP, is
928 characterized by an increase of Poaceae, a drop of arboreal taxa (*Quercus*, *Betula*) and wetland changes
929 (Fig. 7). The decrease of *Betula* is also recorded in Armenia (Cromartie et al., 2020), Turkey (Wick et
930 al., 2003), and at a larger scale in East Asia (Qian et al., 2019). At Vanevan, the vegetation changes
931 around 5100 a cal BP can be discussed in light of the presence of important fires (detected by macro-
932 charcoals) that have affected the landscape and the wetland itself (Leroyer et al., 2016). Several
933 hypotheses explain the ignition of fires: (1) an anthropogenic cause with the lighting of fires by the local
934 population living around Gilli wetland; (2) a volcanic origin due to nearby lava flows from Porak
935 volcano dated to the Mid-Holocene (Fig. 1C, Karakhanian et al., 2017; Meliksetian et al., 2021) or (3)
936 a climatic driver linked with the aridification period around 5000 a cal BP recorded in Armenia (Joannin
937 et al., 2014), Georgia (Connor and Kvadadze, 2008; Connor, 2011), Turkey (Wick et al., 2003), Iran
938 (Stevens et al., 2001, 2006) and in Israel (Bar-Matthews et al., 1997). Although this event could be
939 multifactorial, the regional scale of the changes points towards a climatic cause.

940 From 4200 to 800 a cal BP, the steppe vegetation continues to dominate the landscape with
941 Poaceae (Fig. 7) in accordance with the Zarishat (Joannin et al., 2014) and Shenkani records (Cromartie
942 et al., 2020). According to the modern pollen-vegetation relationships (Fig. 3), Chenopodiaceae is better
943 recorded in pollen assemblages at low and mid-elevations in Armenia (<1900 m) where the climate
944 conditions are more arid. The increase of Chenopodiaceae between 4400-3500 a cal BP may therefore
945 be an indicator of aridification. A decline of agriculture is also highlighted around 4000 a cal BP and
946 abandoned crops may have favored the expansion of Chenopodiaceae. However, this dynamic is not
947 visible during other agriculture abandonments at Vanevan, therefore the climate appears as the main
948 driver of vegetation change at 4.2 cal yr BP (e.g. Kaniewski et al., 2018; Bini et al., 2019).

949

950 5.4 Holocene climate reconstructions for the Lesser Caucasus

951

952 *5.4.1 Pertinence and reliability of climate reconstructions*

953 **Pollen-based climate reconstructions**

954 The results of the four quantitative pollen-based climate reconstructions are consistent (Fig. 5),
955 whether for commonly-used transfer functions/assemblages methods (WAPLS, MAT) or recent

956 “machine-learning” methods (RF, BRT). The minor discrepancies observed in the climate
957 reconstructions at Vanevan can be method-dependent. For the MAT, a major limitation can be the
958 occurrence of no-analogs, however, at Vanevan, it is clearly not the case because the fossil assemblages
959 mainly correspond to the modern Armenian analogs added in this study, as demonstrated by the
960 comparison of modern and core samples (Fig. 4). This method also tends to select analogs that are
961 geographically close to each other (spatial autocorrelation; Telford and Birks, 2005, 2009, 2011),
962 however, at Vanevan the spatial autocorrelation is relatively low (Moran’s $I < 0.26$, $p\text{-value} < 0.01$). The
963 MAT shows a high variability among the reconstructed values of close samples, and this variability is
964 linked to the high degree of sensitivity of the method (Brewer et al., 2008) but is probably overestimated
965 for the Holocene period (Fig. 5). The WAPLS performs well and this method is particularly useful for
966 local to regional scale reconstructions (Chevalier et al., 2020); its main disadvantage is the
967 overestimation of the values (Fig. 5) linked to the implicit inverse regression in WAPLS that “pulls” the
968 predicted values toward the mean of the training set (Birks, 1998). The reconstructed values of the RF
969 show low amplitude variations in contrast to the values of other methods. The BRT include the
970 “boosting” which increases the performance of the model, however the curves present a high sample-to-
971 sample variability. The BRT results are preferred for the regional climate comparison (Fig. 8) since this
972 method is the most performant (maximum R^2 and the minimum RMSE values for all climatic parameters
973 - Supplementary Table S4).

974 At Vanevan, the pollen-based climate reconstructions are problematic for two periods: (1)
975 between 9700 to 9400 a cal BP, the high temperature and precipitation trends are contradictory to all
976 other climate reconstructions available in the South Caucasus (Fig. 8) and to the brGDGT results,
977 suggesting that this overestimation is probably due to the low pollen taxa diversity and the dominance
978 of Cichorioideae, a very resistant pollen grain (Lebreton et al., 2010); (2) From 2300 a cal BP onwards,
979 the climate trends of the different methods diverge, when the percentages of *Cerealia*-type become
980 important (19-44%). There, it is expected that human activities (agriculture, pastoralism) modified the
981 vegetation structure, composition, and diversity, influencing the paleoclimate reconstructions (St
982 Jacques et al., 2015). Therefore, the pollen-based climate reconstructions for these two periods (9700-
983 9400, and 2300-800 a cal BP) are not considered in the comparison of climate reconstructions and in
984 the climate synthesis (Fig. 8).

985

986 **BrGDGT temperature reconstructions**

987 At Vanevan, the wetland dynamic changes along the Holocene with a lake system from 9700 a
988 cal BP, a drying phase at 5000 a cal BP and finally the development of a peatland. The type of wetland,
989 the water level and the surrounding vegetation may influence the brGDGT distribution and origins
990 (catchment soils, rivers, in situ production in waters or sediments) (Martin et al., 2019; Martinez-Sosa
991 et al., 2021). The water level and aquatic plant community changes of the wetland may have largely
992 impacted the brGDGT distribution. For example, between 4800 and 3000 a cal BP, the high Δ MAAT is

993 associated with a low water-level and a switch to ferns. The peak of ΔMAAT at 1820 a cal BP is also
994 associated to a change in plant aquatic distribution, Cyperaceae largely decrease whereas *Potamogeton*
995 and *Sparganium/Typha* increase. The local dynamic has therefore largely impacted the brGDGT
996 distribution and could overprint the climate signal. The type of sediment has also impacted the
997 distribution of brGDGTs. The tetramethylated brGDGTs are more abundant in peat sediments whereas
998 the hexamethylated brGDGTs, brGDGTs ΣIIb and brGDGTs ΣIIc are more abundant in lake sediments
999 (Fig. 6BC), confirming the distributions of brGDGTs reported in lakes, peats and soils (Naafs et al.,
1000 2018; Russell et al., 2018). Due to the difference in brGDGT distributions and the in-situ production in
1001 lakes, if a soil-based MBT-CBT calibration is applied on lake samples, the reconstructed temperatures
1002 are generally underestimated (e.g. Sun et al., 2011; Loomis et al., 2011, 2012; Russel et al., 2018).

1003 In the Vanevan core, the difference in the distribution of brGDGTs according to the type of
1004 sediment is well identified (Fig. 6C), for this reason a lake calibration was applied from 9700 to 5100 a
1005 cal BP whereas a soil calibration was applied from 4900 to 790 a cal BP (Fig. 6D). A soil calibration is
1006 applied because the peat samples of Vanevan core are closer to global soils than global peats (Fig. 6B).
1007 Moreover, the temperature reconstructed for the surface sample of Vanevan peat is closer to modern
1008 temperatures when soil calibration is applied. The $\Sigma\text{IIIa}/\Sigma\text{IIa}$ values suggest important terrigenous
1009 sources of brGDGTs in the Vanevan peat (Xiao et al., 2016; Martin et al., 2020).

1010 Global lake calibrations applied to our modern lake samples (Sevan core top and Vanevan
1011 surface sample) tend to overestimate the reconstructed temperatures, with values close to warmest month
1012 mean (MTWA). The overestimation of reconstructed temperatures has already been evidenced in
1013 middle- and high-latitude lakes and could be linked to a seasonal bias (e.g. Foster et al., 2016; Dang et
1014 al., 2018; Cao et al., 2020). Both higher brGDGT production during warm seasons (Pearson et al., 2011;
1015 Shanahan et al., 2013) or winter ice formation on lake surfaces limiting air/lake water exchanges (Cao
1016 et al., 2020) could explain this seasonal bias. To account for the overestimated temperature values in our
1017 sequence, they were normalized to their mean values on each part of the record in the following
1018 discussion (ΔMAAT , Fig. 6D). The development of local and regional calibrations

1019

1020 **Comparison of climate reconstructions based on pollen and brGDGTs (Fig. 8)**

1021 The Early Holocene is characterized by cold and dry conditions as indicated by pollen and
1022 brGDGT climate reconstructions. The Mid-Holocene (8200-5500 a cal BP) shows warmer conditions
1023 associated with a decrease in precipitation by pollen and in temperature by brGDGTs at 6000 a cal BP.
1024 Between 5100 and 4800 a cal BP, an important change in wetland dynamic and a drying phase are
1025 recorded and have largely impacted the distribution of brGDGTs and the pollen conservation. Therefore,
1026 this part will not be considered for climate reconstructions. Then, the climate reconstructions based on
1027 pollen and brGDGTs during the last 5000 a cal BP differ because of (1) the change in water level and
1028 aquatic plant which impact the bacterial community and therefore the brGDGT distribution and (2) the
1029 strong human impact during the last 3000 a cal BP which biased the climate reconstruction based on

1030 pollen. However, both climate reconstructions based on pollen and brGDGTs recorded a decrease in
1031 temperature between 6300-5700 a cal BP and 4200-3700 a cal BP.

1032

1033 *5.4.2 Millennial-scale climate changes in the Lesser Caucasus*

1034 **A cold and arid Early Holocene (9700-8200 a cal BP)**

1035 Vanevan climate reconstructions clearly indicate low annual temperature and precipitation
1036 during the Early Holocene (Fig. 8), followed by a rise from 8700 a cal BP. This climate improvement is
1037 also accompanied by the increase in water level in Vanevan wetland. This climate pattern is echoed in
1038 Armenia and in Georgia: due to time resolution difference between these archives, the climate change
1039 goes from more progressive in Georgia (Connor and Kvavadze, 2008) to more abrupt in Armenia
1040 (Joannin et al., 2014; Cromartie et al., 2020). In Arid Central Asia, the Early Holocene is also
1041 characterized by arid conditions (Chen, et al., 2008). In contrast, in the Near and Middle East (Iran,
1042 Turkey and Israel), low values of the oxygen isotopes are generally interpreted as responding to higher
1043 water levels, suggesting higher precipitation during the Early Holocene (Roberts et al., 2001; Stevens et
1044 al., 2001, 2006; Wick et al., 2003; Bar-Matthews et al., 2003). However, the openness of the vegetation
1045 recorded at such a large extent (South Caucasus, Near East, Central Asia) brings into question this
1046 climate interpretation. Therefore, our study brings a new argument to attribute cold and dry conditions
1047 during the Early Holocene for the whole Near East region. Going into details, several studies in Armenia
1048 (Joannin et al., 2014), Iran (Stevens et al., 2001), and Turkey (Wick et al., 2003) attributed the vegetation
1049 changes to low spring precipitation, a limiting factor for the plants' growing season, controlled by the
1050 Siberian High (Wick et al., 2003). This is not contradictory with the wet Early Holocene identified by
1051 isotope data of the Near East if it is the result of high winter precipitation, a parameter typical of the
1052 Mediterranean climate (Stevens et al., 2001, 2006; Djamali et al., 2010). Indeed, the winter snows have
1053 lower $\delta^{18}\text{O}$ values leading to more negative values and a lower total precipitation (Stevens et al., 2001,
1054 2006). Moreover, according to Messenger et al. (2017), the winter snow accumulated can melt during
1055 spring and summer, generating higher water level in lakes. However, isotopic and lake-level studies are
1056 rarely conducted together rendering this interpretation difficult to extrapolate for the Early Holocene. In
1057 addition, lake variations depicted in Sevan by our study and Sayadyan's works (1977-1983) do not
1058 corroborate a high lake level during the second half of the Early Holocene.

1059

1060 **Abrupt installation of warm and humid Mid Holocene progressively shifting to cooler and drier** 1061 **conditions**

1062 The Mid Holocene starts with high precipitation and temperature suggested by brGDGTs, pollen
1063 and water-level changes (Fig. 8). This agrees well with the warm and humid Mid-Holocene documented
1064 in Armenia and Georgia (Connor and Kvavadze, 2008; Joannin et al., 2014; Cromartie et al., 2020), and
1065 in Arid Central Asia (Chen et al., 2008). In contrast, the isotopic curves of the Near East show a
1066 progressive decrease of precipitation throughout this period (Roberts et al., 2001; Stevens et al., 2001,

1067 2006; Wick et al., 2003; Bar-Matthews et al., 2003). Our study thus records a mid-Holocene climatic
1068 optimum and supports an increase of spring precipitation linked to the Westerlies (Wick et al., 2003;
1069 Joannin et al., 2014). This change marks the installation of the present-day climate dominated by late
1070 spring rainfall over the East Anatolia and North Iran. Since 5100 a cal BP, pollen and low water levels
1071 suggest a large decrease in precipitation, while brGDGTs shows a temperature decrease (Fig. 8). This
1072 trend agrees with Georgian and Central Asia records for declining precipitation. At the scale of the Near
1073 East, our study clarifies the climate pattern with conditions becoming colder, and aridification (Roberts
1074 et al., 2001; Stevens et al., 2001, 2006; Wick et al., 2003; Bar-Matthews et al., 2003). Since this period,
1075 humans were able to live and cultivate nearer Gilli wetland thanks to the water level drop.

1076

1077 *5.4.3 Rapid/abrupt climate events in the Lesser Caucasus*

1078 **6.2 and 5.2 ka arid events**

1079 At Vanevan, the Mid-Holocene is marked by two arid events. The first one is recorded at 6300-
1080 5700 a cal BP and appears both in pollen and brGDGT reconstructions (Fig. 8). In the South Caucasus,
1081 the fire frequency history and abundance variations of sedge at Zarishat in Armenia show a drier phase
1082 at 6400 a cal BP (Joannin et al., 2014). At a larger scale, a drop in rainfall occurs at Lake Zeribar (Iran)
1083 at 6200 a cal BP (Stevens et al., 2006), at Sofular cave (Turkey) at 6200-6000 a cal BP (Zanchetta et al.,
1084 2014) and in East Asia at 6.2 ka, linked to an abrupt monsoon event (Yu et al., 2006; Wu et al., 2018).
1085 Considering temperature, there is no clear trends according to our results (Fig. 8) and the other studies
1086 carried out in the South Caucasus and the Near East.

1087 The second arid event recorded at Vanevan occurs at 5100-4800 a cal BP and is marked by a
1088 drop in arboreal trees, a drying wetland phase, high fire activity, and changes in brGDGT distribution
1089 (Fig. 8). Major changes are also recorded in Armenia: at Zarishat, by fire frequency history and sedge
1090 changes, which show a dry phase at 5300-4900 a cal BP (Joannin et al., 2014); at Shenkani, by an
1091 increase of fire activity for the same period (Cromartie et al., 2020); and in Georgia at Lake Aligol, by
1092 an increase of fires accompanied by a drop in rainfall at 5000-4500 a cal BP (Connor and Kvavadze,
1093 2008). In the Caucasus, glacier advances are recorded at 5000-4500 a cal BP, supporting the hypothesis
1094 of a colder climate in the Caucasus (Solomina et al., 2015). In the Near East, an arid phase is visible in
1095 isotopic data at Lake Mirabad and Zeribar in Iran at 5200 a cal BP (Stevens et al., 2001, 2006), at
1096 Gölhisar in Turkey at 4900 a cal BP (Eastwood et al., 2007) and at Soreq cave in Israël at 5200 a cal BP
1097 (Bar-Matthews et al., 1997; Bar-Matthews and Ayalon, 2011). Magny et al. (2006) define the '5.2 ka
1098 event' as a global climate event, characterized by drier conditions around the Mediterranean basin.
1099 Although agriculture practices are present around Gilli wetland since 5200 a cal BP, the changes of
1100 vegetation and fire between 5300 and 4800 a cal BP are regional and seem to be largely affected by the
1101 aridification event.

1102

1103 **The 4.2 ka arid event**

1104 At Vanevan, a period of aridity between 4200 and 3700 a cal BP is recorded by the pollen
1105 climate reconstruction, water-level, and brGDGT changes. This event is characterized by a drop in
1106 annual and summer precipitation and an increase in summer temperature. The brGDGT reconstructions
1107 confirm warm conditions for this period (Fig. 8). In the South Caucasus, the other pollen sequences do
1108 not clearly record this arid event, except at Shenkani where an increase of the Br/Ti ratio indicates a
1109 decrease in terrigenous inputs between 4300 and 4100 a cal BP (Cromartie et al., 2020). In the Near
1110 East, the isotopic data of Lake Zeribar in Iran (Stevens et al., 2001), Eski Acigöl in Turkey and Soreq
1111 cave in Israel (Bar-Matthews et al., 2003) show a climate aridification around 4000 a cal BP. At Lake
1112 Van in Turkey, arid conditions at 4200-4000 a cal BP are expressed through the increase of fire, the
1113 decrease of *Quercus* and low lake-level (Wick et al., 2003). This arid event is also characterized by an
1114 increase of dust deposits in the Near East (Ön et al., 2021) as at Lake Van in Turkey (Lemcke and Sturm
1115 1997) and at Lake Neor in Iran (Sharifi et al., 2015). However, this dust event is not recorded in the
1116 South Caucasus (Cromartie et al., 2020). The 4.2 ka event is defined by a severe and prolonged drought
1117 around the Mediterranean basin (global “megadrought”, Weiss, 2016). It was first proposed by Weiss et
1118 al. (1993) for the Near East and is recorded at a global scale although not evidenced in all records (Cullen
1119 et al., 2000). The 4.2 ka event is today considered as the formal boundary of Late and Middle Holocene.
1120 This event is often characterized as a cold event (Cullen et al., 2000; Dixit et al., 2014), however for the
1121 Eastern Mediterranean the records show warmer conditions (this study; Bini et al., 2019). In this region,
1122 the 4.2 ka event is defined by climatic and environmental changes that extend between 4.3 and 3.8 ka
1123 (Bini et al., 2019). In the South Caucasus, the Vanevan sequence is the first to report the impact of a
1124 warm and arid 4.2 ka event. The concordance between the 4.2 ka event and the decline of agricultural
1125 practices is easily linkable to the decline of local population but cannot tell whether it is due to societal
1126 collapse or migrations of population in the South Caucasus and the Near East (Kaniewski et al., 2018;
1127 Palmisano et al., 2021).

1128

1129 **The 2.8 ka climate event**

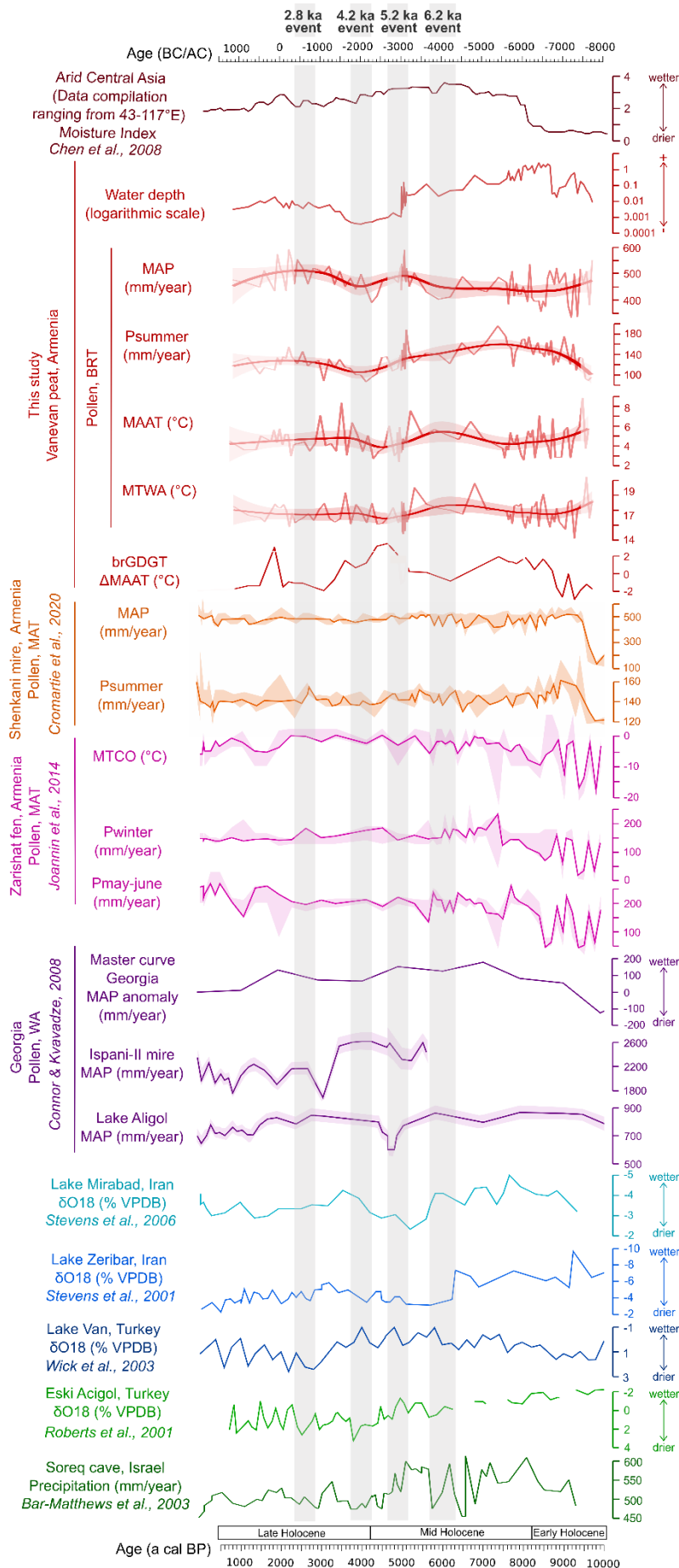
1130 Between 2900 and 2400 a cal BP, a cold and arid event appears at Vanevan, mainly with the
1131 WAPLS method (Fig. 8). This pattern is consistent with the glacier advances recorded in the Greater
1132 Caucasus at 2900-2800 a cal BP (Solomina et al., 2015) and the drop in rainfall at Lake Van, in Turkey
1133 (Wick et al., 2003) and Soreq Cave, in Israël (Bar-Matthews et al., 2003). The 2.8 ka event is defined
1134 by cold conditions at a global scale and several studies have also identified its impact in East Asia
1135 (Fukumoto et al., 2012) and Europe (Ivy-Ochs et al., 2009; Van Geel et al., 2014). In the South Caucasus,
1136 our climate reconstructions marked the impact of the 2.8 ka event, which is accompanied by a decline
1137 of agricultural practices around Lake Sevan, certainly due to a decline of local population (Fig. 8). This
1138 climate event may have contributed to the decline of the Urartian empire centered around Lake Sevan

1139 and it coincides with the arrival of the Persians in Armenia. At the scale of the Caucasus, [Palmisiano et](#)
1140 [al. \(2021\)](#) also showed a decline of population at 2700 a cal BP although the data are limited for this
1141 period. According to several studies focused on the Near East, the demographic trends become
1142 dissociated from climate from 4000-3500 a cal BP because populations are more resilient due to the
1143 technological advancement ([Lawrence et al., 2016](#); [Roberts et al., 2019](#)). This hypothesis might need to
1144 be revisited in the light of the present study, at least for the South Caucasus.

1145

1146 **Atmospheric processes**

1147 The abrupt climate events described here are all characterized by arid conditions in the Caucasus
1148 and the Near East. Temperature shows colder conditions for the 5.2 ka and 2.8 ka events whereas the
1149 4.2 ka event is characterized by warmer conditions. Several studies indicate that the North Atlantic
1150 Oscillation (NAO) is the main driver of precipitation variability in the Near East and the Caucasus during
1151 the Mid- and Late Holocene ([Joannin et al., 2014](#); [Jones et al., 2019](#)). Therefore, arid events in the
1152 Eastern Mediterranean can be caused by a weak westerly flow associated to multi-centennial cyclicity
1153 of the NAO system (e.g. [Magny et al., 2013](#); [Zielhofer et al., 2017](#); [Bini et al., 2019](#)). Many studies
1154 suggest that the Westerlies decreasing influence is accompanied by the reinforcement and latitudinal
1155 expansion of the Siberian High and subtropical systems ([Djamali et al., 2008](#); [Joannin et al., 2014](#);
1156 [Zanchetta et al., 2016](#); [Bini et al., 2019](#); [Ön et al., 2021](#)). The southward expansion of the Siberian High
1157 provides the incursion of cold-dry air masses in southern Europe ([Zanchetta et al., 2016](#); [Perşoiu et al.,](#)
1158 [2019](#)). We hypothesize that the 5.2 ka and 2.8 ka events are mainly under the influence of the winter
1159 Siberian High as cold conditions are recorded in the South Caucasus and the Near East. According to
1160 [Perşoiu et al. \(2019\)](#), the 4.2 ka event is also characterized by a dominance of the winter Siberian High
1161 in Europe, however, the records of the South Caucasus and the Near East show warm conditions ([this](#)
1162 [study](#); [Bini et al., 2019](#)). Other atmospheric systems could come into play in these regions during the
1163 4.2 ka event. According to [Ön et al. \(2021\)](#), precipitation of the southeastern Mediterranean is mainly
1164 controlled by the latitudinal migration of the Intertropical Convergence Zone and the subtropical high
1165 pressure belt but the model does not specify clear trends on the aridity or temperature in the Near East.
1166 Noteworthy, the study of [Sharifi et al. \(2015\)](#) evidences the arrival of dust from the Middle East coming
1167 from the south, but does not identify the origins. We hypothesize that the 4.2 ka event in the South
1168 Caucasus and the Near East is influenced by the northward migration of subtropical systems providing
1169 warm and arid conditions. This migration is also reflected through the arrival of dust from the Near East
1170 but not reaching the South Caucasus. Considering the 6.2 ka event, it is also linked to the NAO variations
1171 ([Joannin et al., 2014](#)), however, the contradicting temperature reconstructions from Vanevan do not
1172 allow us to hypothesize whether the 6.2 ka arid event is due to polar or Arabian subtropical influences.



1174 Figure 8. Synthesis of paleoenvironmental records over the last 10,000 yrs based on pollen, brGDGTs and $\delta^{18}\text{O}$
1175 data. Gray vertical shading represents abrupt climate events. MAAT: mean annual air temperature. MTWA: mean
1176 temperature of the warmest month. MAP: mean annual precipitation. Psummer: summer precipitation. For
1177 location, refer to [Fig. 1](#).

1178

1179 6. Conclusions

1180 Environmental dynamic, climate changes and human practices are reconstructed using multi-
1181 proxies at Vanevan peat in Armenia during the last 9700 years. This study extends the Mid-Holocene
1182 record documented at Vanevan peat by [Leroyer et al. \(2016\)](#) and proposes new proxies as brGDGTs.

- 1183 • For the first time in the South Caucasus and the Near East, our study provides climate
1184 reconstructions based on brGDGTs and pollen coupled with a multimethod approach (MAT,
1185 WAPLS, RF, BRT). The climate reconstructions are complementary and show a good
1186 correspondence between the proxies and the methods used. However, our results reveal that it is
1187 essential to understand the local dynamic of the wetland to properly interpret the climate
1188 reconstructions based on brGDGTs and pollen. The results show an arid and cold Early Holocene,
1189 a more humid and warmer Mid Holocene, and a more arid and cooler Late Holocene. Several abrupt
1190 events are detected at 6.2 ka, 5.2 ka, 4.2 ka, 2.8 ka and allow us to highlight the atmospheric
1191 processes in the Caucasus and the Near East. The four climate events are arid and seem linked to
1192 weak westerlies associated to multi-centennial cyclicity (NAO-like). The 5.2 ka and 2.8 ka are
1193 characterized by cold conditions and could be associated to a strong Siberian High. On the contrary,
1194 the 4.2 ka is characterized by warm conditions and would be influenced by the northward migration
1195 of Arabian subtropical systems.
- 1196 • This study is also the first to investigate the modern relationship between vegetation and pollen in
1197 Armenia. It complements the study of [Connor and Kvavadze \(2008\)](#) for Georgia. The results show
1198 an abundance of Chenopodiaceae in semi-desert/steppe regions and Poaceae in steppes, subalpine
1199 and alpine meadows. Chenopodiaceae and *Artemisia* are over-represented whereas Poaceae is
1200 reliably associated with the local vegetation. In the South Caucasus, Chenopodiaceae percentages
1201 seem to be a better aridity index than A/C ratio.
- 1202 • The vegetation during the last 9700 years shows a dominance of steppes predominantly composed
1203 of Poaceae. The surrounding vegetation of Lake Sevan was poorly forested, even during the Mid-
1204 Holocene and contrasts with the previous hypotheses which suggested the occurrence of a deciduous
1205 forest. This result brings into question the existence of open woodland around Lake Sevan and new
1206 studies are necessary to better estimate the vegetation around the entire lake and the relationship to
1207 open woodland.
- 1208 • Humans have been able to live and cultivate when the Gilli wetland level dropped at around 5200 a
1209 cal BP. The expansion and decline phases of agricultural practices are remarkably correlated with
1210 the occupation and abandonment phases of archeological sites of Lake Sevan but also with
1211 demographic trends of the South Caucasus ([Palmisano et al., 2021](#)).

1212 • Major changes in paleohydrological conditions are recorded by abundances of aquatic plants and
1213 algae at Vanevan during the last 9700 a cal BP. A lake system is initially present following by a
1214 drying phase at 4950 a cal BP associated with fire and finally a peatland dominated by Cyperaceae
1215 appears. The water level changes are consistent with the previously established variations of Lake
1216 Sevan in [Sayadyan's works \(1977-1983\)](#) and they are congruent with our climate reconstructions
1217 proposed for the South Caucasus.

1218 • Contrary to several studies, which conclude to the dissociation between demographic trends and
1219 climate from 4000-3500 a cal BP in the Near East, our study suggests a significant impact of abrupt
1220 climate changes on populations. The different events are consistent with the population
1221 abandonment phases and question the human enfranchisement in the face of climate changes due to
1222 their technological advancements. In our study, climate changes appear as one of the main drivers
1223 of vegetation and demographic changes in the South Caucasus. However, further research is needed
1224 to understand all the social complexities related to these changes although our study clearly shows
1225 links between climatic changes and demographic shifts.

1226 In the line with the previous studies of [Joannin et al. \(2014\)](#), [Leroyer et al. \(2016\)](#) and [Cromartie et al.](#)
1227 [\(2020\)](#) for Armenia, this new study brings a better understanding of vegetation dynamics and the
1228 respective role of climate and humans in the South Caucasus. The multiproxy approach provided a
1229 robust chronicle of climate changes occurring during the Holocene.

1230

1231 **Funding**

1232 This research was co-founded by the International PhD course in “Agriculture Technologies and
1233 Biotechnologies” (34° Cycle, Code: DOT1339335). Financial support for this study was provided by
1234 the French–Armenian International Associated Laboratory HEMHA “Humans and Environments in
1235 Mountainous Habitats, the case of Armenia” supervised by C. Chataigner and P. Avetisyan. This
1236 programme between Armenia and France was founded by the French National Centre for Scientific
1237 Research (CNRS). Field trip campaigns and analyses were founded by CNRS program INSU
1238 INTERRVIE (PI: C. Colombié) and Labex OT Med and ECCOREV program from Aix-Marseille
1239 University through the GeoArT and SoCCER project (PI: V. Ollivier). For the analytical work
1240 completed at LGLTPE-ENS de Lyon, this research was funded by Institut Universitaire de France funds
1241 to G. Ménot. The travels between Italy and France were financed by VINCI funding. The conference
1242 funding was provided by the Association des Palynologues de Langue Française (APLF).

1243

1244 **Author contributions**

1245 M. Robles: Conceptualization, Field work, Laboratory work, Formal analysis, Writing draft
1246 manuscript, Review, Funding acquisition. S. Joannin: Project administration, Conceptualization, Field
1247 work, Supervision, Review, Funding acquisition; O. Peyron: Conceptualization, Formal analysis,
1248 Supervision, Review, Funding acquisition. G. Ménot: Conceptualization, Supervision, Review, Funding

1249 acquisition; E. Brugiapaglia: Conceptualization, Supervision, Review. L. Dugerdil: Formal analysis,
1250 Review. V. Ollivier: Field work, Review, Funding acquisition. S. Ansanay-Alex and A.-L. Develle:
1251 Laboratory work. P. Tozalakyan and K. Sahakyan: Field work. K. Meliksetian and L. Sahakyan: Field
1252 supervision. R. Badalyan and B. Perello: Field supervision, Review. C. Colombié: Field work, Review,
1253 Funding acquisition.

1254

1255 **Declaration of competing interest**

1256 The authors declare that they have no known competing financial interests or personal
1257 relationships that could have appeared to influence the work reported in this paper.

1258

1259 **Acknowledgements**

1260 The authors would like to express their appreciation to David Etienne for the NPP identification
1261 help, to Laurent Bouby and Isabelle Figueiral for seed or wood identifications used for radiocarbon
1262 datings, and to Sandrine Canal for the preparation of moss samples. We would like to thank Amy
1263 Cromartie for the proofreading and comments on the manuscript.

1264

1265 **References**

- 1266 Alekin, O., Ulyanova, D., 1986. Super-saturation of Sevan water with CaCO₃. *Water Resources Moscow I*, 117-
1267 122 (in Russian).
- 1268 Arimura, M., Gasparyan, B., Chataigner, C., 2012. Prehistoric sites in Northwest Armenia: Kmlo-2 and
1269 Tsaghkahovit, in: Matthews, R.J., Curtis, J. (Eds.), *Proceedings of the 7th International Congress of the*
1270 *Archaeology of the Ancient Near East. Volume 3: Fieldwork and Recent Research e Posters*. Harrasowitz,
1271 Wiesbaden, pp. 135-150.
- 1272 Arnaud, F., Révillon, S., Debret, M., Revel, M., Chapron, E., Jacob, J., Giguët-Covex, C., Poulénard, J., Magny,
1273 M., 2012. Lake Bourget regional erosion patterns reconstruction reveals Holocene NW European Alps soil
1274 evolution and paleohydrology. *Quaternary Science Reviews* 51, 81–92.
1275 <https://doi.org/10.1016/j.quascirev.2012.07.025>
- 1276 Badalyan, R.S., Smith A.T., Avetisyan P.S., 2003. The Emergence of Socio-Political Complexity in Southern
1277 Caucasia: An Interim Report on the Research of Project ArAGATS, in: Smith, A.T. and Rubinson K.S.
1278 (Eds.), *Archaeology in the Borderlands: Investigations in Caucasia and Beyond*. The Cotsen Institute of
1279 Archaeology, Los Angeles, pp. 144-166.
- 1280 Badalyan, R., Lombard, P., Chataigner, C., Avetisyan, P., 2004. The Neolithic and Chalcolithic phases in the
1281 Ararat Plain (Armenia): The view from Aratashen, in: Sagona, A. (Eds.), *A View from the Highlands-*
1282 *Archaeological Studies in Honour of Charles Burney*. *Ancient Near Eastern Studies Supplement 12*, Peters,
1283 pp. 399-420.
- 1284 Badalyan, R.S., 2014. New data on the periodization and chronology of the Kura-Araxes culture in Armenia.
1285 *Paléorient* 40, 71–92. <https://doi.org/10.3406/paleo.2014.5636>
- 1286 Badalyan, R., Harutyunyan, A., 2014. Aknashen-the Late Neolithic Settlement of the Ararat Valley: Main Results
1287 and Prospects for the Research, in: Gasparyan, B., Arimura, M. (Eds.), *Stone age of Armenia*. Kanazawa
1288 University, Kanazawa, pp. 161-177.
- 1289 Baghdasaryan, A.B., 1958. *Klimat Armyanskoy, SSR, Yerevan*, pp. 108-118.
- 1290 Bar-Matthews, M., Ayalon, A. and Kauffman, A., 1997. Late Quaternary paleoclimate in the eastern
1291 Mediterranean region from stable isotope analysis of speleothems at Soreq Cave, Israel. *Quaternary Res.* 47,
1292 155–168. <https://doi.org/10.1006/qres.1997.1883>
- 1293 Bar-Matthews, M., Ayalon, A., Gilmour, M., Matthews, A., Hawkesworth, C.J., 2003. Sea–land oxygen isotopic
1294 relationships from planktonic foraminifera and speleothems in the Eastern Mediterranean region and their
1295 implication for paleorainfall during interglacial intervals. *Geochimica et Cosmochimica Acta* 67, 3181–
1296 3199. [https://doi.org/10.1016/S0016-7037\(02\)01031-1](https://doi.org/10.1016/S0016-7037(02)01031-1)

- 1297 Bar-Matthews, M., Ayalon, A., 2011. Mid-Holocene climate variations revealed by high-resolution speleothem
1298 records from Soreq Cave, Israel and their correlation with cultural changes. *The Holocene* 21, 163–171.
1299 <https://doi.org/10.1177/0959683610384165>
- 1300 Behre, K.E., 1981. The interpretation of anthropogenic indicators in pollen diagrams. *Pollen et spores*, 23(2), 225-
1301 245.
- 1302 Beug, H.-J., 2004. Leitfaden der Pollenbestimmung für Mitteleuropa und angrenzende Gebiete, Pfeil, München.
- 1303 Bini, M., Zanchetta, G., Perşoiu, A., Cartier, R., Català, A., Cacho, I., Dean, J.R., Di Rita, F., Drysdale, R.N.,
1304 Finnè, M., Isola, I., Jalali, B., Lirer, F., Magri, D., Masi, A., Marks, L., Mercuri, A.M., Peyron, O., Sadori,
1305 L., Sicre, M.-A., Welc, F., Zielhofer, C., Brisset, E., 2019. The 4.2 ka BP Event in the Mediterranean region:
1306 an overview. *Clim. Past* 15, 555–577. <https://doi.org/10.5194/cp-15-555-2019>
- 1307 Birks, H.J.B., 1998. Numerical tools in palaeolimnology-progress, potentialities, and problems. *J. Paleolimnol.* 20,
1308 307–332.
- 1309 Biscione, R., Hmayakyan, S., Parmegiani, N., 2002. The North-Eastern frontier: Urartians and Non-Urartians in
1310 the Sevan Lake Basin, The Southern Shores. CNR istituto di studi sulle civiltà dell'Egeo e del Vicino
1311 Oriente, Rome.
- 1312 Blaauw, M., 2010. Methods and code for “classical” age-modelling of radiocarbon sequences. *Quat. Geochronol.*
1313 5, 512–518. <https://doi.org/10.1016/j.quageo.2010.01.002>
- 1314 Blaauw, M., Christen, J.A., 2011. Flexible paleoclimate age-depth models using an autoregressive gamma process.
1315 *Bayesian analysis* 6, 457–474. <https://doi.org/10.1214/11-BA618>
- 1316 Bohn, U., Gollub, G., Hettwer, C., 2000. Karte der natürlichen Vegetation Europas, Bundesamt für Naturschutz,
1317 Bonn.
- 1318 Bottema, S., 1992. Prehistoric cereal gathering and farming in the Near East: the pollen evidence. *Rev. Palaeobot.*
1319 *Palynol.* 73, 21–33.
- 1320 Braun-Blanquet, J., Schoenichen, W. 1964. Grundzüge der Vegetationskunde, Springer, Vienna.
- 1321 Breiman, L., 2001. Random forests. *Machine learning* 45, 5–32.
- 1322 Brewer, S., Guiot, J., Sánchez-Goni, M.F., Klotz, S., 2008. The climate in Europe during the Eemian: a multi-
1323 method approach using pollen data. *Quaternary Science Reviews*, 27, 2303-315.
1324 <https://doi.org/10.1016/j.quascirev.2008.08.029>
- 1325 Briant, P., 1996. Histoire de l'Empire perse de Cyrus à Alexandre. Fayard, Paris, 1247p.
- 1326 Brown, E., Johnson, T., Scholz, C., Cohen, A., King, J., 2007. Abrupt change in tropical African climate linked to
1327 the bipolar seesaw over the past 55,000 years. *Geophys. Res. Lett.*, 34, L20702.
1328 <https://doi.org/10.1029/2007GL031240>
- 1329 Cao, X., Tian, F., Xu, Q.H., Li, Y.C., Zhang, Z.Q., Jia, H.J., Zhang, L.Y., Wang, X., 2007. Pollen influx and
1330 comparison with surface pollen in the east part of Yinshan Mountains. *Acta Palaeontologica Sinica*, 46(4),
1331 418 (in Chinese).
- 1332 Cao, J., Rao, Z., Shi, F., Jia, G., 2020. Ice formation on lake surfaces in winter causes warm-season bias of
1333 lacustrine brGDGT temperature estimates. *Biogeosciences* 17, 2521–2536. [https://doi.org/10.5194/bg-17-
1334 2521-2020](https://doi.org/10.5194/bg-17-2521-2020)
- 1335 Chataigner, C., Gratuze, B., 2014. New data on the exploitation of obsidian in the Southern Caucasus (Armenia,
1336 Georgia) and eastern Turkey, Part 2: obsidian procurement from the Upper Palaeolithic to the Late Bronze
1337 Age. *Archaeometry* 56 (2), 569-577. <https://doi.org/10.1111/arcm.12007>
- 1338 Chataigner, C., Gratuze, B., Tardy, N., Abbès, F., Kalantaryan, I., Hovsepian, R., Chahoud, J., Perello, B., 2020.
1339 Diachronic variability in obsidian procurement patterns and the role of the cave-sheepfold of Getahovit-2
1340 (NE Armenia) during the Chalcolithic period. *Quaternary International* 550, 1–19.
1341 <https://doi.org/10.1016/j.quaint.2020.02.010>
- 1342 Chen, F., Yu, Z., Yang, M., Ito, E., Wang, S., Madsen, D.B., Huang, X., Zhao, Y., Sato, T., John B. Birks, H.,
1343 Boomer, I., Chen, J., An, C., Wünnemann, B., 2008. Holocene moisture evolution in arid central Asia and
1344 its out-of-phase relationship with Asian monsoon history. *Quat. Sci. Rev.* 27, 351–364.
1345 <https://doi.org/10.1016/j.quascirev.2007.10.017>
- 1346 Chevalier, M., Davis, B.A.S., Heiri, O., Seppä, H., Chase, B.M., Gajewski, K., Lacourse, T., Telford, R.J.,
1347 Finsinger, W., Guiot, J., Köhl, N., Maezumi, S.Y., Tipton, J.R., Carter, V.A., Brussel, T., Phelps, L.N.,
1348 Dawson, A., Zanon, M., Vallé, F., Nolan, C., Mauri, A., de Vernal, A., Izumi, K., Holmström, L., Marsicek,
1349 J., Goring, S., Sommer, P.S., Chaput, M., Kupriyanov, D., 2020. Pollen-based climate reconstruction
1350 techniques for late Quaternary studies. *Earth-Science Reviews* 210, 103384.
1351 <https://doi.org/10.1016/j.earscirev.2020.103384>
- 1352 Cohen, A.S., 2003. *Paleolimnology: the history and evolution of lake systems*. Oxford University Press, New
1353 York, 528p.
- 1354 Connor, S.E., Thomas, I., Kvavadze, E.V., Arabuli, G.J., Avakov, G.S., Sagona, A., 2004. A survey of modern
1355 pollen and vegetation along an altitudinal transect in southern Georgia, Caucasus region. *Review of*
1356 *Palaeobotany and Palynology* 129, 229–250. <https://doi.org/10.1016/j.revpalbo.2004.02.003>

- 1357 Connor, S.E., Kvavadze, E.V., 2008. Modelling late Quaternary changes in plant distribution, vegetation and
1358 climate using pollen data from Georgia, Caucasus. *Journal of Biogeography* 36, 529–545.
1359 <https://doi.org/10.1111/j.1365-2699.2008.02019.x>
- 1360 Connor, S.E., 2011. A promethean legacy: late quaternary vegetation history of southern Georgia, the Caucasus.
1361 Peeters, Leuven.
- 1362 Connor, S.E., Colombaroli, D., Confortini, F., Gobet, E., Ilyashuk, B.P., Ilyashuk, E.A., van Leeuwen, J.F.N.,
1363 Lamentowicz, M., van der Knaap, W.O., Malysheva, E., Marchetto, A., Margalitadze, N., Mazei, Y.,
1364 Mitchell, E.A.D., Payne, R.J., Ammann, B., 2018. Long-term population dynamics: Theory and reality in a
1365 peatland ecosystem. *J. Ecol.* 106, 333–346. <https://doi.org/10.1111/1365-2745.12865>
- 1366 Cromartie, A., Blanchet, C., Barhoumi, C., Messenger, E., Peyron, O., Ollivier, V., Sabatier, P., Etienne, D.,
1367 Karakhanyan, A., Khatchadourian, L., Smith, A.T., Badalyan, R., Perello, B., Lindsay, I., Joannin, S., 2020.
1368 The vegetation, climate, and fire history of a mountain steppe: A Holocene reconstruction from the South
1369 Caucasus, Sherkani, Armenia. *Quat. Sci. Rev.* 246, 106485.
1370 <https://doi.org/10.1016/j.quascirev.2020.106485>
- 1371 Croudace, I.W., Rothwell, R.G., 2015. *Micro-XRF Studies of Sediment Cores: Applications of a Non-destructive*
1372 *Tool for the Environmental Sciences*. Springer, Dordrecht.
- 1373 Cullen, H.M., deMenocal, P.B., Hemming, S., Hemming, G., Brown, F.H., Guilderson, T., Sirocko, F., 2000.
1374 Climate change and the collapse of the Akkadian empire: Evidence from the deep sea. *Geology* 28, 379–
1375 382. <https://doi.org/10.1130/0091-7613>
- 1376 Dang, X., Ding, W., Yang, H., Pancost, R.D., Naafs, B.D.A., Xue, J., Lin, X., Lu, J., Xie, S., 2018. Different
1377 temperature dependence of the bacterial brGDGT isomers in 35 Chinese lake sediments compared to that in
1378 soils. *Organic Geochemistry* 119, 72–79. <https://doi.org/10.1016/j.orggeochem.2018.02.008>
- 1379 Davtian, N., Bard, E., Ménot, G., Fagault, Y., 2018. The importance of mass accuracy in selected ion monitoring
1380 analysis of branched and isoprenoid tetraethers. *Org. Geochem.* 118, 58–62.
1381 <https://doi.org/10.1016/j.orggeochem.2018.01.007>
- 1382 Dearing Crampton-Flood, E., Tierney, J.E., Peterse, F., Kirkels, F.M.S.A., Sinninghe Damsté, J.S., 2020.
1383 BayMBT: A Bayesian calibration model for branched glycerol dialkyl glycerol tetraethers in soils and peats.
1384 *Geochimica et Cosmochimica Acta* 268, 142–159. <https://doi.org/10.1016/j.gca.2019.09.043>
- 1385 De'ath, G., 2007. Boosted trees for ecological modeling and prediction. *Ecology* 88, 243–251.
1386 [https://doi.org/10.1890/0012-9658\(2007\)88\[243:BTFEMA\]2.0.CO;2](https://doi.org/10.1890/0012-9658(2007)88[243:BTFEMA]2.0.CO;2)
- 1387 De Jonge, C., Hopmans, E.C., Zell, C.I., Kim, J.-H., Schouten, S., Sinninghe Damsté, J.S., 2014. Occurrence and
1388 abundance of 6-methyl branched glycerol dialkyl glycerol tetraethers in soils: implications for palaeoclimate
1389 reconstruction. *Geochim. Cosmochim. Acta* 141, 97–112. <https://doi.org/10.1016/j.gca.2014.06.013>
- 1390 Ding, S., Schwab, V.F., Ueberschaar, N., Roth, V.-N., Lange, M., Xu, Y., Gleixner, G., Pohnert, G., 2016.
1391 Identification of novel 7-methyl and cyclopentanyl branched glycerol dialkyl glycerol tetraethers in lake
1392 sediments. *Org. Geochem.* 102, 52–58. <https://doi.org/10.1016/j.orggeochem.2016.09.009>
- 1393 Dixit, Y., Hodell, D.A., Petrie, C.A., 2014. Abrupt weakening of the summer monsoon in northwest India ~4100
1394 yr ago. *Geology* 42, 339–342. <https://doi.org/10.1130/G35236.1>
- 1395 Djamali, M., de Beaulieu, J.-L., Shah-hosseini, M., Andrieu-Ponel, V., Ponel, P., Amini, A., Akhiani, H., Leroy,
1396 S.A.G., Stevens, L., Lahijani, H., Brewer, S., 2008. A late Pleistocene long pollen record from Lake Urmia,
1397 Nw Iran. *Quat. res.* 69, 413–420. <https://doi.org/10.1016/j.yqres.2008.03.004>
- 1398 Djamali, M., de Beaulieu, J.-L., Campagne, P., Andrieu-Ponel, V., Ponel, P., Leroy, S.A.G., Akhiani, H., 2009.
1399 Modern pollen rain–vegetation relationships along a forest–steppe transect in the Golestan National Park,
1400 NE Iran. *Review of Palaeobotany and Palynology* 153, 272–281.
1401 <https://doi.org/10.1016/j.revpalbo.2008.08.005>
- 1402 Djamali, M., Akhiani, H., Andrieu-Ponel, V., Braconnot, P., Brewer, S., de Beaulieu, J.-L., Fleitmann, D., Fleury,
1403 J., Gasse, F., Guibal, F., Jackson, S.T., Lézine, A.-M., Médail, F., Ponel, P., Roberts, N., Stevens, L., 2010.
1404 Indian Summer Monsoon variations could have affected the early-Holocene woodland expansion in the Near
1405 East. *The Holocene* 20, 813–820. <https://doi.org/10.1177/0959683610362813>
- 1406 Djamali, M., Cilleros, K., 2020. Statistically significant minimum pollen count in Quaternary pollen analysis; the
1407 case of pollen-rich lake sediments. *Rev. Palaeobot. Palynol.*, 275, 104156.
1408 <https://doi.org/10.1016/j.revpalbo.2019.104156>
- 1409 Dugerdil, L., Joannin, S., Peyron, O., Jouffroy-Bapicot, I., Vannièrè, B., Bazartseren, B., Unkelbach, J., Behling,
1410 H., Ménot, G., 2021. Climate reconstructions based on GDGT and pollen surface datasets from Mongolia
1411 and Siberia: calibrations and applicability to extremely cold-dry environments over the Late Holocene.
1412 *Climate of the Past Discussions*, pp.1–39. <https://doi.org/10.5194/cp-2020-154>
- 1413 Eastwood, W.J., Leng, M.J., Roberts, N., Davis, B., 2007. Holocene climate change in the eastern Mediterranean
1414 region: a comparison of stable isotope and pollen data from Lake Gölhisar, southwest Turkey. *J. Quaternary*
1415 *Sci.* 22, 327–341. <https://doi.org/10.1002/jqs.1062>

- 1416 El-Moslimany, A., 1990. Ecological significance of common non-arboreal pollen: examples from drylands of the
1417 Middle East. *Review of Palaeobotany and Palynology* 69, 343-350.
- 1418 Elith, J., Leathwick, J.R., Hastie, T., 2008. A working guide to boosted regression trees. *J. Anim. Ecol.* 77, 802-
1419 813
- 1420 Fægri, K., Iversen, J., Kaland, P.E., Krzywinski, K., 1989. Textbook of pollen analysis, IV, John Wiley & Sons,
1421 Chichester.
- 1422 Fayvush, G., Tamanyan, K., Kalashyan, M., Vitek, E., 2013. Biodiversity Hotspots in Armenia. *Annalen des*
1423 *Naturhistorischen Museums Wien B* 115, 11–20.
- 1424 Fayvush, G., Aleksanyan, A., Bussmann, R.W., 2017. Ethnobotany of the Caucasus – Armenia, in: Bussmann,
1425 R.W. (Eds.), *Ethnobotany of the Caucasus, European Ethnobotany*. Springer International Publishing, Cham,
1426 pp. 21–36. https://doi.org/10.1007/978-3-319-49412-8_18
- 1427 Fick, S.E., Hijmans, R.J., 2017. Worldclim 2: new 1-km spatial resolution climate surfaces for global land areas:
1428 New climate surfaces for global land areas. *International Journal of Climatology* 37, 4302–4315.
1429 <https://doi.org/10.1002/joc.5086>
- 1430 Fletcher, W.J., Debret, M., Goñi, M.F.S., 2013. Mid-Holocene emergence of a low-frequency millennial
1431 oscillation in western Mediterranean climate: Implications for past dynamics of the North Atlantic
1432 atmospheric westerlies. *The Holocene* 23, 153–166. <https://doi.org/10.1177/0959683612460783>
- 1433 Foster, L.C., Pearson, E.J., Juggins, S., Hodgson, D.A., Saunders, K.M., Verleyen, E., Roberts, S.J., 2016.
1434 Development of a regional glycerol dialkyl glycerol tetraether (GDGT)–temperature calibration for
1435 Antarctic and sub-Antarctic lakes. *Earth and Planetary Science Letters* 433, 370–379.
1436 <https://doi.org/10.1016/j.epsl.2015.11.018>
- 1437 Fukumoto, Y., Kashima, K., Orkhonselenge, A., Ganzorig, U., 2012. Holocene environmental changes in northern
1438 Mongolia inferred from diatom and pollen records of peat sediment. *Quaternary International* 254, 83–91.
1439 <https://doi.org/10.1016/j.quaint.2011.10.014>
- 1440 Ge, Y., Li, Y., Bunting, M.J., Li, B., Li, Z., Wang, J., 2017. Relation between modern pollen rain, vegetation and
1441 climate in northern China: Implications for quantitative vegetation reconstruction in a steppe environment.
1442 *Science of The Total Environment* 586, 25–41. <https://doi.org/10.1016/j.scitotenv.2017.02.027>
- 1443 Göktürk, O.M., 2011. Climate on the southern Black Sea coast during the Holocene: implications from the Sofular
1444 Cave record. *Quaternary Science Reviews* 30, 2433-2445. <https://doi.org/10.1016/j.quascirev.2011.05.007>
- 1445 Grachev, A.M., Novenko, E.Y., Grabenko, E.A., Alexandrin, M.Y., Zazovskaya, E.P., Konstantinov, E.A.,
1446 Shishkov, V.A., Lazukova, L.I., Chepurnaya, A.A., Kuderina, T.M., Ivanov, M.M., Kuzmenkova, N.V.,
1447 Darin, A.V., Solomina, O.N., 2020. The Holocene paleoenvironmental history of Western Caucasus (Russia)
1448 reconstructed by multi-proxy analysis of the continuous sediment sequence from Lake Khuko. *The Holocene*
1449 31, 368–379. <https://doi.org/10.1177/0959683620972782>
- 1450 Grieser, J., Giommes, R., Bernardi, M., 2006. New LocClim – the Local Climate Estimator of FAO, *Geophys. Res.*
1451 *Abstr.*, 8, 08305.
- 1452 Grimm, E., 1987. CONISS: a Fortran 77 Program for stratigraphically constraint cluster analysis by the 655
1453 method of incremental squares. *Computers and Geosciences* 13, 13-35.
- 1454 Gudbrandsson, S., Wolff-Boenisch, D., Gislason, S.R., Oelkers, E.H., 2011. An experimental study of crystalline
1455 basalt dissolution from 2<pH<11 and temperatures from 5 to 75°C. *Geochimica et Cosmochimica Acta* 75,
1456 5496–5509. <https://doi.org/10.1016/j.gca.2011.06.035>
- 1457 Guiot, J., 1990. Methodology of the last climatic cycle reconstruction in France from pollen data. *Palaeogeography,*
1458 *Palaeoclimatology, Palaeoecology* 80, 49–69.
- 1459 Guiot, J., de Beaulieu, J. L., Cheddadi, R., David, F., Ponel, P., Reille, M., 1993. The climate in Western Europe
1460 during the last Glacial/Interglacial cycle derived from pollen and insect remains. *Palaeo-geography,*
1461 *Palaeoclimatology, Palaeoecology* 103, 73–93.
- 1462 Günther, F., Thiele, A., Gleixner, G., Xu, B., Yao, T., Schouten, S., 2014. Distribution of bacterial and archaeal
1463 ether lipids in soils and surface sediments of Tibetan lakes: Implications for GDGT-based proxies in saline
1464 high mountain lakes. *Organic Geochemistry* 67, 19–30. <https://doi.org/10.1016/j.orggeochem.2013.11.014>
- 1465 Herzsuh, U., 2007. Reliability of pollen ratios for environmental reconstructions on the Tibetan Plateau. *J.*
1466 *Biogeography* 34, 1265–1273. <https://doi.org/10.1111/j.1365-2699.2006.01680.x>
- 1467 Hijmans, R.J., Phillips, S., Leathwick, J., Elith, J., 2020. Dismo: Species Distribution Modeling. R package version
1468 1.3-3. <https://cran.r-project.org/web/packages/dismo/>
- 1469 Hopmans, E.C., Schouten, S., Sinninghe Damsté, J.S., 2016. The effect of improved chromatography on GDGT-
1470 based palaeoproxies. *Org. Geochem.* 93, 1-6. <https://doi.org/10.1016/j.orggeochem.2015.12.006>
- 1471 Hovsepyan, R., Willcox, G., 2008. The earliest finds of cultivated plants in Armenia: evidence from charred
1472 remains and crop processing residues in pise from the Neolithic settlements of Aratashen and Aknashen.
1473 *Vegetation History and Archaeobotany*, 17(1), 63-71. <https://doi.org/10.1007/s00334-008-0158-6>
- 1474 Hovsepyan, R. 2013. First archaeobotanical data from the basin of Lake Sevan. *Archäologie in Armenien II* 67,
1475 93-10.

- 1476 Hovsepyan, R. 2017. New data on archaeobotany of the Lake Sevan basin. *Iran and the Caucasus* 21(3), 251-276.
- 1477 Huguet, C., Hopmans, E.C., Febo Ayala, W., Thompson, D.H., Sinninghe Damsté, J.S., Schouten, S., 2006. An
1478 improved method to determine the absolute abundance of glycerol dibiphytanyl glycerol tetraether lipids.
1479 *Org. Geochem.* 37, 1036-1041. <https://doi.org/10.1016/j.orggeochem.2006.05.008>
- 1480 Ivy-Ochs, S., Kerschner, H., Maisch, M., Christl, M., Kubik, P.W., Schlüchter, C., 2009. Latest Pleistocene and
1481 Holocene glacier variations in the European Alps. *Quat. Sci. Rev.* 28, 2137–2149.
1482 <https://doi.org/10.1016/j.quascirev.2009.03.009>
- 1483 Joannin, S., Brugiapaglia, E., de Beaulieu, J.-L., Bernardo, L., Magny, M., Peyron, O., Goring, S., Vanni re, B.,
1484 2012. Pollen-based reconstruction of Holocene vegetation and climate in southern Italy: the case of Lago
1485 Trifoglietti. *Clim. Past.* 8, 1973–1996. <https://doi.org/10.5194/cp-8-1973-2012>
- 1486 Joannin, S., Ali, A.A., Ollivier, V., Roiron, P., Peyron, O., Chevaux, S., Nahapetyan, S., Tozalakyan, P.,
1487 Karakhanyan, A., Chataigner, C., 2014. Vegetation, fire and climate history of the Lesser Caucasus: a new
1488 Holocene record from Zarishat fen (Armenia). *J. Quat. Sci.* 29, 70–82. <https://doi.org/10.1002/jqs.2679>
- 1489 Joannin, S., in prep.
- 1490 Jacobson, G. L., Bradshaw, R. H., 1981. The selection of sites for paleovegetational studies. *Quaternary research*
1491 16, 80-96.
- 1492 Jenderedjian, K., 2005. Peatlands of Armenia, in: Steiner, G.M. (Eds.), *Moore von Sibirien bis Feuerland / Mires-*
1493 *from Siberia to Tierra Del Fuego.* Biologiezentrum/ Ober sterreichische Landesmuseen, Linz, pp. 323-333.
- 1494 Jones, M.D., Abu-Jaber, N., AlShdaifat, A., Baird, D., Cook, B.I., Cuthbert, M.O., Dean, J.R., Djamali, M.,
1495 Eastwood, W., Fleitmann, D., Haywood, A., Kwiecien, O., Larsen, J., Maher, L.A., Metcalfe, S.E., Parker,
1496 A., Petrie, C.A., Primmer, N., Richter, T., Roberts, N., Roe, J., Tindall, J.C.,  nal- mer, E., Weeks, L., 2019.
1497 20,000 years of societal vulnerability and adaptation to climate change in southwest Asia. *WIREs Water* 6.
1498 <https://doi.org/10.1002/wat2.1330>
- 1499 Juggins, S., 2020. Rioja: Analysis of Quaternary Science Data. R package version 0.9-26. [https://cran.r-](https://cran.r-project.org/package=rioja)
1500 [project.org/package=rioja](https://cran.r-project.org/package=rioja)
- 1501 Kaniewski, D., Marriner, N., Cheddadi, R., Guiot, J., Van Campo, E., 2018. The 4.2 ka BP event in the Levant.
1502 *Clim. Past* 14, 1529-1542. <https://doi.org/10.5194/cp-14-1529-2018>
- 1503 Karakhanian, A., Tozalakyan, P., Grillot, J.C., Philip, H., Melkonyan, D., Paronyan, P., Arakelyan, S., 2000.
1504 Tectonic impact on the Lake Sevan environment (Armenia). *Environmental geology* 40(3), 279-288.
- 1505 Karakhanian, A., Djrashian, R., Trifonov, V., Philip, H., Arakelian, S., Avagian, A., 2002. Holocene-historical
1506 volcanism and active faults as natural risk factors for Armenia and adjacent countries. *Journal of*
1507 *Volcanology and Geothermal Research* 113, 319–344. [https://doi.org/10.1016/S0377-0273\(01\)00264-5](https://doi.org/10.1016/S0377-0273(01)00264-5)
- 1508 Karakhanian, A., Arakelyan, A., Avagyan, A., & Sadoyan, T., 2017. Aspects of the seismotectonics of Armenia:
1509 New data and reanalysis. Tectonic evolution, collision, and seismicity of Southwest Asia, in: Sorkhabi, R.
1510 (Eds.), *Honor of Manuel Berberian’s Forty-Five Years of Research Contributions: Geological Society of*
1511 *America Special Paper* 525, pp. 445-477.
- 1512 Kom rek, J., Jankovsk , V., 2001. Review of the green algal genus *Pediastrum*: implications for pollen analytical
1513 research, J. Cramer, Berlin, Germany.
- 1514 Kuhry, P., 1985. Transgressions of a raised bog across a coversand ridge originally covered with an oak-lime
1515 forest. *Rev. Palaeobot. Palynol.* 44, 313–353.
- 1516 Lalayan, E., 1931. Mavzoleys’ excavations in Soviet Armenia, Publication of Academy of Sciences of USSR,
1517 Yerevan. (In Armenian)
- 1518 Lawrence, D., Philip, G., Hunt, H., Snape-Kennedy, L., Wilkinson, T.J., 2016. Correction: Long Term Population,
1519 City Size and Climate Trends in the Fertile Crescent: A First Approximation. *PLoS ONE* 11, e0157863.
1520 <https://doi.org/10.1371/journal.pone.0157863>
- 1521 L , S., Josse, J., Husson, F., 2008. FactoMineR: An R Package for Multivariate Analysis. *Journal of Statistical*
1522 *Software*, 25(1), 1-18.
- 1523 Lebreton, V., Messenger, E., Marquer, L., Renault-Miskovsky, J., 2010. A neotaphonomic experiment in pollen
1524 oxidation and its implications for archaeopalynology. *Review of Palaeobotany and Palynology* 162, 29–38.
1525 <https://doi.org/10.1016/j.revpalbo.2010.05.002>
- 1526 Lemcke, G., Sturm, M., 1997. $\delta^{18}O$ and trace element measurements as proxy for the reconstruction of climate
1527 changes at Lake Van (Turkey): preliminary results, in: Dalfes, H.N., Kukla, G., Weiss, H. (Eds.), *Third*
1528 *Millennium BC Climate Change and Old World Collapse*, NATO ASI Series 49, Springer, Berlin, pp. 653–
1529 678.
- 1530 Leroy, S.A.G., Tudryn, A., Chali , F., L pez-Merino, L., Gasse, F., 2013. From the Aller d to the mid-Holocene:
1531 palynological evidence from the south basin of the Caspian Sea. *Quat. Sci. Rev.* 78, 77–97.
1532 <https://doi.org/10.1016/j.quascirev.2013.07.032>
- 1533 Leroyer, C., Joannin, S., Aoustin, D., Ali, A. A., Peyron, O., Ollivier, V., Tozalakyan, P., Karakhanyan, A., Fany,
1534 J., 2016. Mid Holocene vegetation reconstruction from Vanevan peat (south eastern shore of Lake Sevan,
1535 Armenia). *Quaternary International*, 395, 5-18. <http://dx.doi.org/10.1016/j.quaint.2015.06.008>

- 1536 Li, Y., Xu, Q., Yang, X., Chen, H., Lu, X., 2005. Pollen-vegetation relationship and pollen preservation on the
1537 Northeastern Qinghai-Tibetan Plateau. *Grana* 44, 160–171. <https://doi.org/10.1080/00173130500230608>
- 1538 Li, J., Pancost, R.D., Naafs, B.D.A., Yang, H., Zhao, C., Xie, S., 2016. Distribution of glycerol dialkyl glycerol
1539 tetraether (GDGT) lipids in a hypersaline lake system. *Organic Geochemistry* 99, 113–124.
1540 <https://doi.org/10.1016/j.orggeochem.2016.06.007>
- 1541 Liaw, A., Wiener, M., 2002. Classification and regression by randomForest. *R news* 2, 18–22.
- 1542 Lind, D., Taslakyan, L., 2005. Restoring the fallen blue sky: management issues and environmental legislation for
1543 Lake Sevan, Armenia. *Environ* 29, 29–103.
- 1544 Lindsay, I., Smith, A.T., 2006. A History of Archaeology in the Republic of Armenia. *Journal of Field*
1545 *Archaeology*, 31(2), pp. 165–184
- 1546 Loomis, S.E., Russell, J.M., Sinninghe Damsté, J.S., 2011. Distributions of branched GDGTs in soils and lake
1547 sediments from western Uganda: Implications for a lacustrine paleothermometer. *Organic Geochemistry* 42,
1548 739–751. <https://doi.org/10.1016/j.orggeochem.2011.06.004>
- 1549 Loomis, S.E., Russell, J.M., Ladd, B., Street-Perrott, F.A., Sinninghe Damsté, J.S., 2012. Calibration and
1550 application of the branched GDGT temperature proxy on East African lake sediments. *Earth and Planetary*
1551 *Science Letters* 357–358, 277–288. <https://doi.org/10.1016/j.epsl.2012.09.031>
- 1552 Lytle, D.E., Wahl, E.R., 2005. Palaeoenvironmental reconstructions using the modern analogue technique: the
1553 effects of sample size and decision rules. *The Holocene* 15, 554–566.
1554 <https://doi.org/10.1191/0959683605hl830rp>
- 1555 Ma, Y., Liu, K., Feng, Z., Sang, Y., Wang, W., Sun, A., 2008. A Survey of Modern Pollen and Vegetation along
1556 a South-North Transect in Mongolia. *J. Biogeogr.* 35, 1512–1532. <https://doi.org/10.1111/j.1365-2699.2007.01871.x>
- 1557
- 1558 Magny, M., Leuzinger, U., Bortenschlager, S., Haas, J.N., 2006. Tripartite climate reversal in Central Europe
1559 5600–5300 years ago. *Quat. res.* 65, 3–19. <https://doi.org/10.1016/j.yqres.2005.06.009>
- 1560 Martin, C., Ménot, G., Thouveny, N., Davtian, N., Andrieu-Ponel, V., Reille, M., Bard, E., 2019. Impact of human
1561 activities and vegetation changes on the tetraether sources in Lake St Front (Massif Central, France). *Org.*
1562 *Geochem.* 135, 38–52. <https://doi.org/10.1016/j.orggeochem.2019.06.005>
- 1563 Martin, C., Ménot, G., Thouveny, N., Peyron, O., Andrieu-Ponel, V., Montade, V., Davtian, N., Reille, M., Bard,
1564 E., 2020. Early Holocene Thermal Maximum recorded by branched tetraethers and pollen in Western Europe
1565 (Massif Central, France). *Quat. Sci. Rev.* 228, 106109. <https://doi.org/10.1016/j.quascirev.2019.106109>
- 1566 Martínez-Sosa, P., Tierney, J.E., Stefanescu, I.C., Dearing Crampton-Flood, E., Shuman, B.N., Routsom, C., 2021.
1567 A global Bayesian temperature calibration for lacustrine brGDGTs. *Geochimica et Cosmochimica Acta* 305,
1568 87–105. <https://doi.org/10.1016/j.gca.2021.04.038>
- 1569 McGovern, P., Jalabazde, M., Batiuk, S., Callahan, M.P., Smith, K.E., Hall, G.R., Kavadze, E., Maghradze, D.,
1570 Rusishvili, N., Bouby, L., Failla, O., Cola, G., Mariani, L., Boaretto, E., Bacilieri, R., This, P., Wales, N.,
1571 Lordkipanidze, D., 2017. Early Neolithic wine of Georgia in the South Caucasus. *Proc Natl Acad Sci USA*
1572 114, E10309–E10318. <https://doi.org/10.1073/pnas.1714728114>
- 1573 Meliksetian, K., Neill, I., Barfod, D.N., Milne, E.J.M., Waters, E.C., Navasardyan, G., Grigoryan, E., Olive, V.,
1574 Odling, N., Karakhanian, A., 2021. Pleistocene-Holocene volcanism at the Karkar geothermal prospect,
1575 Armenia. *Quaternary Geochronology*, 66, 101201. <https://doi.org/10.1016/j.quageo.2021.101201>
- 1576 Messenger, E., Belmecheri, S., Von Grafenstein, U., Nomade, S., Ollivier, V., Voinchet, P., Puaud, S., Courtin-
1577 Nomade, A., Guillou, H., Mgeladze, A., Dumoulin, J.-P., Mazuy, A., Lordkipanidze, D., 2013. Late
1578 Quaternary record of the vegetation and catchment-related changes from Lake Paravani (Javakheti, South
1579 Caucasus). *Quat. Sci. Rev.* 77, 125–140. <https://doi.org/10.1016/j.quascirev.2013.07.011>
- 1580 Messenger, E., Nomade, S., Wilhelm, B., Joannin, S., Scao, V., Von Grafenstein, U., Martkoplshvili, I., Ollivier,
1581 V., Mgeladze, A., Dumoulin, J.-P., Mazuy, A., Belmecheri, S., Lordkipanidze, D., 2017. New pollen
1582 evidence from Nariani (Georgia) for delayed postglacial forest expansion in the South Caucasus. *Quat. res.*
1583 87, 121–132. <https://doi.org/10.1017/qua.2016.3>
- 1584 Mezhlumyan, S.K., 1972. Paleo-fauna of eneolith, bronze and iron periods in Armenia, Publication of Academy
1585 of Sciences of Armenia, Yerevan (In Russian).
- 1586 Mnatsakanyan, H.H., 1952. Archaeological excavations in drained part of Lake Sevan, Publication of Academy
1587 of Sciences of Armenia, Yerevan (In Armenian).
- 1588 Moore, P., Webb, J.A., Collinson, M.E., 1991. Pollen analysis, Blackwell Scientific Publications, London.
- 1589 Moreno-Sanchez, R., Sayadyan, H.Y., 2005. Evaluation of the forest cover in Armenia. *International Forestry*
1590 *Review* 7, 113–127. <https://doi.org/10.1505/ifer.2005.7.2.113>
- 1591 Mudie, P.J., Leroy, S.A.G., Marret, F., Gerasimenko, N.P., Kholeif, S.E.A., Sapelko, T., Filipova-Marinova, M.,
1592 2011. Nonpollen palynomorphs: Indicators of salinity and environmental change in the Caspian–Black Sea–
1593 Mediterranean corridor, in : Buynevich, I., Yanko-Hombach, V., Gilbert, A.S, Martin, R.E. (Eds.), *Geology*
1594 *and Geoarchaeology of the Black Sea Region: Beyond the Flood Hypothesis*, Geological Society of America
1595 Special Paper 473, pp. 89–115.

- 1596 Naafs, B.D.A., Gallego-Sala, A.V., Inglis, G.N., Pancost, R.D., 2017a. Refining the global branched glycerol
1597 dialkyl glycerol tetraether (brGDGT) soil temperature calibration. *Org. Geochem.* 106, 48–56.
1598 <https://doi.org/10.1016/j.orggeochem.2017.01.009>
- 1599 Naafs, B.D.A., Inglis, G.N., Zheng, Y., Amesbury, M.J., Biester, H., Bindler, R., Blewett, J., Burrows, M.A., del
1600 Castillo Torres, D., Chambers, F.M., Cohen, A.D., Evershed, R.P., Feakins, S.J., Galka, M., Gallego-Sala,
1601 A., Gandois, L., Gray, D.M., Hatcher, P.G., Honorio Coronado, E.N., Hughes, P.D.M., Huguet, A.,
1602 Könönen, M., Laggoun-Défarge, F., Lähteenoja, O., Lamentowicz, M., Marchant, R., McClymont, E.,
1603 Pontevedra-Pombal, X., Ponton, C., Pourmand, A., Rizzuti, A.M., Rochefort, L., Schellekens, J., De
1604 Vleeschouwer, F., Pancost, R.D., 2017b. Introducing global peat-specific temperature and pH calibrations
1605 based on brGDGT bacterial lipids. *Geochimica et Cosmochimica Acta* 208, 285–301.
1606 <https://doi.org/10.1016/j.gca.2017.01.038>
- 1607 Ning, D., Zhang, E., Shulmeister, J., Chang, J., Sun, W., Ni, Z., 2019. Holocene mean annual air temperature
1608 (MAAT) reconstruction based on branched glycerol dialkyl glycerol tetraethers from Lake Ximenglongtan,
1609 southwestern China. *Organic Geochemistry* 133, 65–76. <https://doi.org/10.1016/j.orggeochem.2019.05.003>
- 1610 Ollivier, V., Joannin, S., Roiron, P., Nahapetyan, S., Chataigner, C., 2011. Travertinization and Holocene
1611 morphogenesis in Armenia: A reading grid of rapid climatic changes impact on the landscape and societies
1612 between 9500-4000 cal. BP in the Circumcaspien regions? *European Archaeologist* 36, 26–31.
- 1613 Ollivier V., Fontugne M., Hamon C., Decaix A., Hatté C., Jalabazde M., 2018. Neolithic water management and
1614 flooding in the Lesser Caucasus (Georgia). *Quaternary Science Reviews* 197, 267-287.
- 1615 Ön, Z.B., Greaves, A.M., Akçer-Ön, S., Özeren, M.S., 2021. A Bayesian test for the 4.2 ka BP abrupt climatic
1616 change event in southeast Europe and southwest Asia using structural time series analysis of paleoclimate
1617 data. *Climatic Change* 165, 7. <https://doi.org/10.1007/s10584-021-03010-6>
- 1618 Palmisano, A., Lawrence, D., de Gruchy, M.W., Bevan, A., Shennan, S., 2021. Holocene regional population
1619 dynamics and climatic trends in the Near East: A first comparison using archaeo-demographic proxies. *Quat.*
1620 *Sci. Rev.* 252, 106739. <https://doi.org/10.1016/j.quascirev.2020.106739>
- 1621 Parmegiani, N., Poscolieri, M., 2003. DEM data processing for a landscape archaeology analysis (Lake Sevan-
1622 Armenia). *International archives of photogrammetry remote sensing and spatial information sciences*, 34,
1623 255-258.
- 1624 Pearson, E. J., Juggins, S., Talbot, H. M., Weckström, Jan., Rosén, P., Ryves, D. B., Roberts, S. J., and Schmidt,
1625 R., 2011. A lacustrine GDGT-temperature calibration from the Scandinavian Arctic to Antarctic: renewed
1626 potential for the application of GDGT-paleothermometry in lakes. *Geochim. Cosmochim. Ac.* 75, 6225–
1627 6238, <https://doi.org/10.1016/j.gca.2011.07.042>
- 1628 Perşoiu, A., Ionita, M., Weiss, H., 2019. Atmospheric blocking induced by the strengthened Siberian High led to
1629 drying in west Asia during the 4.2 ka BP event – a hypothesis. *Clim. Past* 15, 781–793.
1630 <https://doi.org/10.5194/cp-15-781-2019>
- 1631 Peyron, O., Magny, M., Goring, S., Joannin, S., de Beaulieu, J.-L., Brugiapaglia, E., Sadori, L., Garfi, G., Kouli,
1632 K., Ioakim, C., Combourieu-Nebout, N., 2013. Contrasting patterns of climatic changes during the Holocene
1633 across the Italian Peninsula reconstructed from pollen data. *Clim. Past* 9, 1233–1252.
1634 <https://doi.org/10.5194/cp-9-1233-2013>
- 1635 Peyron, O., Combourieu-Nebout, N., Brayshaw, D., Goring, S., Andrieu-Ponel, V., Desprat, S., Fletcher, W.,
1636 Gambin, B., Ioakim, C., Joannin, S., Kotthoff, U., Kouli, K., Montade, V., Pross, J., Sadori, L., Magny, M.,
1637 2017. Precipitation changes in the Mediterranean basin during the Holocene from terrestrial and marine
1638 pollen records: a model–data comparison. *Clim. Past* 13, 249–265. <https://doi.org/10.5194/cp-13-249-2017>
- 1639 Prasad, A.M., Iverson, L.R. and Liaw, A., 2006. Newer classification and regression tree techniques: bagging and
1640 random forests for ecological prediction. *Ecosystems* 9(2), 181-199.
- 1641 Prentice, I.C., 1985. Pollen representation, source area, and basin size: toward a unified theory of pollen analysis.
1642 *Quaternary Research*, 23(1), 76-86.
- 1643 Prentice, C., Guiot, J., Huntley, B., Jolly, D., Cheddadi, R., 1996. Reconstructing biomes from palaeoecological
1644 data: a general method and its application to european pollen data at 0 and 6 ka. *Climate Dynamics* 12, 185–
1645 194.
- 1646 Qian, H., Hongyan, L., Shilei, Y., Weihua, Y., Zhaoliang, S., 2019. Differentiated roles of mean climate and
1647 climate stability on post-glacial birch distributions in northern China. *The Holocene* 29, 1758–1766.
1648 <https://doi.org/10.1177/0959683619862038>
- 1649 Ramezani, E., Marvie Mohadjer, M.R., Knapp, H.-D., Theuerkauf, M., Manthey, M., Joosten, H., 2013. Pollen–
1650 vegetation relationships in the central Caspian (Hyrcanian) forests of northern Iran. *Review of Palaeobotany*
1651 *and Palynology* 189, 38–49. <https://doi.org/10.1016/j.revpalbo.2012.10.004>
- 1652 Reille, M., 1992-1998. *Pollen et Spores d'Europe et d'Afrique du nord*, Laboratoire de Botanique Historique et
1653 Palynologie, Université d'Aix-Marseille, Marseille.
- 1654 Reimer, P.J., Austin, W.E.N., Bard, E., Bayliss, A., Blackwell, P.G., Ramsey, C.B., Butzin, M., Cheng, H.,
1655 Edwards, R.L., Friedrich, M., Grootes, P.M., Guilderson, T.P., Hajdas, I., Heaton, T.J., Hogg, A.G., Hughen,

1656 K.A., Kromer, B., Manning, S.W., Muscheler, R., Palmer, J.G., Pearson, C., vander Plicht, J., Reimer, R.W.,
1657 Richards, D.A., Scott, E.M., Southon, J.R., Turney, C.S.M., Wacker, L., Adophi, F., Büntgen, U., Capano,
1658 M., Fahrni, S., Fogtmann-Schulz, A., Friedrich, R., Kudsk, S., Miyake, F., Olsen, J., Reinig, F., Sakamoto,
1659 M., Sookdeo, A., Talamo, S., 2020. The IntCal20Northern Hemisphere radiocarbon calibrationcurve (0–55
1660 cal kBP). *Radiocarbon* 62 (4), 725–757. <https://doi.org/10.1017/RDC.2020.41>
1661 Ricci, A., D’Anna, M.B., Lawrence, D., Helwing, B., Aliyev, T., 2018. Human mobility and early sedentism: the
1662 Late Neolithic landscape of southern Azerbaijan. *Antiquity* 92, 1445–1461.
1663 <https://doi.org/10.15184/ajqy.2018.230>
1664 Ritchie, K., Wouters, W., Mirtskhulava, G., Jokhadze, S., Zhvania, D., Abuladze, J., Hansen, S., 2021. Neolithic
1665 fishing in the South Caucasus as seen from Aruchlo I, Georgia. *Archaeological Research in Asia* 25, 100252.
1666 <https://doi.org/10.1016/j.ara.2020.100252>
1667 Roberts, N., Reed, J.M., Leng, M.J., Kuzucuoğlu, C., Fontugne, M., Bertaux, J., Woldring, H., Bottema, S., Black,
1668 S., Hunt, E., Karabiyikoğlu, M., 2001. The tempo of Holocene climatic change in the eastern Mediterranean
1669 region: new high-resolution crater-lake sediment data from central Turkey. *The Holocene* 11, 721–736.
1670 <https://doi.org/10.1191/09596830195744>
1671 Roberts, N., 2002. Did prehistoric landscape management retard the post-glacial spread of woodland in Southwest
1672 Asia? *Antiquity* 76, 1002–1010. <https://doi.org/10.1017/S0003598X0009181X>
1673 Roberts, N., Eastwood, W.J., Kuzucuoğlu, C., Fiorentino, G., Caracuta, V., 2011. Climatic, vegetation and cultural
1674 change in the eastern Mediterranean during the mid-Holocene environmental transition. *The Holocene* 21,
1675 147–162. <https://doi.org/10.1177/0959683610386819>
1676 Roberts, C.N., Woodbridge, J., Palmisano, A., Bevan, A., Fyfe, R., Shennan, S., 2019. Mediterranean landscape
1677 change during the Holocene: Synthesis, comparison and regional trends in population, land cover and
1678 climate. *The Holocene* 29, 923–937. <https://doi.org/10.1177/0959683619826697>
1679 Russell, J.M., Hopmans, E.C., Loomis, S.E., Liang, J., Sinninghe Damsté, J.S., 2018. Distributions of 5- and 6-
1680 methyl branched glycerol dialkyl glycerol tetraethers (brGDGTs) in East African lake sediment: Effects of
1681 temperature, pH, and new lacustrine paleotemperature calibrations. *Organic Geochemistry* 117, 56–69.
1682 <https://doi.org/10.1016/j.orggeochem.2017.12.003>
1683 Ryabogina, N., Borisov, A., Idrisov, I., Bakushev, M., 2018. Holocene environmental history and populating of
1684 mountainous Dagestan (Eastern Caucasus, Russia). *Quaternary International* 516, 111–126.
1685 <https://doi.org/10.1016/j.quaint.2018.06.020>
1686 Sagona, A., Kiguradze, T., 2003. On the origins of the Kura-Araxes cultural complex. *Archaeology*, in: Smith, T.,
1687 Rubinson, K.S. (Eds.), *Archaeology in the borderlands: investigations in Caucasia and beyond*. Cotsen
1688 Institute of Archaeology, Los Angeles, pp. 38-94
1689 Sagona, A., 2017. *The Archaeology of the Caucasus: from Earliest Settlements to the Iron Age*. Cambridge
1690 University Press, Cambridge.
1691 St Jacques, J.M., Cumming, B.F., Sauchyn, D.J., Smol, J.P., 2015. The bias and signal attenuation present in
1692 conventional pollen-based climate reconstructions as assessed by early climate data from Minnesota, USA.
1693 *PLoS One* 10, 1–17. <https://doi.org/10.1371/journal.pone.0113806>
1694 Salonen, J.S., Verster, A.J., Engels, S., Soininen, J., Trachsel, M., Luoto, M., 2016. Calibrating aquatic microfossil
1695 proxies with regression-tree ensembles: Cross-validation with modern chironomid and diatom data. *The*
1696 *Holocene* 26, 1040–1048. <https://doi.org/10.1177/0959683616632881>
1697 Salonen, J.S., Korpela, M., Williams, J.W., Luoto, M., 2019. Machine-learning based reconstructions of primary
1698 and secondary climate variables from North American and European fossil pollen data. *Scientific reports* 9,
1699 1–13.
1700 Sayadyan, Y.V., Aleshinskaya, Z.V., Khanzadyan, E.V., 1977. Late glacial deposits and archaeology of the Sevan
1701 Lake, in: Sayadyan, Y.V. (Eds.), *Geology of the Quaternary Period (Pleistocene)*, Akad. Nauk Arm. SSR,
1702 Yerevan, pp. 91-109 (in Russian).
1703 Sayadyan, Y.V., 1978. Postglacial Times in Armenia and Adjacent Regions, vol. XII. *Studia Geomorphologica*
1704 *Carpatho-Balcanica*, Krakow, pp. 77-93.
1705 Sayadyan, Y.V., 1983. Men and environment in postglacial period in Lake Sevan basin and neighbourhood areas.
1706 In: *Problems of Quaternary Geology in Armenia*. Yerevan, pp 67-73 (In Russian).
1707 Sayadyan, Y.V., 2009. *The Newest Geological History of Armenia*. Gitun publish, Nat. Acad. Sciences, Yerevan
1708 (In Russian).
1709 Sayadyan, H.Y., 2011. Valuation of mountain forests: case study Armenia. *Annals of agrarian science*. Republic
1710 of Georgia, 9(1), 144-148.
1711 Schouten, S., van der Meer, M. T., Hopmans, E. C., Rijpstra, W. I. C., Reysenbach, A.-L., Ward, D. M., Sinninghe
1712 Damsté, J.S., 2007. Archaeal and bacterial glycerol dialkyl glycerol tetraether lipids in hot springs of
1713 Yellowstone National Park. *Applied and Environmental Microbiology* 73(19), 6181–6191.
1714 Shanahan, T.M., Huguen, K.A., Van Mooy, B.A.S., 2013. Temperature sensitivity of branched and isoprenoid
1715 GDGTs in Arctic lakes, *Org. Geochem.* 64, 119–128. <https://doi.org/10.1016/j.orggeochem.2013.09.010>

- 1716 Sharifi, A., Pourmand, A., Canuel, E.A., Ferer-Tyler, E., Peterson, L.C., Aichner, B., Feakins, S.J., Daryaei, T.,
 1717 Djamali, M., Beni, A.N., Lahijani, H.A.K., Swart, P.K., 2015. Abrupt climate variability since the last
 1718 deglaciation based on a high-resolution, multi-proxy peat record from NW Iran: The hand that rocked the
 1719 Cradle of Civilization? *Quat. Sci. Rev.* 123, 215–230. <https://doi.org/10.1016/j.quascirev.2015.07.006>
- 1720 Shumilovskikh, L.S., Tarasov, P., Arz, H.W., Fleitmann, D., Marret, F., Nowaczyk, N., Plessen, B., Schlütz, F.,
 1721 Behling, H., 2012. Vegetation and environmental dynamics in the southern Black Sea region since 18kyr BP
 1722 derived from the marine core 22-GC3. *Palaeogeography, Palaeoclimatology, Palaeoecology* 337–338, 177–
 1723 193. <https://doi.org/10.1016/j.palaeo.2012.04.015>
- 1724 Sinninghe Damsté, J.S., Rijpstra, W.I.C., Foesel, B.U., Huber, K.J., Overmann, J., Nakagawa, S., Kim, J.J.,
 1725 Dunfield, P.F., Dedysh, S.N., Villanueva, L., 2018. An overview of the occurrence of ether- and ester-linked
 1726 iso-diabolic acid membrane lipids in microbial cultures of the Acidobacteria: Implications for brGDGT
 1727 paleoproxies for temperature and pH. *Organic Geochemistry* 124, 63–76.
 1728 <https://doi.org/10.1016/j.orggeochem.2018.07.006>
- 1729 Smith, A.T., 2015. *The Political Machine: Assembling Sovereignty in the Bronze Age Caucasus*. Princeton
 1730 University Press, Princeton.
- 1731 Solomina, O.N., Bradley, R.S., Hodgson, D.A., Ivy-Ochs, S., Jomelli, V., Mackintosh, A.N., Nesje, A., Owen,
 1732 L.A., Wanner, H., Wiles, G.C., Young, N.E., 2015. Holocene glacier fluctuations. *Quat. Sci. Rev.* 111, 9–
 1733 34. <https://doi.org/10.1016/j.quascirev.2014.11.018>
- 1734 Solomon, J.C., Shulkinia, T.V., Schatz, G.E., 2014. *Red List of the Endemic Plants of the Caucasus: Armenia,*
 1735 *Azerbaijan, Georgia, Iran, Russia, and Turkey*, Missouri Botanical Garden Press, Saint Louis.
- 1736 Sosson, M., Rolland, Y., Müller, C., Danelian, T., Melkonyan, R., Kekelia, S., Adamia, S., Babazadeh, V.,
 1737 Kangarli, T., Avagyan, A., Galoyan, G., Mosar, J., 2010. Subductions, obduction and collision in the Lesser
 1738 Caucasus (Armenia, Azerbaijan, Georgia), new insights, in: Sosson, M., Kaymakci, N., Stephenson, R.,
 1739 Bergerat, F., Starostenko, V. (Eds.), *Sedimentary Basin Tectonics from the Black Sea and Caucasus to the*
 1740 *Arabian Platform*, Geological Society of London, Special Publication 340, pp. 329–352.
 1741 <https://doi.org/10.1144/SP340.14>
- 1742 St Jacques, J.M., Cumming, B.F., Sauchyn, D.J., Smol, J.P., 2015. The bias and signal attenuation present in
 1743 conventional pollen-based climate reconstructions as assessed by early climate data from Minnesota, USA.
 1744 *PLoS One* 10, 1–17. <https://doi.org/10.1371/journal.pone.0113806>.
- 1745 Stanyukovich, K. V., 1973. *Vegetation of the Mountains of the USSR*. The Tadjik Academy of Sciences Presse,
 1746 Dushanbe (in Russian).
- 1747 Stevens, L.R., Wright, H.E., Ito, E., 2001. Proposed changes in seasonality of climate during the Lateglacial and
 1748 Holocene at Lake Zeribar, Iran. *The Holocene* 11, 747–755. <https://doi.org/10.1191/09596830195762>
- 1749 Stevens, L.R., Ito, E., Schwalb, A., Wright, H.E., 2006. Timing of Atmospheric Precipitation in the Zagros
 1750 Mountains Inferred from a Multi-Proxy Record from Lake Mirabad, Iran. *Quat. res.* 66, 494–500.
 1751 <https://doi.org/10.1016/j.yqres.2006.06.008>
- 1752 Stockhecke, M., Bechtel, A., Peterse, F., Guillemot, T., Schubert, C.J., 2021. Temperature, precipitation, and
 1753 vegetation changes in the Eastern Mediterranean over the last deglaciation and Dansgaard-Oeschger events.
 1754 *Palaeogeography, Palaeoclimatology, Palaeoecology* 577, 110535.
 1755 <https://doi.org/10.1016/j.palaeo.2021.110535>
- 1756 Sun, Q., Chu, G.Q., Liu, M.M., Xie, M.M., Li, S.Q., Ling, Y., Wang, X.H., Shi, L.M., Jia, G.D., Lü, H.Y., 2011.
 1757 Distributions and temperature dependence of branched glycerol dialkyl glycerol tetraethers in recent
 1758 lacustrine sediments from China and Nepal. *J. Geophys. Res.* 116, G01008.
 1759 <https://doi.org/10.1029/2010jg001365>
- 1760 Takhtajyan, A.L., 1941. Botanical-geographic overview of Armenia. *Work Papers of Institute of Botany of*
 1761 *Armenian Academy of Sciences/Branch of USSR Academy of Sciences* 2, 180 (in Russian).
- 1762 Telford, R.J., Birks, H.J.B., 2005. The secret assumption of transfer functions: problems with spatial
 1763 autocorrelation in evaluating model performance. *Quat. Sci. Rev.* 24, 2173–2179.
 1764 <https://doi.org/10.1016/j.quascirev.2005.05.001>
- 1765 Telford, R.J., Birks, H.J.B., 2009. Evaluation of transfer functions in spatially structured environments. *Quat. Sci.*
 1766 *Rev.* 28, 1309–1316. <https://doi.org/10.1016/j.quascirev.2008.12.020>
- 1767 Telford, R.J., Birks, H.J.B., 2011. QSR Correspondence “is spatial autocorrelation introducing biases in the
 1768 apparent accuracy of palaeoclimatic reconstructions?”. *Quat. Sci. Rev.* 30, 3210–3213.
 1769 <https://doi.org/10.1016/j.quascirev.2011.07.019>
- 1770 Ter Braak, C.J.F., Van Dam, H., 1989. Inferring pH from diatoms: A comparison of old and new calibration
 1771 methods. *Hydrobiologia* 178, 209–223.
- 1772 Ter Braak, C.J.F., Juggins, S., Birks, H.J.B., Van der Voet, H., 1993. Weighted averaging partial least squares
 1773 regression (WA-PLS): definition and comparison with other methods for species–environment calibration,
 1774 chap. 25, Elsevier Science Publishers, Amsterdam, pp. 525–560.

- 1775 Tumanyan, M.R., 1971. On the history of lake Sevan basin vegetation in holocene. Academy of Sciences of
1776 Armenian SSR, Biological Journal, T.XXIV 11, 57-61 (in Russian).
- 1777 Tumajanov, I.I., Tumanyan, M.R., 1973. New data on the history of forest vegetation in Masrik plain in Holocene.
1778 Academy of Sciences of Armenian SSR, Biological Journal, T.XXVI 12, 24-28 (in Russian).
- 1779 Turner, R., Roberts, N., Jones, M.D., 2008. Climatic pacing of Mediterranean fire histories from lake sedimentary
1780 microcharcoal. *Global and Planetary Change* 63, 317–324. <https://doi.org/10.1016/j.gloplacha.2008.07.002>
- 1781 Turner, R., Roberts, N., Eastwood, W.J., Jenkins, E., Rosen, A., 2010. Fire, climate and the origins of agriculture:
1782 micro-charcoal records of biomass burning during the last glacial-interglacial transition in Southwest Asia.
1783 *J. Quaternary Sci.* 25, 371–386. <https://doi.org/10.1002/jqs.1332>
- 1784 Van Geel, B., van der Hammen, T., 1978. Zygnemataceae in Quaternary Colombian sediments. *Rev. Palaeobot.*
1785 *Palynol.* 25, 377–392.
- 1786 Van Geel, B., Coope, G.R., van der Hammen, T., 1989. Palaeoecology and stratigraphy of the Lateglacial type
1787 section at Usselo (The Netherlands). *Rev. Palaeobot. Palynol.* 60, 25–129.
- 1788 Van Geel, B., Grenfell, H.R., 1996. Spores of Zygnemataceae, in: Jansonius, J., McGregor D.C. (Eds.) *Palynology:*
1789 *principles and applications*, Am. Ass. Strat. Palynol. Found., Vol. 1, pp. 173–179.
- 1790 Van Geel, B., 2002. Non-Pollen Palynomorphs, in: Smol, J.P., Birks, H.J.B., Last, W.M., Bradley, R.S., Alverson,
1791 K. (Eds.), *Tracking Environmental Change Using Lake Sediments. Developments in Paleoenvironmental*
1792 *Research*. Springer, Dordrecht, pp. 99–119. https://doi.org/10.1007/0-306-47668-1_6
- 1793 Van Geel, B., Heijnis, H., Charman, D.J., Thompson, G., Engels, S., 2014. Bog burst in the eastern Netherlands
1794 triggered by the 2.8 kyr BP climate event. *The Holocene* 24, 1465–1477.
1795 <https://doi.org/10.1177/0959683614544066>
- 1796 Van Zeist, W., Woldring, H., Stapert, D., 1975. Late Quaternary vegetation and climate of southwestern Turkey.
1797 *Palaeohistoria* 17, 53–143.
- 1798 Volodicheva, N., 2002. The Caucasus, in: Shahgedanova, M. (Eds.), *The Physical Geography of Northern Eurasia*.
1799 Oxford University Press, New York, pp. 350-376.
- 1800 Wang, H. Y., Liu, W. G., Zhang, C. L., Wang, Z., Wang, J. X., Liu, Z. H., Dong, H. L., 2012. Distribution of
1801 glycerol dialkyl glycerol tetraethers in surface sediments of Lake Qinghai and surrounding soil, *Org.*
1802 *Geochem.* 47, 78–87. <https://doi.org/10.1016/j.orggeochem.2012.03.008>
- 1803 Watson, B.I., Williams, J.W., Russell, J.M., Jackson, S.T., Shane, L., Lowell, T.V., 2018. Temperature variations
1804 in the southern Great Lakes during the last deglaciation: Comparison between pollen and GDGT proxies.
1805 *Quaternary Science Reviews* 182, 78–92. <https://doi.org/10.1016/j.quascirev.2017.12.011>
- 1806 Weber, Y., Sinninghe Damsté, J.S., Zopfi, J., De Jonge, C., Gilli, A., Schubert, C.J., Lepori, F., Lehmann, M.F.,
1807 Niemann, H., 2018. Redox-dependent niche differentiation provides evidence for multiple bacterial sources
1808 of glycerol tetraether lipids in lakes. *Proc. Natl. Acad. Sci. USA* 115, 10926–10931.
1809 <https://doi.org/10.1073/pnas.1805186115>
- 1810 Wei, H., Zhao, Y., 2015. Surface pollen and its relationships with modern vegetation and climate in the Tianshan
1811 Mountains, northwestern China. *Veget. Hist. Archaeobot.* 25, 19–27. [https://doi.org/10.1007/s00334-015-](https://doi.org/10.1007/s00334-015-0530-2)
1812 [0530-2](https://doi.org/10.1007/s00334-015-0530-2)
- 1813 Weijers, J.W., Schouten, S., Linden, M., Geel, B., Sinninghe Damsté, J.S., 2004. Water table related variations in
1814 the abundance of intact archaeal membrane lipids in a Swedish peat bog. *FEMS Microbiology Letters* 239,
1815 51–56.
- 1816 Weijers, J.W., Schouten, S., Hopmans, E.C., Genevassen, J.A., David, O.R., Coleman, J.M., Pancost, R.D.,
1817 Sinninghe Damsté, J.S., 2006. Membrane lipids of mesophilic anaerobic bacteria thriving in peats have
1818 typical archaeal traits. *Environmental Microbiology* 8(4), 648–657. [https://doi.org/10.1111/j.1462-](https://doi.org/10.1111/j.1462-2920.2005.00941.x)
1819 [2920.2005.00941.x](https://doi.org/10.1111/j.1462-2920.2005.00941.x)
- 1820 Weijers, J.W., Schouten, S., van den Donker, J.C., Hopmans, E.C., Sinninghe Damsté, J.S., 2007. Environmental
1821 controls on bacterial tetraether membrane lipid distribution in soils. *Geochem. Cosmochim. Acta* 71, 703–
1822 713. <https://doi.org/10.1016/j.gca.2006.10.003>
- 1823 Weiss, H., Courty, M.-A., Wetterstrom, W., Guichard, F., Senior, L., Meadow, R., Curnow, A., 1993. The genesis
1824 and collapse of third millennium north Mesopotamian civilization. *Science* 261, 995–1004.
- 1825 Weiss, H., 2016. Global megadrought, societal collapse and resilience at 4.2–3.9 ka BP across the Mediterranean
1826 and west Asia. *Magazine* 24, 62–63. <https://doi.org/10.22498/pages.24.2.62>
- 1827 Wick, L., Lemcke, G., Sturm, M., 2003. Evidence of Lateglacial and Holocene climatic change and human impact
1828 in eastern Anatolia: high-resolution pollen, charcoal, isotopic and geochemical records from the laminated
1829 sediments of Lake Van, Turkey. *The Holocene* 13, 665–675. <https://doi.org/10.1191/0959683603hl653rp>
- 1830 Wright, H.E., Ammann, B., Stefanova, I., Atanassova, J., Margalitadze, N., Wick, L., Blyakharchuk, T., 2003.
1831 Late-glacial and Early-Holocene Dry Climates from the Balkan Peninsula to Southern Siberia, in: Tonkov,
1832 S. (Eds.), *Aspects of Palynology and Palaeoecology – Festschrift in Honour of Elissaveta Bozilova*. Pensoft
1833 Publishers, Sofia, pp. 127-136. <https://doi.org/10.1016/j.quascirev.2009.02.001>

1834 Wu, W., Zheng, H., Hou, M., Ge, Q., 2018. The 5.5 cal ka BP climate event, population growth, circumscription
1835 and the emergence of the earliest complex societies in China. *Sci. China Earth Sci.* 61, 134–148.
1836 <https://doi.org/10.1007/s11430-017-9157-1>

1837 Wünnemann, B., Demske, D., Tarasov, P., Kotlia, B.S., Reinhardt, C., Bloemendal, J., Diekmann, B., Hartmann,
1838 K., Krois, J., Riedel, F., Arya, N., 2010. Hydrological evolution during the last 15kyr in the Tso Kar lake
1839 basin (Ladakh, India), derived from geomorphological, sedimentological and palynological records. *Quat.*
1840 *Sci. Rev.* 29, 1138–1155. <https://doi.org/10.1016/j.quascirev.2010.02.017>

1841 Xiao, W., Wang, Y., Zhou, S., Hu, L., Yang, H., Xu, Y., 2016. Ubiquitous production of branched glycerol dialkyl
1842 glycerol tetraethers (brGDGTs) in global marine environments: a new source indicator for brGDGTs.
1843 *Biogeosciences* 13, 5883–5894. <https://doi.org/10.5194/bg-13-5883-2016>.

1844 Xu, Q.H., Li, Y.C., Zhou, L.P., Li, Y.Y., Zhang, Z.Q., Lin, F.Y., 2007. Pollen flux and vertical dispersion in
1845 coniferous and deciduous broadleaved mixed forest in the Changbai Mountains. *Chinese Science Bulletin*
1846 52 (11), 1540–1544.

1847 Xu, Q., Li, Y., Tian, F., Cao, X., Yang, X., 2009. Pollen assemblages of tauber traps and surface soil samples in
1848 steppe areas of China and their relationships with vegetation and climate. *Review of Palaeobotany and*
1849 *Palynology* 153, 86–101. <https://doi.org/10.1016/j.revpalbo.2008.07.003>

1850 Xu, Q., Cao, X., Tian, F., Zhang, S., Li, Y., Li, M., Li, J., Liu, Y., Liang, J., 2014. Relative pollen productivities
1851 of typical steppe species in northern China and their potential in past vegetation reconstruction. *Sci. China*
1852 *Earth Sci.* 57, 1254–1266. <https://doi.org/10.1007/s11430-013-4738-7>

1853 Yang, H., Pancost, R.D., Dang, X., Zhou, X., Evershed, R.P., Xiao, G., Tang, C., Gao, L., Guo, Z., Xie, S., 2014.
1854 Correlations between microbial tetraether lipids and environmental variables in Chinese soils: Optimizing
1855 the paleo-reconstructions in semi-arid and arid regions. *Geochimica et Cosmochimica Acta* 126, 49–69.
1856 <https://doi.org/10.1016/j.gca.2013.10.041>

1857 Yu, X., Zhou, W., Franzen, L.G., Xian, F., Cheng, P., Jull, A.J.T., 2006. High-resolution peat records for Holocene
1858 monsoon history in the eastern Tibetan Plateau. *Sci. China* 49, 615–621. <https://doi.org/10.1007/s11430-006-0615-y>

1860 Zanchetta, G., Bar-Matthews, M., Drysdale, R.N., Lionello, P., Ayalon, A., Hellstrom, J.C., Isola, I., Regattieri,
1861 E., 2014. Coeval dry events in the central and eastern Mediterranean basin at 5.2 and 5.6ka recorded in
1862 Corchia (Italy) and Soreq caves (Israel) speleothems. *Global and Planetary Change* 122, 130–139.
1863 <https://doi.org/10.1016/j.gloplacha.2014.07.013>

1864 Zanchetta, G., Regattieri, E., Isola, I., Drysdale, R. N., Bini, M., Baneschi, I., and Hellstrom, J. C., 2016. The so-
1865 called “4.2 event” in the central Mediterranean and its climatic teleconnections, *Alp. Med. Quat.* 29, 5–17.

1866 Zhao, Y., Herzschuh, U., 2009. Modern pollen representation of source vegetation in the Qaidam Basin and
1867 surrounding mountains, north-eastern Tibetan Plateau. *Veget. Hist. Archaeobot.* 18, 245–260.
1868 <https://doi.org/10.1007/s00334-008-0201-7>

1869 Zhao, Y., Yu, Z., Chen, F., 2009. Spatial and temporal patterns of Holocene vegetation and climate changes in
1870 arid and semi-arid China. *Quaternary International* 194, 6–18. <https://doi.org/10.1016/j.quaint.2007.12.002>

1871 Zhang, Y.-J., Duo, L., Pang, Y.-Z., Felde, V.A., Birks, H.H., Birks, H.J.B., 2018. Modern pollen assemblages and
1872 their relationships to vegetation and climate in the Lhasa Valley, Tibetan Plateau, China. *Quaternary*
1873 *International* 467, 210–221. <https://doi.org/10.1016/j.quaint.2018.01.040>

1874 Zheng, Z., Huang, K., Xu, Q., Lu, H., Cheddadi, R., Luo, Y., Beaudouin, C., Luo, C., Zheng, Y., Li, C., Wei, J.,
1875 Du, C., 2008. Comparison of climatic threshold of geographical distribution between dominant plants and
1876 surface pollen in China. *Sci. China Ser. D-Earth Sci.* 51, 1107–1120. <https://doi.org/10.1007/s11430-008-0080-x>

1877

1878 Zielhofer, C., Fletcher, W.J., Mischke, S., De Batist, M., Campbell, J.F.E., Joannin, S., Tjallingii, R., El Hamouti,
1879 N., Junginger, A., Stele, A., Bussmann, J., Schneider, B., Lauer, T., Spitzer, K., Strupler, M., Brachert, T.,
1880 Mikdad, A., 2017. Atlantic forcing of Western Mediterranean winter rain minima during the last 12,000
1881 years, *Quat. Sci. Rev.* 157, 29–51, 2017. <http://dx.doi.org/10.1016/j.quascirev.2016.11.037>

1882 Zink, K.-G., Vandergoes, M.J., Bauersachs, T., Newnham, R.M., Rees, A.B.H., Schwark, L., 2016. A refined
1883 paleotemperature calibration for New Zealand limnic environments using differentiation of branched
1884 glycerol dialkyl glycerol tetraether (brGDGT) sources. *Journal of Quaternary Science* 31, 823–835.
1885 <https://doi.org/10.1002/jqs.2908>

1886

1887

1888